

# The added value of 4D microgravimetry to the understanding of how volcanoes work

Daniele Carbone<sup>1</sup>, Michael P. Poland<sup>2</sup>, Michel Diament<sup>3</sup> and Filippo Greco<sup>1</sup>

*1 Istituto Nazionale di Geofisica e Vulcanologia, Sezione di Catania - Osservatorio Etneo, Catania, Italy*

*2 U.S. Geological Survey - Cascades Volcano Observatory, Vancouver, Washington, USA*

*3 Institut de Physique du Globe de Paris (UMR CNRS 7154), Sorbonne Paris Cité, Paris, France*

## Abstract

During the last few decades, 4D volcano gravimetry has shown great potential for illuminating subsurface processes at active volcanoes (including some that might otherwise remain “hidden”), especially when combined with other methods (e.g., ground deformation, seismicity, and gas emissions). By supplying information on changes in the distribution of bulk mass over time, gravimetry can provide unique information regarding such processes as magma accumulation in void space, gas segregation at shallow depths, and mechanisms driving volcanic uplift and subsidence.

Despite its potential, 4D volcano gravimetry is an underexploited method, not widely adopted by volcano researchers or observatories. The cost of instrumentation and the difficulty in using it under harsh environmental conditions is a significant impediment to the exploitation of gravity at many volcanoes. In addition, retrieving useful information from gravity changes in noisy volcanic environments is a major challenge. While these difficulties are not trivial, neither are they insurmountable; indeed, creative efforts in a variety of volcanic settings highlight the value of 4D gravimetry for understanding hazards as well as revealing fundamental insights into how volcanoes work.

Building on previous work, we provide a comprehensive review of 4D volcano gravimetry, including discussions of instrumentation, modeling and analysis techniques, and case studies that emphasize what can be learned from, campaign, continuous, and hybrid gravity observations. We are hopeful that this exploration of 4D volcano gravimetry will excite more scientists about the potential of the method, spurring further application, development, and innovation.

## 1. Introduction

The dynamics of active volcanic systems are governed by complex coupled phenomena that are manifested at the surface in different ways, both as unrest and eruptive activity. The assessment and mitigation of volcanic hazards rely upon interpreting these manifestations, which requires a thorough understanding of the physical and chemical processes that drive volcanism—particularly those associated with magma ascent and transport. Over the past few decades, volcanology has undergone a substantial transformation in this respect, with limited, often qualitative, discipline-bounded observations giving way to multidisciplinary, high-spatiotemporal-resolution datasets that are quantitatively analyzed using principles from thermodynamics, fluid dynamics, rock mechanics, and other fields. This transformation has occurred largely as a result of two developments: (1) improvements in volcano monitoring systems due to increasing numbers of observation techniques, technological advancements in geophysical and geochemical sensors, and growth in areas such as computer science, telecommunications, and information technology; and (2) development of analytical, semi-analytical and numerical methods aimed at modelling the effect of multiphase dynamics triggered by a wide range of processes within magmatic plumbing systems.

The field of volcano gravimetry has benefitted substantially from these advances, with improvements in instrumentation coupled with new modelling approaches allowing for novel insights into subsurface mass changes. During the past few decades, many studies have shown that volcano gravimetry can supply information of exceptional value regarding the source mechanisms of volcanic unrest (Battaglia et al., 2008; Williams-Jones et al., 2008; and references therein). As an example, the accumulation of magma and the exsolution of gas within an existing magma chamber both induce a pressure increase resulting in a similar pattern of ground deformation at the surface. The key parameter needed to discriminate between these sources is mass, which will increase in the case of intrusion but show much less variation in the case of vesiculation. Under some circumstances, mass change may represent the only factor that can be used to constrain processes occurring in the subsurface. For instance, magma accumulation in pre-existing void space (such as a network of fractures) may not trigger changes in pressure that would result in measureable seismicity or ground deformation, but the mass signature of the intrusion can be recognized by measuring gravity changes at the surface (e.g., Rymer et al. 1993). Microgravity monitoring can also shed light on the causes of unrest—for example, are seismicity and surface inflation caused by the buildup and expansion of hydrothermal fluids, or is magma accumulation the source of the observed changes (e.g., Battaglia et al., 1999, 2003, 2006)? The answers to this and similar questions are critical for assessing the hazards posed by the unrest and represent

information that civil defense organizations require to design and implement appropriate response plans. Indeed, past studies have shown that microgravity changes are detectable before, during, and after volcanic crises (Rymer et al., 1993; Battaglia et al., 1999; Carbone et al., 2003a; Jousset et al., 2000, 2003; Bonvalot et al., 2008; Bagnardi et al., 2014), with signal strengths varying from a few to several hundred  $\mu\text{Gal}$  ( $1 \mu\text{Gal} = 10^{-8} \text{ms}^{-2}$ ).

Despite its promise in revealing potentially “hidden” magmatic activity and elucidating the cause-effect relations between complex subsurface processes and their geophysical manifestations at the surface (e.g., Battaglia et al., 2006; Carbone et al., 2014), time-variable gravity monitoring has not been widely adopted by volcano researchers and observatories. This is likely a result of several factors, including: (i) the cost of instrumentation (the most common gravimeters are about an order of magnitude more expensive than, for example, broadband seismometers), (ii) problems that are inherent with the use and deployment of instruments intended for laboratory conditions in the harsh environments that characterize the summit zones of most active volcanoes, and (iii) difficulty in interpreting gravity changes that are a function of not only magmatic, volcanic, and tectonic activity, but also hydrological effects, environmental conditions, and instrumental artifacts. Nevertheless, microgravity surveys aimed at detecting subsurface mass changes have been completed at several dozen volcanoes worldwide (Fig. 1), and results from many of these studies have provided valuable constraints on magma dynamics and eruptive activity.

Here, we review the instrumentation and methodologies used to characterize gravity change at volcanoes, and we describe many case studies that highlight the results achieved by coupling other, more established methods (like deformation, seismicity, and gas geochemistry) with gravity observations to better understand volcanic processes. Our intent is to provide a comprehensive review of volcano gravimetry, building on discussions in Battaglia et al. (2008) and Williams-Jones et al. (2008). First, we introduce instruments and techniques used to perform gravity measurements at active volcanoes (section 2). We then describe the most commonly used models to interpret gravity data from volcanoes (section 3). Next, we discuss the results of past studies focused on (i) long-term gravity changes from time-lapse (campaign) measurements (section 4), (ii) short-term gravity changes revealed by continuous measurements (section 5), and (iii) the joint use of discrete and continuous methods, as well as coupled relative and absolute measurements (section 6). We conclude by reviewing the inherent challenges in volcano gravimetry and suggesting how these challenges can be overcome, with a view toward expanding future exploitation of the capability (section 7).

## 2. Instrumentation and measurement techniques

Gravity measurements at active volcanoes are performed to fulfil two main purposes: (i) to understand volcanic processes that induce bulk mass/density changes, and thus gravity changes over time (time-varying gravimetry; e.g., Battaglia et al., 2008; Williams-Jones et al., 2008), and (ii) to image the subsurface density structure of a volcanic edifice (static gravimetry; e.g., Schiavone and Loddo, 2007). To achieve (i), gravity measurements must be repeated over time, in either campaign or continuous mode (see sections 4 and 5), to estimate how the gravity field has changed at a single point or along an array of fixed observation points during the interval spanned. To achieve (ii), tens to hundreds of points over a broad area are measured to attain sufficient spatial resolution for mapping density variations beneath the surface. When used for the purpose of static gravimetry, data must be made consistent with each-other, i.e. reflective only of the density structure beneath the ground. Corrections are thus applied (Deroussi et al., 2009) to account for the different elevation of the observation points (free-air correction) and the different distribution of above-ground masses around each measurement point (Bouguer and terrain corrections).

As our focus is on time-varying gravimetry at volcanoes, we do not discuss static gravimetry and we refer readers to Schiavone and Loddo (2007) and to Gailler et al. (2009) for more information on the topic.

### 2.1. Instrumentation

The magnitude of time-varying gravity changes associated with active volcanic systems is between a few and a few hundred  $\mu\text{Gal}$  (Rymer, 1989)—between one part in  $10^6$  and one part in  $10^8$  of the standard gravity on Earth ( $g = 9.8 \text{ m}\cdot\text{s}^{-2}$ ). High-precision instruments are therefore needed to detect such small signals. These instruments come in two varieties: relative and absolute. Relative gravimeters measure gravity differences over space, between pairs of stations, or over time, at a single point with respect to the gravity value at an arbitrary starting time. The absolute gravity value at a given station is not measurable by relative instruments. Conversely, using absolute gravimeters, it is possible to measure the actual value of the gravitational acceleration at the observation point.

#### 2.1.1. Relative gravimeters

##### 2.1.1.1. Spring-based gravimeters

Spring gravimeters—the most widely used relative instruments—measure the change in the equilibrium position of a proof mass suspended from a spring that results from a change in the gravity field. To achieve the extraordinary precision required for measuring gravity changes due to volcanic activity (typically on the order of 10  $\mu\text{Gal}$ ), a number of different strategies have been adopted by various instrument manufacturing companies. Since 1930, more than 30 types of spring gravimeters have been introduced (Nabighian et al., 2005), one of the most successful being that developed by LaCoste & Romberg (L&R) in 1939. The working principle of L&R gravimeters is based on the concept of a “zero-length” spring (LaCoste, 1988)—a spring that is wound in a pre-stressed condition, so that, if the force acting on it was zero, the spring would collapse to zero length. In L&R instruments, an inclined zero-length metal counter-spring holds a horizontal beam supporting the proof mass (Fig. 2c; Torge, 1989). The beam is displaced by a change in gravity, which is compensated for, and thus measured, by forcing the beam back to the horizontal position. An increase in the mechanical sensitivity is achieved by designing the system so that the torque characteristics of gravity and spring forces are very close to each-other (astatization). In early L&R instruments, the horizontal position of the beam was restored only mechanically, by lifting the top end of the zero-length spring through a sophisticated system including levers, a high-precision screw, and a gear box (LaCoste & Romberg, 2004). Since the beginning of the 2000s, L&R gravimeters have been optionally fitted with a capacitive position indicator, to monitor the position of the beam, and an electrostatic feedback system, to keep the beam in the null position (the Aloid-100 feedback system, featuring a dynamic range of 100 (early models) to 200 mGal).

The L&R D- and G-models are no longer in production but are still widely utilized. The D-meter (Fig. 2a and d) features a reading resolution of about 5  $\mu\text{Gal}$  and, when used to reoccupy networks of stations, has an accuracy of between 15 to 20  $\mu\text{Gal}$  (Rymer, 1989; Torge, 1989). When an electronic feedback system is used to null the beam, the accuracy of the recordings (1 Hz sampling rate) can be better than 1  $\mu\text{Gal}$  for averages over time-windows of 1 minute. Spring-based gravimeters are affected by instrumental drift due to changes in the elastic properties of the spring that occur slowly over time. For L&R gravimeters, the drift is on the order of 1 mGal per month, but decreases as the meter ages down to less than 0.5 mGal per month. Drift is usually linear over some days, but strong nonlinearities arise over longer periods because ambient parameters (mainly temperature but also humidity) induce instrumental effects that modulate the rate of the drift (El Wahabi et al., 2001).

A new generation of relative spring gravimeters has been developed by Scintrex Ltd. since 1989. Scintrex gravimeters are microprocessor-based, automated instruments with a reading resolution of 1

$\mu\text{Gal}$ . They feature a vertically hanging quartz spring and a capacitive displacement transducer/electrostatic feedback system able to detect movements of the proof mass and to force it back to a null position. The high-resolution displacement transducer, able to determine changes in the length of the spring to 0.2 nm, removes the need for astatization, largely eliminating errors arising from mechanical imperfections in the zeroing system. The quartz spring offers some advantages with respect to the metal spring in L&R instruments: it is less affected by mechanical shocks, less sensitive to changes in external magnetic fields, and has limited fatigue and memory effects. However, quartz springs are more fragile than metal springs, feature a higher temperature coefficient than the special alloy metal of L&R springs, and have a tendency towards stronger long-term drift. Budetta and Carbone (1997) studied the performances of the (at the time) newly released Scintrex CG-3M gravimeter and found that, under the severe field condition encountered on active volcanoes, the more rugged and automated Scintrex devices provide a better measurement precision than L&R instruments. Budetta and Carbone (1997) also showed that the strong drift of Scintrex gravimeters ( $\sim 1 \text{ mGal d}^{-1}$ ) can be reduced to acceptable standards (within about  $20 \mu\text{Gal d}^{-1}$ ) by the real-time automatic compensation.

For the ten years after their release, Scintrex was the major competitor of L&R. In 2001, however, the two companies merged to form LaCoste & Romberg - Scintrex, Inc. (LRS), which later became the parent company of Micro-g. Nowadays, LRS and Micro-g capture most of the market available for land spring-based relative gravimeters with two products: the Micro-g/LaCoste gPhone and the Scintrex CG-5 gravimeters (the successor to the CG-3M). With its compact shape, limited size/weight, insensitivity to shocks, and automated features, the CG-5 (Fig. 3) is well suited for measurements at active volcanoes and has been the standard for time-lapse observations since the mid-to-late 2000s (e.g., Bagnardi et al., 2014).

The gPhone (Fig. 2d) is primarily intended for recording gravity time series (continuous observations). The instrument is based upon the L&R zero-length spring suspension system; however, with respect to previous L&R models (e.g., the D- and G-meters), it features significant upgrades, including: (i) a double-oven system, allowing for a higher degree of temperature stabilization; (ii) a fully vacuum-sealed chamber enclosing the sensor, to eliminate the effect of external pressure changes; and (iii) a feedback nulling system with  $0.1 \mu\text{Gal}$  resolution. The gPhone is also characterized by small instrumental drift (common to L&R meters), a high precision ( $1 \mu\text{Gal}$ ), and low system noise ( $3 \mu\text{Gal}/\sqrt{\text{Hz}}$ ). Some features, however, make it difficult to use the instrument in hostile field environments. In many cases, measurement sites in the active zones of tall volcanoes must be reached

on foot and do not offer much space for the setup, implying that the weight and size of the instrumentation are critical issues. A gPhone is nearly 3 times larger (Fig. 2d) and more than 4 times heavier (13 vs 3.2 kg) than a L&R D- or G-meter, is controlled by a dedicated acquisition system that includes a laptop computer, and requires a continuous power supply of about 100 Watts (by comparison, the power supply required by a L&R D- or G-meter with an electronic feedback system is about 10 W). gPhone installations therefore require sites with AC power (or a very large array of solar panels and batteries), large footprints, good access, and a hardened vault. Finally, the gPhone is not fitted with indicators of tilt and beam position (Fig. 2d)—a condition that probably arose from the need to minimize the number of vents in the chassis of the instrument and better insulate the sensor against ambient temperature and pressure changes. Nevertheless, it implies that communication between the meter and the computer must be active during setup operations, including unclamping and leveling the meter, as well as centering the proof mass in the feedback range. Once again, this is not ideal in hostile field environments where the operator must deploy tools that are as easy to use as possible.

While companies producing other geophysical instrumentation (e.g., broadband seismometers) tend to reduce sensor size and power consumption to facilitate use in adverse field conditions (e.g., <http://www.nanometrics.ca/seismology/products/trillium-compact>), LRS/Micro-g seem to favor continuous gravity observation under laboratory conditions, rather than the field of volcano monitoring. This explains why most studies of continuous gravity at active volcanoes have been accomplished using either old L&R meters (e.g., Carbone et al., 2012; 2015; Poland and Carbone, 2016) or the only competitor to LRS/Micro-g spring gravimeters, namely, the Burris gravity meter, produced by ZLS Corporation (e.g., Carbone and Poland, 2012; Gottsmann et al., 2011).

#### 2.1.1.2. Superconducting gravimeters

Superconducting gravimeters (SGs) are based on the same principle as spring-based instruments, but instead of a mechanical spring, the magnetic levitation of a superconducting Niobium sphere in a field of superconducting persistent coils is exploited. By utilizing the perfect stability of supercurrents, a completely reliable, non-mechanical spring is created (Goodkind, 1999). The SG was first introduced by Prothero and Goodkind (1968) as an elegant realization of the principles of superconductivity. The basic sensor configuration has remained unchanged since that time (Fig. 4); nevertheless, improvements in many aspects of the original design have transformed the SG from a prototype experiment into a reliable research tool (Hinderer et al., 2007), now produced and commercialized by GWR Instruments.

In an SG instrument, both the coils and the sphere become superconducting at very low temperatures ( $< 9.2$  K). The SG sensor is therefore operated inside a dewar filled with liquid helium. Displacements of the sphere due to gravity changes or inertial accelerations are measured by a capacitance bridge formed by three aluminum plates. The feedback force needed to hold the sphere in the null position is derived from the signal of the capacitance bridge, which represents the gravity signal. Thanks to the design of the magnetic levitation, large displacements of the sphere correspond to small gravity changes, enabling higher sensitivity. Persistent superconducting currents and operation at cryogenic temperatures eliminate the sources of noise and drift commonly found in mechanical-spring gravity meters, allowing higher sensitivity and long-term stability. In early SG models, helium in the dewar had to be replenished every 3 weeks or so, and each of these refills, besides being expensive and time-consuming, caused disturbances to the data stream. GWR therefore developed a refrigerated dewar system for their instrument, where a cryogenic refrigerator (coldhead and compressor) is utilized to intercept and reduce the flow of heat via radiation and conduction from the outside of the dewar to its belly, thereby reducing the rate of boil-off and lengthening the ‘hold time’ of the liquid helium.

Following earlier reports on the development of a transportable SG to be used in the field of hydrology (Wilson et al., 2007), GWR released a more portable version of early observatory SGs, the iGrav (Fig. 4), which was first available for widespread use in 2012 and is the most well-suited SG to monitor and study active volcanoes. Indeed, it is much smaller and lighter than an Observatory SG, needs less power, and, thanks to an efficient refrigeration system, can operate indefinitely without the need for refilling with liquid helium. The iGrav features sub- $\mu\text{Gal}$  precision ( $0.05 \mu\text{Gal}$  over 1-minute averaging), negligible drift ( $< 0.5 \mu\text{Gal}/\text{month}$ ), and very low instrumental noise ( $0.3 \mu\text{Gal}/\sqrt{\text{Hz}}$ ). Despite its reduced size and weight with respect to a GWR OSG (Observatory Superconducting Gravimeter), however, the iGrav is still not ideal for installation in the vicinity of active volcanic structures. Indeed, the refrigeration system consumes more than 1 kW of electricity, and thus AC power is required at the installation site. Furthermore, some kind of hut or vault is needed to house the instrumentation, which includes the dewar and base plate, the cryogenic refrigerator (and helium tank), and the control box with its portable computer. The choice to install (or not) an SG at an active volcano requires careful study to assess whether the installation site is suitably well located with respect to the locus of volcanic activity to ensure that signals will be detected.

At Mt. Etna, the installation of a mini-array of three iGrav instruments was begun in September 2014. To our knowledge, these are the first SGs ever installed on an active volcano. iGrav#16, installed at a site 6.5 km away from the active craters of Etna, has recorded small (a few  $\mu\text{Gal}$ ) gravity changes

likely related to volcanic processes over periods ranging from a few hours to several days. Such changes would not be observable by spring gravimeters due to their intrinsic limitations regarding precision and long-term stability.

#### 2.1.1.3. MEMS devices

One factor that has limited the full development of volcano gravimetry is the relatively high cost of instrumentation. A spring-based relative gravimeter costs about 100,000 US Dollars (ten times more than a broadband seismometer, for example), while an SG is nearly three times that amount. Such high costs have often discouraged institutions in charge of monitoring and researching active volcanoes from initiating microgravity observation—especially continuous measurements that, ideally, would require the installation of an array of instruments (Williams-Jones et al., 2008). The future development of volcano gravimetry, therefore, requires new instrumentation that goes significantly beyond the current state of the art. The latter, for spring-based meters and SGs, is based on designs that date back 80 and 50 years, respectively.

Middlemiss et al. (2016) showed the potential of microelectromechanical system (MEMS) devices to measure changes in the gravity field. MEMS are microscopic mechanical devices that are mass-producible, light-weight and inexpensive. They are made from semiconductor materials and have been used in both accelerometers (e.g., in smartphones) and seismometers. The MEMS device developed by Middlemiss et al. (2016) is based on a smart geometrical (“anti-spring”) design and, through the use of servo control loops able to keep the temperature of the system within 1 mK, it has sufficient stability to detect low-frequency gravimetric signals, such as Earth tides (around 10  $\mu\text{Hz}$ ). Indeed, over an interval of 5 days, the authors found that the signal observed and the theoretical Earth tide had a correlation coefficient of 0.86, implying a device sensitivity of 40  $\mu\text{Gal}/\sqrt{\text{Hz}}$ . The instrumental drift was found to be less than 150  $\mu\text{Gal}/\text{day}$ . MEMS gravimeters are not yet suited to detect changes of a few tens of  $\mu\text{Gal}$  in adverse environmental conditions, and the strategy to stabilize the temperature to a suitable level seems to be the main limitation (a change in temperature of 1 mK gives an uncertainty in the gravity reading of about 25  $\mu\text{Gal}$ ). Nevertheless, these devices represent a promising new opportunity to advance volcano gravimetry in the near future. If reliable, small-sized MEMS gravimeters can be produced at low cost, there is the possibility of improving the signal-to-noise ratio by stacking the signal from many sensors in a cluster configuration.

#### 2.1.2. Absolute gravimeters

### 2.1.2.1. Free-fall absolute gravimeters

Due to the difficulty in measuring time with sufficient accuracy, the free fall method of absolute gravity could not be implemented until the wide availability of crystal and atomic clocks. Starting in 1960, a number of free fall interferometric measurements were accomplished at different laboratories. The first transportable free-fall absolute gravimeter (FFAG), the so-called IMGC, was developed starting in 1968 at the Istituto di Metrologia “G. Colonnetti” (now Istituto Nazionale di Ricerca Metrologica, Torino; Cerutti, et al., 1974). Today, the most widely used FFAG in gravimetry and geophysics is the FG5 (Niebauer et al., 1995; Fig. 5), developed at the Joint Institute for Laboratory Astrophysics (JILA) and sold commercially by Micro-g/LaCoste. The FG5 operates by monitoring the descent of a corner-cube reflector, contained in a co-falling servo-controlled chamber at vacuum pressure. During a drop, the corner cube is in absolute free fall and not in mechanical contact with the chamber. The free-fall trajectory of the corner cube is monitored very accurately using a laser interferometer and referenced to the so-called Superspring, which provides seismic-isolation for the reference optic and improves the performance of the instrument. Drops can be reproduced every two seconds. The accuracy is 2  $\mu\text{Gal}$ , while the system noise is 15  $\mu\text{Gal}/\sqrt{\text{Hz}}$  at a quiet site (i.e., not a seismically active volcano). The FG5 is, in general, not well-suited for portable use on active volcanoes, since it is large and heavy (the system weights about 300 kg and requires a floor space of 3  $\text{m}^2$ ), has a limited operating temperature range (10 to 30  $^{\circ}\text{C}$ ) and requires facilities to house the instrumentation. Nevertheless, it has been used on active volcanoes (Fig. 5; e.g., Kazama and Okubo, 2009; Greco et al., 2012; Kazama et al., 2015). Micro-g/LaCoste also produces the A-10 (Fig. 6), an absolute gravimeter optimized for fast data acquisition in harsh field conditions. While the A-10 is less accurate and less precise than the FG5 (accuracy = 10  $\mu\text{Gal}$ ; precision = 10  $\mu\text{Gal}$  after 10 minutes at a quiet site), it is lighter (total weight = 100 kg), more compact, less power-hungry (average power consumption is 200W), and can operate under a broad temperature range (-18 $^{\circ}\text{C}$  to +38 $^{\circ}\text{C}$ ). An A-10 has been used, jointly with CG-5 meters, to perform hybrid gravity measurements (see Section 6) at La Soufrière de Guadeloupe volcano (Fig. 6; Deroussi, pers. Comm.).

### 2.1.2.2. Absolute gravimeters based on atom interferometry

Atom absolute gravimeters use cold atoms as the test mass, whose free-fall acceleration is measured by means of a laser interferometer. Contrary to classical free-fall gravimeters that employ macroscopic test masses, atom gravimeters do not suffer from mechanical wear and thus offer the possibility of performing continuous and high-rate absolute measurements over long time periods. Since the

beginning of the 1990s, the principle of atom interferometry has been employed for a variety of applications, including precise determination of the gravitational constant ( $G$ ; e.g., Rosi et al., 2014), testing predictions from the theory of general relativity, and high-precision measurement of the absolute value of local gravitational acceleration ( $g$ ; Peters et al., 2001). During its early stages, this technology remained confined to laboratory environments due to the bulkiness and fragility of the setup. Over the last two decades, however, research groups based in France, China and the USA have worked on the development of portable cold atom gravimeters intended (at least in part) for geophysical applications (Dickerson et al., 2013; Gillot et al., 2014; Zhou et al., 2015). The LNE-SYRTE cold atom gravimeter, in development since 2009 by a research group based at the Observatoire de Paris (Le Gouët et al., 2008), supplied the know-how for the first commercially available gravimeter exploiting laser-cooled atoms—the Absolute Quantum Gravimeter (AQG), produced by Muquans. The AQG features an accuracy of a few  $\mu\text{Gal}$  and a sensitivity of  $50 \mu\text{Gal}/\sqrt{\text{Hz}}$ . The manufacturer claims that the AQG is stable over the long-term (within about  $1 \mu\text{Gal}$ ) and can attain a station-to-station repeatability of  $2 \mu\text{Gal}$ . The AQG is the only instrument that allows the execution of high-rate ( $2 \text{ Hz}$ ) absolute measurements on a continuous basis for several years. Furthermore, the measuring system can be set up in a relatively short time (ready to measure within 1h from arrival at the observation point), thereby allowing for the execution of campaign measurements involving several stations within a reasonable amount of time. Using an AQG, an instrument that records continuously at a given reference site could be occasionally moved between other points to take time-lapse measurements and then returned to the reference station, where the absolute continuous time series could be restarted without the need to apply any compensating corrections. A measurement campaign involving the use of the AQG, however, must take into account several constraints, including the size of the instrumentation, the required power (300W), and, most importantly, the currently limited operating temperature range.

## 2.2. Strategies for reducing measurement uncertainty during campaign observations.

Changes in gravity with time can be assessed by repeated measurements or continuous observations. In the case of repeated measurements, the time between successive surveys should match the period of the expected gravity changes, which, on active volcanoes, is a function of the evolution rate of the driving magmatic processes. Nevertheless, in most cases, the interval at which the surveys are performed is constrained by logistic factors (e.g., accessibility of the survey area that depends on the eruptive

activity and/or weather conditions, availability of personnel and funding), rather than scientific considerations. Precision gravity networks are established for monitoring changes over relatively long periods (months to years), and measurements can be carried out using both relative and absolute gravimeters. Very high precision is required to detect the relatively small gravity changes caused by volcanic activity, implying that sources of error must be understood and minimized. Repeated measurements on active volcanoes are mostly accomplished through spring-based relative instruments, which are small and light and thus easily transportable from one station to the other. Spring gravimeters also do not require much time to set up and record a measurement (a few to a few tens of minutes), allowing a survey of tens of stations to be completed in a matter of a few days.

Rymer (1989) analyzed sources of errors that can affect gravity measurements acquired by spring gravimeters. The most important are instrumental effects, namely drift and tares. While instrumental drift is a gradual change of the zero position due to fading spring tension over time, tares are sudden and irreversible jumps in meter reading due to mechanical or thermal shocks. In the framework of a gravity survey, drift coefficients and tare sizes are determined by reoccupying the same point at different times during the same day, or by repeated connection of adjacent stations. Watermann (1957) proposed and tested various measurement schedules aimed at monitoring instrumental drift. When a strict survey procedure is adopted, errors in the gravity differences between adjacent stations can be restricted to  $<10 \mu\text{Gal}$  (Rymer, 1989) or better (Budetta and Carbone, 1997). To make gravity data acquired in the framework of different measurement campaigns comparable with one another, and thereby recognize changes over time, each campaign must be related to a reference outside the active area, where it is assumed that the gravity field is stable. Naturally, this contributes to the error budget of a time-lapse survey, since small variations at the reference station(s) due to man-made, hydrological, and other effects will be propagated through the entire network. The use of portable absolute gravimeters would overcome these limitations; however, not all institutions can afford these instruments (on the order of 500,000 US Dollars) and, due to their characteristics, they are difficult to use in challenging environmental conditions. Absolute gravity measurements are required in areas where there is no guarantee of temporally constant gravity at the reference site (e.g., small volcanic islands where there are no points far enough away from the active structures; Furuya et al., 2003).

### **3. Models**

The instrumentation described in the previous section is essential for detecting and characterizing gravity changes at active volcanoes. On its own, however, the technology only provides an indication of an anomaly. Relating temporal variations in gravity to causative source mechanisms requires the use of models.

Inverse methods (Tarantola, 1987) are commonly used to investigate spatio-temporal gravity variations, as they provide a means of estimating, from the observed gravity changes, potential causative underground mass/density redistributions. The source parameters (position, size, shape, mass change, etc.) that best fit the measured gravity changes are constrained using a combination of forward models and optimization algorithms (Tiampo et al. 2000; Jousset et al. 2003, Bonvalot et al., 2008; Carbone et al., 2008a; Greco et al., 2016). The choice of the most appropriate forward model, however, is not straightforward—volcanoes are complex systems in which multiphase mass transfer occurs through a medium that can be porous, viscoelastic and fractured. Simplifying assumptions are therefore essential. Several closed-form solutions have been derived to calculate the gravity effect of simple-shaped underground bodies that have a constant density contrast with respect to the embedding medium. In active volcanic areas, underground mass redistributions are often associated with pressure changes that cause ground deformation. Therefore, whenever possible, gravity changes must be analyzed jointly with the corresponding ground deformation (see section 4).

A number of analytical formulations are widely used to interpret gravity changes and ground deformation from active volcanoes. Perhaps the most common is the “Mogi” model (Mogi, 1958), which envisages a magma chamber with spherical symmetry undergoing pressure increase/decrease as magma is injected or withdrawn. The Mogi model involves 6 parameters (Fig. 7a), and gravity and elevation change are related linearly through the solution (Hagiwara, 1977). In spite of its popularity, the application of the Mogi model requires some caution. Indeed, the simplification that holds true for a spherical point source, i.e., that the only deformation effect on gravity is the free-air effect, is not generally true for nonspherically symmetric sources (Walsh and Rice, 1979; Segall, 2010) and may lead to bias in the interpretation of the results if applied to, e.g., even slightly elliptical magma chambers (Battaglia et al., 2003). The “fissure eruption” model, proposed by Okubo and Watanabe (1989), approximates the opening of cracks in a narrow fracture zone due to the action of tensile tectonic stress. These cracks may channel the flow of magma to the surface, thus triggering an eruption. The model involves 9 parameters (Fig. 7b) and does not predict a linear relation between gravity and elevation changes (Jousset et al., 2003). By combining the analytical expressions derived by Okubo (1992) and Okada (1985, 1992), it is possible to calculate the gravity changes and corresponding ground deformation due to a dike-like intrusion (activation of a rectangular tensile dislocation). This

model is described by 10 parameters (Fig. 7c) and involves a nonlinear relationship between gravity and ground deformation (Carbone et al., 2008a). Further analytical models have been derived to calculate gravity change and ground deformation induced by mass/pressure sources featuring other simple shapes. For example, the sets of equations proposed by Clark et al. (1986) and Yang et al. (1988) allow calculation of the effect of a pipe-like (prolate spheroid) source that can be used to approximate a volcanic conduit, and the equations derived by Fialko et al. (2001) can be used to evaluate the effect of a horizontal penny-shaped body (sill-like intrusions).

Closed-form analytical formulations are computationally tractable and relatively easy to implement; hence, they are often used as forward models for the inversion of gravity and deformation data from active volcanoes—especially in the framework of real-time monitoring, where computation time is a critical issue. Analytical models, however, involve several simplifications and assumptions, for instance, that the crust surrounding the source is a homogenous, isotropic, elastic, semi-infinite medium with a flat upper surface (elastic half-space), and that the source has a simple geometry and features a uniform density contrast with respect to the embedding medium. These assumptions make analytical models easy to utilize but can result in misleading volcanological interpretations (Fernández and Rundle, 1994; Trasatti and Bonafede, 2008). To take into account the mechanical discontinuities and heterogeneities of the medium, topography, complex source geometries, and non-uniform density distributions throughout the source, numerical modelling schemes are necessary.

Numerical modeling of both gravity change and surface deformation is not as widespread a practice as analytical modeling, but several efforts are worthy of highlight. Charco et al. (2007) used a 3-D indirect boundary element method and showed that accounting for topography alters both the pattern and magnitude of surface deformation and gravity changes induced by a magmatic intrusion. Trasatti and Bonafede (2008) and Currenti (2014) performed numerical computations based on the finite element method and showed that, during pressurization of an ellipsoidal magma chamber, the deformation of the medium may make a significant contribution to the gravity changes observable at the surface through displacement of layer interfaces (density boundaries) and medium compressibility. Furthermore, the introduction of medium complexities such as layering and plastic rheologies may change the inferences arising from gravity data in terms of mass gain/loss (Trasatti and Bonafede, 2008).

Numerical solutions can also be utilized to explore the effect of sources with complex geometry. Camacho et al. (2011) proposed a non-linear inversion scheme for gravity and deformation data that determines a general geometrical configuration of the source, assuming homogenous elastic conditions and taking the topography into account. This method is based on the 3D aggregation of density and

pressure point sources through an automated growth process, and it finds a free 3D geometry of the anomalous body (or bodies) that matches the observed data as best as possible. While this method is appropriate for the inversion of spatially dense (e.g., InSAR) data (Camacho et al., 2011), its application to often-sparse (both spatially and temporally) 4D gravity data from volcanoes may not be appropriate. Indeed, when applied to gravity data from Montserrat, the inversion scheme by Camacho et al. (2011) did not furnish results statistically more significant than those obtained through the use of finite source models (Hautmann et al., 2014).

Another application of numerical solutions is to forward-model the gravity effect of mass sources whose complex geometry is known from independent information. For example, Carbone et al. (2013) developed a numerical model (Fig. 8) of the summit eruptive vent at Kīlauea that was based on measurements of vent dimensions and could be used to calculate the gravity effect of changes in lava level within the vent. Gravity changes estimated using this model were applied to adjust the results of time-variable gravity surveys to better detect changes associated with shallow magma storage (Bagnardi et al., 2014) and to investigate the density of the lava within the eruptive vent from a continuous gravity time series (Carbone et al., 2013; Poland and Carbone, 2016).

Numerical models also offer an opportunity to approximate variable source density on models of gravity observations. Carbone and Poland (2012) used a numerical model where the density in the different parts of the source volume could be set independently of each other. This approximation was utilized to forward-model the gravity effect of convection-driven density inversions within the shallow magma reservoir at Kīlauea.

While numerical schemes are well-suited to perform direct calculations aimed at retrieving the relative importance that some complexities of the system may have on the budget of the observed gravity changes, they are, in general, not well suited to data inversions. Furthermore, complex models that make use of numerical techniques require numerous model parameters. Because gravity and ground deformation data from active volcanoes are often limited and noisy, there is a risk of over-interpreting the results of numerical models based on such datasets (Battaglia et al., 2008). The choice of model—analytical versus numerical—to derive information related to source parameters must therefore be carefully evaluated, taking into account the constraints relevant to the case under study.

#### **4. Gravity surveys to detect long-term volcanic processes**

Not long after their development, portable gravimeters were put to use for measuring temporal changes in gravity associated with volcanic activity. Gravity surveys to measure such changes typically occupy a network of points around a given volcano and are repeated every few months to years; thus, gravity campaigns are best suited to investigate long-term variations in volcanic processes. An early application of campaign gravity to track volcanic unrest was the case of Izu-Oshima, Japan, where Iida et al. (1952) measured a pre-eruptive, several-hundred-microgal gravity increase and subsequent co-eruptive decrease in 1950–1951, possibly related to magma accumulation before, and withdrawal during, eruptive activity. In the decades that followed, studies of time-variable gravity at active volcanoes were rare, perhaps reflecting the inherent uncertainty in the mechanism of gravity change when coincident deformation measurements are not available. Uplift causes a decrease in gravity, and subsidence an increase, due to the changing distance between the surface and the center of the Earth, following a theoretical “free-air” gradient (FAG) of  $-0.3086$  mGal/m. Gravity changes detected at Izalco, El Salvador (Rose and Stoiber, 1969), Mt. Baker, Washington, USA (Malone, 1979), and Pacaya, Guatemala (Eggers et al., 1976; Eggers and Chavez, 1979), could not be interpreted unambiguously because of the lack of elevation control. One of the first studies that measured coincident and consistent changes in gravity and elevation over time was at Kīlauea Volcano, Hawai‘i, during and following the 1975 M7.7 earthquake (Dzurisin et al., 1980; Jachens and Eaton, 1980). During the 1980s, surveys of temporally variable gravity and deformation at volcanoes began to flourish (e.g., Eggers, 1983; Rymer and Brown, 1984, 1987, 1989; Berrino et al., 1984; Johnson, 1987; Okubo and Watanabe, 1989). It soon became plain that gravity held great potential for elucidating the source mechanisms of volcanic unrest, perhaps best exemplified at Long Valley caldera, where gravity change associated with inflation during the 1980s and 1990s was consistent with fluid densities indicative of magma accumulation and not a hydrothermal source (Battaglia et al., 1999, 2003). The advent of interferometric synthetic aperture radar (InSAR) in the 1990s further facilitated volcano gravimetry, as ground-based field campaigns were no longer critical for providing surface displacement information (e.g., de Zeeuw-van Dalssen, 2006; Bagnardi et al., 2014).

In many cases, long-term gravity changes are triggered by magmatic processes that also induce measurable ground deformation. The joint collection of deformation and gravity data is needed not only to assess the contribution of the FAG to the gravity signal, but also to constrain the driving mechanism of any measured geodetic changes. Indeed, the nature of the processes at work can result in different relations between gravity change and ground deformation. When gravity and deformation data are analyzed jointly, it is possible to recognize, for example, densification of stored magma (Bagnardi et al., 2014), filling of void space by magma (Carbone et al., 2008a), compression of bubbles (Bonvalot

et al., 2008), the efficiency of long-term eruptions (Kauahikaua and Miklius, 2003), and magma drainage (de Zeeuw-van Dalssen et al., 2004). Furthermore, at volcanoes that host active hydrothermal systems, gravity studies can distinguish processes involving magma from those driven by water and volatiles—critical information for characterizing hazards (e.g., Battaglia et al., 2006).

#### 4.1 $\Delta g/\Delta h$ as an indicator of subsurface processes

Rymer and Williams-Jones (2002) proposed that, in situations where volcanic activity is regulated by the dynamics of a pressurized magma chamber whose behavior can be approximated by a point-source model (Mogi, 1958; see section 3), the ratio between gravity and elevation changes ( $\Delta g/\Delta h$ ) provides a framework from which to assess the likelihood and type of volcanic processes at work—including potential future eruptive activity (Gottsmann et al., 2003; Fig. 9). Indeed, from the study of the  $\Delta g/\Delta h$  gradients one can tell whether, for example, inflation (volume increase) is associated with a change in the density of magma within the source reservoir (Williams-Jones and Rymer, 2002). A density decrease might indicate vigorous interaction between the intruding and resident magmas, causing convection and cooling of the new magma, leading to volatile oversaturation and vesiculation. The resulting increase in gas pressure within the reservoir might eventually lead to explosive eruptive activity. The model of Rymer and Williams-Jones (2002) can therefore be applied to hazards assessment, provided that the inherent assumptions and limitations are taken into account. Even in the cases where the Mogi (1958) approximation is not the best model for the actual source of mass and pressure change, the  $\Delta g/\Delta h$  framework can provide a useful starting point when the surface patterns of gravity and elevation changes are in agreement. Evaluating whether or not the change in gravity is commensurate with the observed deformation provides a window into the processes occurring at depth. If the increases (or decreases) in gravity that share a common source as surface deformation are due to a “pure” mechanism of magma accumulation or withdrawal, the  $\Delta g/\Delta h$  will approximate the Bouguer-corrected free-air gradient (BCFAG)—in other words, there is no significant change in subsurface density (Gottsmann et al., 2003). Johnsen et al. (1980) and Torge (1981) both observed a good spatial correlation between gravity and elevation changes at Krafla Volcano (Iceland), obtaining a mean value for  $\Delta g/\Delta h$  that was consistent with processes involving only magma injected to or withdrawn from a shallow magma chamber. Similarly, at Usu Volcano (Japan), Jousset et al. (2003) found that, between July 1998 and November 2000, the displacements and gravity variations—among the largest ever recorded on an active volcano—were caused by a common source process, namely the intrusion of new magma along a subvertical fracture zone prior to the March 2000 eruption. The density of the intruding

material was found to be slightly higher than, but still consistent with, the density of past eruptive products from Mt. Usu, implying again that a mechanism involving only the intrusion of magma in the fracture zone could explain the observations.

In other cases, even though the patterns of gravity changes and deformation are well correlated in space (i.e., deformation and gravity change share the same source), the density of the fluid involved in the source process, deduced from the analysis of the  $\Delta g/\Delta h$  gradient, is not in keeping with a “pure” mechanism of magma intrusion/withdrawal. In other words, explaining the observed gravity change associated with uplift or subsidence would require a density that is unrealistically higher or lower than that expected for subsurface magma ( $\Delta g/\Delta h$  values above or below, respectively, the BCFAG curve in Fig. 9). It is especially these cases where campaign gravity measurements demonstrate their importance as a volcano surveillance and research tool.

#### 4.1.1 $\Delta g/\Delta h$ within the FAG-BCFAG range

In some cases, the mass gain or loss is less than expected if the mechanism of gravity change and deformation were driven by magma accumulation or withdrawal alone—in other words,  $\Delta g/\Delta h$  values plot between the FAG and the BCFAG curves in Fig. 9. For example, a strong gravity decrease during the inflation that preceded the 2005 eruption of Sierra Negra volcano (Galápagos) pointed to an overall density decrease in the magma reservoir. Vigouroux et al. (2008) proposed that pre-eruptive magma vesiculation might explain the observations, consistent with the model of Gottsmann et al. (2003).

Mass deficits can also indicate that a fluid other than magma is driving observed deformation and gravity change. Battaglia et al. (2006) analyzed gravity and deformation data collected at Campi Flegrei and found that the 1980–84 inflation episode could be explained by a common mass/pressure source (a penny-shaped crack) with a mass change indicating a low bulk density (about  $1000 \text{ kg}\cdot\text{m}^{-3}$ ). Rather than assuming a process involving mixing of resident and new magma and leading to an overall density decrease of the reservoir by vesiculation, Battaglia et al. (2006) proposed that the unrest was driven by migration of aqueous fluid to the caldera hydrothermal system. By combining gravity change and deformation data from Yellowstone caldera, Tizzani et al. (2015) found that both magma and hydrothermal fluids play a role in driving caldera unrest.

#### 4.1.2 $\Delta g/\Delta h$ outside the FAG-BCFAG range: too much mass gained/lost!

Several examples now exist of scenarios where the amount of mass required to explain a gravity signal is far more than expected from the deformation signal—in other words, a large gravity change is associated with minor deformation, yet both have the same source.

At Kīlauea Volcano, Bagnardi et al. (2014) measured a gravity changes and inflation centered on a common source located ~1.5 km beneath the caldera, just east of Halema‘uma‘u Crater, between March 2011 and November 2012 (Fig. 10). The volume change modeled from deformation data, however, could explain only a small percentage of the mass change deduced from gravity, assuming a reasonable magma density. The driving process must therefore cause an increase in bulk mass without inducing commensurate surface inflation. The authors proposed several possible mechanisms: 1) substitution of gas-rich magma in the shallow reservoir by denser, degassed magma that had convected up to the summit eruptive vent and lost its volatile load, 2) filling of subsurface void space by magma, 3) compression of bubbles in the resident magma, and 4) formation of olivine cumulates.

Excess mass during inflation has also been measured at Mt. Etna and Piton de la Fournaise (La Réunion). Carbone et al. (2008a) found that gravity changes spanning the March 1981 flank eruption of Mt. Etna were spatially well correlated with the coincident elevation changes. The source model (tensile cracks) that satisfactorily explained ground deformation, however, implied a volume change that underestimated the observed gravity changes (assuming a reasonable magma density). To account for the bulk mass increase without the expected ground deformation, Carbone et al. (2008a) proposed that, besides opening the tensile crack, the ascending magma also filled a network of preexisting interconnected microfractures surrounding the crack itself. Bonvalot et al. (2008) showed that gravity changes associated with the March 1998 major eruption at Piton de la Fournaise could not be fully explained by the intrusive dike model that had been proposed on the grounds of InSAR and tilt data. A satisfactory fit to the observed gravity data was obtained through an additional mass increase below the dike (Fig. 11), suggesting that compression of bubbles in a magma reservoir may have produced the additional mass change without commensurate surface deformation.

The “excess mass” principle applies not only to periods of inflation, but also deflation. For example, Dzurisin et al. (1980) found that more mass was lost from beneath Kīlauea’s summit as a result of the 1975 M7.7 earthquake than could be accounted for by deformation, indicating the formation of void space in the subsurface. Similarly, at Askja (de Zeeuw-van Dalssen et al., 2004) and Krafla (de Zeeuw-van Dalssen et al., 2006), Iceland, mass loss in excess of that predicted from deformation modeling was measured. In both cases, indeed, only a small percent of the volume of magma drained from the chamber is accommodated by magma chamber reduction measurable as deflation at the surface, while

most of it is accommodated by decompression of stored reservoir magma (de Zeeuw-van Dalfts et al., 2004; 2006). These results indicate that volcano deflation could result from complex coupled processes that can be fully understood only if gravity studies are performed.

## 4.2 Gravity change without deformation

### 4.2.1 Magmatic processes

The study of gravity change is especially important when bulk mass redistribution occurs in the absence of pressure changes that induce measureable ground deformation. In such cases, gravity may be the only tool able to recognize the occurrence of magmatic unrest.

Kīlauea provides an excellent example of gravity change without associated deformation. Between November 1975 (after the M7.7 earthquake) and 2008, Johnson et al. (2010) documented a significant mass increase beneath the east margin of Halema‘ūma‘ū Crater, within the volcano’s summit caldera. Deformation during the same time period, however, was focused further south and associated with the known main magma storage area beneath the summit. The long-term mass increase over that time period therefore occurred in the absence of a significant collocated bulk pressure change (Fig. 12). Johnson et al. (2010) thus concluded that the observed gravity changes were induced by magma accumulation in void space—most likely a network of interconnected cracks that may have formed when magma withdrew from the summit in response to the November 1975 earthquake.

Rymer et al. (1998) observed a gravity decrease at Masaya volcano, Nicaragua, at stations near the active crater area but with negligible elevation change (stations outside the area of the summit craters showed no gravity change). The strong 1993–94 gravity decrease was modeled as due to a mass change at shallow depth (~500 m) beneath Santiago pit crater, possibly due to convection-driven replacement of relatively dense, degassed magma by gas-rich material (Rymer et al., 1998). On the grounds of these data, the authors concluded that the activity phase they observed was not caused by the intrusion fresh magma, but rather by overturn of resident magma in the chamber.

At Mt. Etna, the stress field on the volcanic edifice leads to the formation of systems of fractures that can channel the flow of magma, allowing for “passive” magma ascent and transport. Movement of magma can therefore occur without the development of stress changes able to induce seismicity and/or ground deformation (Aloisi et al., 2011). Rymer et al. (1993) measured strong gravity changes in the year preceding the major 1991–93 eruption (Fig. 13), for which the associated surface deformation was small and had an unexpected pattern (based on elastic modeling of likely deformation sources). They

proposed that magma transport was not forceful, but instead occurred in a pre-existing fracture system before reaching the surface (Fig. 13). Budetta et al. (1999) also observed, between 1994 and 1996 (a period that included the 1995–96 summit explosive activity), gravity changes without significant variation in ground elevation, reflective of mass redistributions within Etna's edifice. In particular, it was proposed that a batch of magma intruded passively to a zone about 2 km beneath the summit craters (September 1994 – October 1995; gravity increase) and fed the 1995–96 eruptive activity (October 1995 – July 1996; gravity decrease).

While Etna, Maaya, and Kīlauea highlight some of the best examples of gravity change in the absence of significant deformation, the phenomenon is certainly not restricted to those volcanoes. Similar observations have been made at: Mayon volcano (Philippines), between 1992 and 1994, suggesting mass redistribution at depths of 2–5 km below sea level (see Vajda et al., 2012 and references therein); Askja volcano (Iceland), between 2007 and 2009, possibly reflecting accumulation of magma in void space beneath the caldera (Rymer et al. 2010; de Zeeuw-van Dalssen et al., 2012); and at Miyakejima volcano (Japan) before and after caldera collapse in 2000 (Furuya et al., 2003). In the Miyakejima case, a gravity decrease, recorded soon before the collapse and for almost 2 months after its start (July to late August), was interpreted as due to bulk void formation followed by water invasion of the hot conduit and explosive eruptions. The subsequent (September to November) gravity increase, which exceeded the effect of collapsed topography, was thought to reflect magma ascent and refilling of the evacuated conduit.

#### 4.2.2 Hydrothermal processes

Gravity changes not associated with ground deformation can also develop due to shallow processes involving hydrothermal systems. Jousset et al. (2000a) found that the patterns of gravity change and ground deformation during the 1996–98 crisis at Komagatake volcano (Japan) did not coincide. Indeed, elastic models with a common mass and pressure source failed to satisfactorily explain both datasets. A more complex model involving deeper (5 km below sea level) magma intrusion and shallower (above sea level) boiling and evaporation of water, however, can fully explain the set of observations (Fig. 14). Gottsmann et al. (2006) analyzed gravity changes accompanying the reactivation of the central volcanic complex of Tenerife (Spain) in early 2004. These changes, mostly due to subsurface mass/density variations (accompanying elevation changes were negligible), were shown to reflect migration of hydrothermal fluid along a permeable N-S striking zone.

Gravity measurements at Poás volcano (Costa Rica) also revealed changes over years-long periods without obvious ground deformation (Rymer et al., 2009) that were thought to be triggered by shallow mass changes of either magmatic or hydrothermal origin (i.e., a direct effect of shallow magma intrusion, or an indirect effect through enhanced circulation of hydrothermal fluids). In particular, the strong gravity changes observed between 1985 and 1990 heralded a catastrophic drop in the level of the acidic crater lake (Fig. 15) and was associated with intense outgassing and sulphur eruptions that had serious consequences for local health and environmental conditions (Rymer et al., 2009). The possibility that mass changes occurred at depth years before the manifestation of enhanced eruptive activity highlights the potential of time-lapse gravity as an early indicator of volcanic hazards.

#### 4.3 Gravity changes in the absence of magmatic fluids

Besides imaging processes involving magmatic fluids (i.e., the accumulation and transport of magma, hydrothermal fluids, or volatiles, as well as changes like vesiculation or crystallization in static bodies), gravity changes can develop in response to the emplacement of volcanic deposits or as a result of changes in the rate of microfracturing along bulk weakness zones within or below a volcanic edifice due to modifications in the local or regional stress field.

At Merapi volcano (Indonesia), Jousset et al. (2000b) observed, between 1993 and 1995, strong gravity changes (nearly 400  $\mu\text{Gal}$ ) with negligible deformation (less than 5 cm). The gravitational attraction exerted by the recently extruded lava dome was found to explain most of the observed signal. Residual gravity changes, after reduction for the effect of dome growth, were interpreted as due to a mass increase at shallow depth, possibly driven by the arrival of new magma replacing the extruded dome.

Hautmann et al. (2010) performed gravity measurements at Soufrière Hills Volcano (Montserrat, West Indies) and observed, between 2006 and 2008, gravity changes not accompanied by significant ground deformation (Fig. 16). They were centered at stations relatively far from the volcanic center and thought to be caused by changes in the fracturing rate along a fault zone beneath the central part of the island, in turn controlled by the stress field imposed by the shallow plumbing system of the volcano.

Using gravity and seismic data acquired at Etna between 1994 and 2001, Carbone et al. (2009a; 2014) found a marked coupling between mass changes and release of seismic energy, over both time and space (Fig. 17). Spatial patterns of gravity change and deformation, in contrast, showed little resemblance to one another, indicating that the sources of mass and pressure variations were different. These findings lent support to the view that the observed gravity anomalies reflected changes in the rate of micro-fracturing along the NNW–SSE fracture/weakness zone that crosses the SE slope of Etna

(Greco et al., 2010). Enhanced fracturing would cause a local density (gravity) decrease and an increase in the release of seismic energy, thus explaining the observed anticorrelation. A phase of gravity decrease coupled with an increase in strain release culminated in the 2001 flank eruption, probably because deeper magma used the inferred zone of increasing microfracturing as a path to the surface (Carbone et al. 2003a; 2009a).

## **5. Short-term changes observed through continuous measurements**

### **5.1. Characteristics of continuous gravity time series**

The ability of time-lapse gravity to explore volcano-related subsurface mass redistribution is limited by the repeat time of the campaign measurements, which is generally on the order of 1 year and almost never shorter than 1 month (Torge, 1989). Gravity surveys are therefore not suitable for investigating the most dynamic volcanic processes, which typically develop over time-scales of minutes to days (e.g. Gilbert and Lane, 2008). Instead, continuous measurements of gravity are needed (Williams-Jones et al., 2008).

Although hardly a mature field, continuous gravity measurements have been carried out at a number of volcanoes around the world (Fig. 1), with recording rates in the range of 0.01-1 Hz (Jousset et al., 2000b; Gottsmann et al., 2007; Carbone et al., 2008b; Carbone and Poland, 2012; Poland and Carbone, 2016). Such measurements can be accomplished through either spring or superconducting relative gravimeters (SGs; section 2). SGs provide higher data quality than spring gravimeters, but are larger and require AC power, making field deployments in close proximity to volcanic activity problematic (section 2.1.1.2). SGs are also considerably more expensive than spring gravimeters, and the cost of installing an array of SGs is beyond the financial means of most institutions that are tasked with volcano monitoring and research. Continuous gravity measurements at active volcanoes are therefore usually accomplished using spring gravimeters, which are portable and can be operated on DC power at remote field locations. Unfortunately, these instruments usually do not provide reliable measurements when used in continuous mode for weeks or more because they can be influenced by environmental factors and are subject to instrumental drift.

Andò and Carbone (2004; 2006) studied the effect of environmental parameters on the signal from continuously recording gravimeters and showed that changes in ambient temperature can induce strong apparent gravity changes (admittance up to 200  $\mu\text{Gal}/^\circ\text{C}$  over seasonal variations; El Wahabi et al.,

1997). The transfer functions between ambient temperature and the signal from continuously recording spring gravimeters were shown to be highly nonlinear, instrument-specific, and frequency-dependent (Carbone et al., 2003b; Andò and Carbone, 2004). Furthermore, using records from the same instrument operating in different monitoring sites, Andò and Carbone (2006) demonstrated that the installation setup itself has an important influence on the transfer function. Thus, nonlinear techniques must be applied to remove the effect of ambient temperature, involving the use of frequency-dependent and instrument/setup-specific algorithms. These corrections also require the acquisition of a time series that is much longer than the period of the influencing temperature fluctuations in order to optimize the compensation schemes (the so-called “training process”).

Past studies (e.g., Andò and Carbone, 2001; Carbone et al., 2003a) demonstrated that, if a suitable setup is adopted for the field stations, the effect of ambient temperature on continuously recording spring gravimeters is negligible over short periods (seconds to days; Fig. 18). Given the difficulties in implementing compensation strategies, most past studies at active volcanoes have focused on the analysis of continuous gravity observations over time-scales of minutes (e.g. Carbone et al., 2009; Carbone and Poland, 2012), hours (Branca et al., 2003; Carbone et al., 2006; 2008b; 2012; 2015; Gottsmann et al., 2007), and days (Sainz-Maza Aparicio et al., 2014; Poland and Carbone, 2016). This approach also mitigates against instrument drift, which is difficult to assess for spring gravimeters (e.g., Berrino et al., 2006), but can be a minor factor relative to volcanic signals over timescales of hours to days (e.g., Poland and Carbone, 2016).

Although continuously recording spring gravimeters can detect volcano-related signals over relatively restricted timescales, a variety of processes can still be studied, assuming that the sensor is located in close proximity to the source of the process being investigated. Indeed, magmatic fluids are composed of a multi-phase mixture of liquid, gas and crystals, all with different densities. Changes in the relative proportion of these components within a magmatic system can induce modifications of the density profile in the upper plumbing system which, in turn, can lead to local gravity changes that are measurable at the surface. For example, using a finite element scheme that is able to describe the time-dependent dynamics of magma and determine the contribution to the gravity field of each mass parcel during the simulated dynamics, Vassalli et al. (2009) showed that magma mixing processes in a shallow chamber can induce measurable gravity changes over minutes. These changes are mainly related to density inversions during convective overturns (Longo et al., 2006), when magmas with different compositions (and densities) come into contact.

Simplified calculations based on the model of Wilson and Head (1981) show that, under equilibrium conditions, even small pressure changes in a shallow magma chamber may lead to important bulk density changes via diffusion of water (Fig. 19) and compression/decompression of vesicles. Indeed, water is far more soluble in magma than CO<sub>2</sub> and dominates gaseous processes at shallow depths (e.g., Gerlach, 1986). Pressure changes as small as a few tenths of MPa occurring in a magma body at depths between 1000 and 2000 m (lithostatic pressure of 20–50 MPa) can induce, through diffusion of water, density changes on the order of 10 kg·m<sup>-3</sup> (Fig. 19). If the magma chamber has a size of 1000m, such density change will induce gravity changes of up to 20-30 μGal at the surface, which would be detectable using spring gravimeters. Magma chambers featuring the above geometrical characteristics, in terms of depth and size, are known to exist beneath the summit caldera of Kīlauea Volcano (e.g., Poland et al., 2009), below the summit craters of Mt. Etna (e.g., Aiuppa et al., 2010), and beneath the summit cone of Piton de la Fournaise e.g., Peltier et al., 2009).

For relatively large and shallow magma reservoirs, the gravity signal from a mass redistribution can be significant even if the bulk density of the reservoir remains constant (Carbone and Poland, 2012). As an example, if bubbles dispersed in such a magma body accumulate as a layer of foam at the top of the chamber (closest to the observation point at the surface), a gravity decrease may be observed depending on the amount of gas involved and the position of the gas accumulation zone (Carbone et al., 2006). Similarly, the mass redistribution that takes place when crystals loosely held together below the roof of a cooling magma body are dislodged and form a sinking plume (Hill et al., 2002) may result in the development of short-term gravity changes (Carbone et al., 2009b).

A gravimeter installed in the vicinity of an active crater could also react to the rise of a large gas slug towards the surface, as gas replaces magma in a position progressively closer to the surface observation point. For example, Ripepe and Harris (2008) and Allard (2010) estimated that the amount of gas emitted by the 5 April 2003 paroxysmal explosion of Stromboli, Italy, ranged between 3\*10<sup>6</sup> and 2\*10<sup>7</sup> kg. Allard (2010) proposed that such explosions are triggered by the collapse and rapid ascent of bubble foams that accumulate at a depth as great as 10 km beneath the crater vents. Figure 20 shows simulated gravity changes at a point about 300m from the active vents that would be caused by the rising of a gas slug. The volume of the slug at each depth is calculated starting from the above amount of emitted gas and assuming (i) CO<sub>2</sub> as the main component and (ii) expansion of ideal gas. Results show that measurable gravity changes are induced when the slug reaches a depth shallower than about 1000m below the crater vents (Fig. 20).

Short-term gravity change can also result from rapid magma transport through shallow parts of the plumbing system. For example, the migration of magma from a central conduit to a lateral rift zone can

induce gravity changes over timescales of the order of hours and with positive or negative sign, depending on the relative position of observation point and conduit-rift system.

## 5.2. Case studies of processes detected with continuous gravity

Bonvalot et al. (1998) first suggested the possibility that permanent networks of continuously recording gravity meters could be used to monitor and study active volcanoes. Two years later, Jousset et al. (2000b) presented the first results from continuous gravity observations at an active volcano. They analyzed a years-long sequence from a gravimeter installed 4 km from the summit of Merapi volcano (Indonesia) and found a correlation between gravity changes and volcanic activity, probably driven by pressure oscillations in the magma chamber. Jousset et al. (2000b) also observed a coupling involving volcanic activity and admittance between the amplitude of observed gravity and theoretical Earth tides. This finding suggests that rheological changes in the volcanic edifice may occur due to volcanic processes at depth.

Despite their obvious potential (Carbone and Greco, 2007), continuous gravity measurements at active volcanoes are relatively rare. Most past results come from Mount Etna, where stations for continuously recording gravity were installed in the late 1990s (Carbone et al., 2003b) and have worked intermittently since then, and from Kīlauea, where continuous gravity stations were installed in 2010 (Carbone and Poland, 2012). Nevertheless, some exceptional results have been obtained, demonstrating that continuous gravity stations have the ability to detect processes associated with volatile accumulation and release, magma migration, and hydrothermal activity, and resulting in insights that might not be possible using other types of volcanological data.

### 5.2.1. Volatile accumulation and release

On several occasions, gravity anomalies observed at Etna over time-scales of minutes to hours negatively correlated with the amplitude of volcanic tremor (Carbone et al., 2006; 2008b). This anti-correlation is thought to reflect the activation of a common gravity and seismic source involving the dynamics of magma and exsolved gas in the uppermost part of Etna's plumbing system. Carbone et al. (2006) performed a joint analysis of the data collected by an array of broadband seismometers and a continuously recording gravity station during the 2002–2003 eruption of Etna. On three occasions they observed a strong anti-correlation, involving increases of the tremor amplitude (up to a factor of 4) and

gravity decreases (up to 30  $\mu\text{Gal}$ ), over periods of a few hours (Fig. 21). The tremor/gravity anomalies occurred during periods of temporary eruptive changes from intense lava fountaining to mild strombolian activity. Carbone et al. (2006) proposed that the accumulation of gas in the conduit feeding the eruptive vent could have acted as a joint source for gravity and tremor changes. Indeed, the growth of a bubbly foam layer may act as an efficient radiator of seismic energy and induce a gravity decrease through substitution of magma by gas.

A marked anti-correlation between tremor amplitude and gravity was also observed at Mt. Etna during the December 2005 - January 2006 non-eruptive period (Carbone et al., 2008b). Anti-correlation was found with the gravity signal from one of the two summit stations over 2- to 3-hour periods. Carbone et al. (2008b) noted that, during the period of marked anti-correlation, the tremor sources coincided with the volume that was inferred to contain the gravity source, in a region located about 2 km beneath the surface. Based on this finding, they suggested that the anti-correlation indicated the activation of a joint source process, possibly related to the arrival of fresh magma in the upper part of the feeding system and involving a progressive enrichment in volatiles. The inferred gas segregation during December 2005 to January 2006 did not lead to eruptive activity and could be detected only on the grounds of the joint seismological-gravity studies, demonstrating that, when used in conjunction, they have the ability to detect “hidden” states of unrest at active volcanoes.

Carbone et al. (2015) also proposed that accumulation of gas bubbles at shallow levels below the summit craters of Etna may trigger measurable gravity changes. On various occasions during the summer of 2011, they observed marked gravity decreases over time scales of a few hours, each occurring during the transition from Strombolian to lava fountaining activity (Fig. 22). Relying on the relation between the amount of gas trapped in a foam and amount of gas emitted during each eruption, Carbone et al. (2015) developed a conceptual model of the mechanism controlling the onset of lava fountaining activity at Etna during the summer of 2011. They proposed the establishment of a feedback loop involving an increase in the gas volume fraction in the conduit and a decrease in the magma-static pressure in the trapping zone, resulting in further growth of a foam layer that eventually collapses, triggering the onset of fountaining activity (Fig. 22).

Short-term changes in the relative proportions of magma and gas within the shallow part of the plumbing system were also shown to induce measurable gravity changes at Stromboli volcano (Italy). In the framework of a multiparameter experiment, Carbone et al. (2012) analyzed a continuous time series of gravity data collected at a point about 350 m from the summit craters. The authors did not observe, as in the case of Etna, an anti-correlation between gravity and the amplitude of the volcanic tremor. Rather, they found correlated changes evidenced through wavelet transforms of gravity and

RMS-tremor. These changes occurred over periods of around 50 and 25 min for gravity and tremor, respectively, and were inferred to be controlled by the rate of fresh magma supply to the shallowest part of Stromboli's feeding system, i.e., no more than 800 m below the crater vents (Carbone et al., 2012). The changes in the amplitude of the coupled gravity and volcanic tremor oscillations correlate with changes in the rate of explosions from the summit craters, suggesting that, even if the slug-genesis process behind the explosions occurs at levels deeper than 800 m (Allard, 2010), it is also controlled by the rate of gas-rich magma supply from depth (Fig. 23).

### 5.2.2. Magma dynamics

At Etna, large gravity changes over time-scales of a few hours can also occur due to movement of magma at shallow levels. Branca et al. (2003) analyzed a continuous gravity sequence from a station on the upper northern slope of the volcano and detected a marked decrease (about 400  $\mu\text{Gal}$  in less than one hour) 4 hours before the onset of the 2002 NE Rift eruption. A positive gravity change occurred soon afterward, matching the magnitude of the preceding decrease (Fig. 24). Branca et al. (2003) interpreted the gravity anomaly as due to (i) the opening of a shallow fracture system only 1 km from the gravity station (gravity decrease) and (ii) the filling of this fracture system by magma transported from the central conduit (gravity increase) and that used the fractures as a path to reach lower portions of the NE Rift, where an eruption occurred (Fig. 24).

Rapid and shallow magma transfer also resulted in major gravity change at Kīlauea. Carbone et al. (2013) observed a gravity decrease of about 150  $\mu\text{Gal}$  over less than 10 hours at a station only 150 m from the center of the volcano's summit eruptive vent, where a lava lake experienced a coincident drop in level of over 120 m (Fig. 25). The withdrawal of lava was associated with an intrusion and 4.5-day-long fissure eruption on Kīlauea's East Rift Zone during March 5–9, 2011 (Orr et al., 2015). The gravity decrease observed by Carbone et al. (2013) reflects the loss of mass due to the drop of the lava level in the summit vent and, when combined with measurements of the volume loss from the vent, was used to calculate the density of the part of the lava lake that drained—about  $1,000 \text{ kg}\cdot\text{m}^{-3}$  (Fig. 25). This finding further demonstrates the utility of continuous gravity data as a tool for monitoring rapid mass transfer in the shallow part of the feeding system and also examining physical properties of the magmatic system that cannot be known using other methods.

Expanding the study of continuous gravity data from near Kīlauea's summit lava lake, Poland and Carbone (2016) used a sequence spanning 2011-2015 to show a strong correlation between gravity and lava level change over intervals of hours to days (Fig. 26)—a rare example of the use of a years-long continuous gravity time series at an active volcano. By relating lava level and gravity through a numerical model of the eruptive vent (Carbone et al., 2013; Fig. 8), Poland and Carbone (2016) determined that the density of the upper few tens to hundreds of meters of the lava lake was consistently low—between 1,000 to 1,500 kg\*m<sup>-3</sup>, suggesting that the lake is gas-rich (40–60% bubbles). An overall increase in the modeled density over the time spanned by the sequence may be due to either a real decrease in the proportion of bubbles or a progressive increase in the size and storage capacity of the vent. A few transient “density spikes” were also modeled during the sequence (marked with arrows in Figure 26e) and probably indicate mass changes below the summit eruptive vent (perhaps 500–1,000 m below the surface), possibly due to magma accumulation in, and withdrawal from, void space. The joint analysis of continuous gravity and lava level in near real-time would provide a powerful new monitoring tool, as variations in the ratio of gravity to lava level change could indicate transient phases of disequilibrium in the shallow magmatic system that might not otherwise be detectable.

The continuous gravity stations that were installed in the summit zone of Kīlauea in 2010 also provided the first geophysical evidence for magma convection over time scales of minutes. Carbone and Poland (2012) observed gravity oscillations with a period of ~150s at two continuous gravity stations. The amplitude ratio of changes at these stations suggests a source location that is coincident with the known shallow magma reservoir about ~1–2 km beneath Kīlauea's summit (Poland et al., 2009). The oscillations may therefore indicate variations in subsurface mass caused by convection-related density inversions in the magma reservoir.

### 5.2.3. Hydrothermal systems

Continuous gravity measurements also have the ability to expose short-term oscillatory signals associated with the dynamics of hydrothermal systems. Indeed, simulations of multi-phase and multi-component hydrothermal fluid circulation in active volcanic areas indicate that changes in average fluid density can generate detectable gravity changes (Todesco and Berrino, 2005). In the framework of a multiparameter experiment performed at Nisyros caldera (Greece), Gottsmann et al. (2007) observed non-steady, short-term oscillatory signals with average amplitudes of 20 μGal and a dominant period of

40-60 min. These variations were probably associated with instabilities in the degassing process. Microseismic disturbances in continuous gravity records were also recorded at the Upper Geyser Basin of Yellowstone caldera (Wyoming, USA) where the signals were inferred to be caused by processes associated with the hydrothermal system (Tikku et al., 2006).

The application of continuous gravity to hydrothermal systems is a fertile ground for additional research. A better understanding of the nature of hydrothermal sources of gravity change is critical for strengthening interpretations of magmatic gravity signals, since groundwater changes are a source of noise in such analyses (e.g., Kazama and Okubo, 2009; Kazama et al., 2015), and hydrothermal processes play a key role during phases of volcanic unrest (e.g., Tizzani et al., 2015). Gravity also has the potential to elucidate the nature of geyser plumbing systems, although the problem is clearly not a straightforward one. Vandemeulebrouck et al. (2014) deployed continuous gravimeters as part of a multi-parameter 4-day experiment at Lone Star geyser in Yellowstone caldera, but the gravity data were not helpful in constraining geyser dynamics.

The information supplied by continuous gravity on the dynamics of hydrothermal system would be especially relevant at volcanoes like La Soufrière de Guadeloupe (Lesser Antilles arc), where hydrothermal activity weakens the rocks that form the volcanic edifice, increasing the risk of flank collapse (Voight, 2000), and where hydrothermal processes may play a key role during phases of unrest (Reid, 2004).

### 5.3 Guidelines for continuous gravity deployments at active volcanoes

The examples above demonstrate the clear advantage of continuous gravity measurements for elucidating volcanic processes. Over timescales of minutes to days, the method can detect changes in magmatic and hydrothermal systems and, when coupled with other geophysical datasets, can be used to develop models of subsurface processes that might not otherwise be known.

Continuous gravity deployments should be done judiciously, however, since they are not universally applicable to all volcanoes. For instance, at volcanoes that are dormant, like Vesuvius, continuous gravity yields results that are mostly related to Earth tides and local or distant earthquakes (Berrino et al., 2006). These data are important for assessing instrument response, but have limited applicability to understanding volcanic processes. Similarly, deployments that are too far from the centers of volcanic activity may not record changes related to magmatic processes. At Soufrière Hills Volcano, Montserrat, continuous gravity data collected 7 km from the eruptive vent were most useful for constructing tidal and ocean loading models, and gravity anomalies that were observed during occasional Vulcanian

explosions were thought to represent second-order effects, triggered by either the explosion-induced air pressure wave or by the response of a local aquifer to pressure variations in the magmatic system (Gottsmann et al., 2011; Hautmann et al., 2014). In our experience, continuous gravity measurements are best utilized at volcanoes that are restless or actively erupting and where it is possible to install stations within hundreds of meters, or at most a few km, of the center of activity. Etna, Kīlauea and Stromboli are therefore ideally suited for continuous gravity studies, but they are hardly unique. Other volcanoes where continuous gravity is likely to yield new insights into volcano activity include Piton de la Fournaise, Masaya (Nicaragua), Villarica (Chile), and Erebus (Antarctica), to name a few. In addition, there are ample opportunities to explore hydrothermal systems at active volcanoes, especially in Yellowstone, Iceland and La Soufrière de Guadeloupe. We anticipate many future developments in the field of continuous gravimetry from existing and new deployments at active volcanoes and hydrothermal systems, as well as continued development of instruments and methods that will make the technique more accessible and impactful.

## **6. Hybrid gravity measurement**

The preceding sections have treated absolute and relative gravity, and campaign and continuous measurements, independently. However, these techniques are most powerful when combined, to improve the quality of the data and expand their spatio-temporal resolution. For example, absolute gravity measurements can be used in tandem with relative measurements in time-lapse surveys to reduce uncertainty and make the campaign data more robust. Similarly, quasi-annual gravity campaigns can be combined with continuous measurements to obtain better temporal resolution of gravity change. Given the high cost of gravimeters, it is unlikely that arrays of continuous instruments (i.e., more than 2-3) can be installed on any single volcano (Williams-Jones et al., 2008), so combining continuous and campaign measurements is critical for achieving good spatial and temporal resolution of gravity change (Battaglia et al., 2008).

### **6.1 Relative and absolute campaign measurements**

Absolute gravity measurements can be used in conjunction with relative measurements to improve the quality of 4D gravity data from volcanoes, while keeping the measurement cost (in terms of person-time) relatively low. Usually, the absolute measurements are taken at only one of the stations in the

gravity network (the reference station), while the gravity value at the other benchmarks is measured through relative instruments using a measurement strategy that includes connections to the reference site. This type of hybrid measurement has been performed at small volcanic islands, like Vulcano (Italy; Berrino, 2000) and Miyakejima (Japan; Furuya et al., 2003). Indeed, at small islands the reference station could not be sufficiently far from the zone of volcanic activity to be free of volcanic effects and deep-seated mass/density changes may affect gravity measurements at both the reference station and other stations in the network, introducing significant ambiguity in interpretation. By performing absolute measurements at the reference station, this shortcoming can be overcome. This strategy has also been applied at continental volcanoes, like Vesuvius, where absolute measurements at the reference station have been performed since 1986 (Berrino et al., 2013) using the IMGIC absolute gravimeter (D'Agostino et al. 2008; see section 2.1.2.1).

A step forward in this hybrid measurement technique was made by Greco et al. (2012), who, rather than carrying out absolute measurements only at the reference station, established several absolute stations within a single survey area. Between 2007 and 2009, Greco et al. (2012) integrated the campaign gravity network at Mt. Etna (71 benchmarks covering an area of about 400 km<sup>2</sup>; Budetta et al., 1999) with 12 absolute stations (Fig. 27a), measured using an FG5 instrument (Niebauer et al., 1995; see section 2.1.2.1) and an IMGIC gravimeter. These stations are evenly distributed around the volcano, with the main constraint on their locations being the presence of a facility to house the instrumentation. The gravity values at the other benchmarks of the gravity network were determined using relative instruments by repeated connections with the absolute stations. In most cases, 5 or 6 relative gravity stations were connected to each absolute station (Fig. 27b). The distance between each absolute reference and nearby relative stations was mostly within 2km, allowing each hybrid loop to be completed in a few hours and thus minimizing the influence of instrumental drift of the relative instrument. On a large volcano like Etna, where the reference stations are at distances of 15 to 20km from the active zone (Budetta et al., 1999), hybrid measurements avoid the risk of propagating errors due to (i) nonlinear transport drift of the spring gravimeters (Torge, 1989) and (ii) differential gravity changes of non-volcanic origin possibly occurring at the reference stations. Greco et al. (2012) estimated the uncertainty on the temporal gravity changes obtained through the hybrid method to be less than 10  $\mu$ Gal.

Even though absolute measurements are time-consuming (each requires about 6 hours to complete), there is an overall time savings because of the short distances between the relative measurement sites and absolute stations, allowing for quick repeated connections between adjacent stations (see section

2.2). The total time required by the hybrid gravity campaign is comparable to, or slightly less than, that of a conventional (relative) survey, while the data quality is significantly improved.

Similar hybrid gravity measurements involving the use of an A-10 absolute gravimeter (section 2.1.2.1.) have been performed at Aso Volcano (Japan; Sofyan et al., 2014), La Soufrière de Guadeloupe (Deroussi, pers. comm.), and Campi Flegrei (Berrino, pers. comm.).

## 6.2 Discrete and continuous gravity measurements

The time between successive relative (or hybrid) gravity surveys usually ranges from a few months to a few years, even though gravity changes might be caused by processes occurring over shorter time scales. Aliasing effects may therefore arise, leading to a misinterpretation of the causative subsurface dynamics. To avoid this shortcoming, time-lapse observations should be integrated with continuous measurements at one or more selected sites (Battaglia et al., 2008), in much the same way that campaign and continuous GPS measurement are collected to maximize both temporal and spatial resolution of deformation. If spring gravimeters are used as continuously running devices, however, it is difficult to perform joint analyses of time-lapse and continuous measurements. Indeed, due to intrinsic limitations of the sensors (see section 5.1), data from continuously recording spring gravimeters are often not reliable over time scales longer than a few days, implying the existence of a significant gap between the repetition rate of time-lapse measurements and the maximum period of changes observable through continuously measuring spring gravimeters. Because of this limitation, some studies that have had access to both discrete and continuous gravity measurements from the same volcano (e.g., Bonvalot et al., 2008; Jousset et al., 2000b; Hautmann et al., 2014) could not perform a joint analysis of the two datasets and only gained insight into different processes, mostly occurring over different time-scales.

To our knowledge, the only case-study involving the integration of discrete and continuous gravity observations to obtain a more accurate spatio-temporal picture of an ongoing process was that of Carbone et al. (2003b). These authors performed 4 time-lapse gravity surveys in the summit zone of Etna, at a higher than usual (monthly) rate. The time-lapse data were compared with the data from a continuous gravimeter located 2 km from the active summit craters. After removing the effects of Earth tide, ground tilt, and meteorological perturbations (the latter through a non-linear model; Andò and Carbone, 2001), the continuous gravity time series was in good agreement (within uncertainty) with the time-lapse gravity changes measured at sites very close to the continuous station (Fig. 28). It was thus possible to obtain insight into the magnitude of the subsurface mass changes and the characteristics of

the source (discrete measurements) and into the temporal evolution of the source processes (continuous measurements).

Instead of spring instruments, SGs (section 2.1.1.2.) could be utilized to perform continuous gravity measurements. SGs feature very high precision and long-term stability (negligible instrumental drift), thus allowing straightforward comparison with the results of time-lapse measurements. However, as discussed in section 2.1.1.2., the use of SGs at active volcanoes is limited by logistic constraints.

## 7. Conclusive remarks

The numerous examples cited in this article, and the wide range of volcanoes over which gravity change measurements have been made (Fig. 1), should leave little doubt of the value of microgravity data for elucidating volcanic processes. Microgravity is the only measurement technique that, for example, can detect magma accumulation in void space (e.g., Rymer et al., 1993; Johnson et al., 2010), identify vesiculation and gas segregation at shallow depths (e.g., Carbone et al., 2008b; 2015), distinguish mechanisms for volcanic uplift (Bagnardi et al., 2014) and subsidence (e.g., Dzurisin et al., 1980; de Zeeuw-van Dalssen, 2004, 2006), and recognize formation of bulk fractures due to changes in local stress patterns (e.g., Carbone et al., 2014). Many of these capabilities have direct relevance to hazards assessment. One of the most obvious demonstrations of application to hazards involves caldera systems, which are often characterized by fluid-driven seismicity and deformation, but for which the nature of the driving fluids is uncertain. At Long Valley, microgravity combined with deformation has indicated that accumulation of magma, and not volatiles or hydrothermal fluids, is driving unrest (Battaglia et al., 1999; 2003)—information relevant to hazards assessments and that can help to define future monitoring strategies.

This being the case, why hasn't microgravity been applied on a more widespread basis at volcanoes around the world? The most likely reasons are: (1) instrument cost, (2) a lack of equipment especially designed for field deployment under difficult conditions, and (3) the challenge of retrieving useful information from gravity changes in noisy volcanic environments.

Instrument cost for spring, superconducting, and absolute gravimeters will probably continue to be high, which may prevent many institutions from acquiring such technology (at least in terms of purchasing new equipment); however, a variety of creative solutions can address this problem. L&R D- and G-model gravimeters are relatively common at universities around the world. For comparatively little cost (with respect to the price of a new gravimeter), these can be refurbished and even upgraded

with electrostatic nulling (especially valuable for continuous deployments). New ZLS Burriss and Scintrex CG-5 gravimeters are less than US\$100,000, which, although a major investment, can be supported by grants and institutional funding. Superconducting and absolute gravimeters, with their price tags of many hundreds of thousands of US\$, are beyond the reach of most individual investigators but can be purchased for shared use by research consortiums. Perhaps the most exciting development, though, is the potential for very-low-cost MEMS gravimeters (Middlemiss et al., 2016), possibly within a few years. Such an advance has the potential to revolutionize the field of volcano gravimetry, given that large arrays of gravimeters could be deployed at low cost, thereby facilitating array and imaging studies that might resemble methods for extracting small signals from seismic data. While cost is clearly a barrier to widespread application of microgravity on volcanoes, it is not insurmountable.

The lack of field-appropriate equipment is also a poor excuse for not applying microgravity to active volcanic environments. Certainly many styles of gravimeter are not suited for field deployments. Many spring-based instruments, however, are easily transportable, and some can be modified for continuous use. For example, a L&R G-meter with electrostatic nulling ran continuously at the summit of Kīlauea Volcano for several years, despite the fact that it was located only a few tens of meters from the rim of an active lava lake in the presence of corrosive gases and in a harsh tropical environment (Poland and Carbone, 2016). Similarly, L&R D-meters were installed in sites within 1km from the summit craters of Etna (about 3000m a.s.l.) where they ran continuously for long intervals (Carbone et al., 2008b; 2009b; 2015). Such deployments require an element of creativity to design datalogging and possibly telemetry systems, but similar efforts are required for other types of instruments, including tiltmeters, extensometers, strainmeters, and other geodetic equipment (none of which are specifically designed for use at active volcanoes). Superconducting and absolute gravimeters are much less mobile and require robust field enclosures and a steady power supply, but their greater accuracy means they can be utilized farther from the active areas on a given volcano, perhaps in a volcano observatory or instrumentation vault. Certainly most gravimeters are not intended for use on volcanoes, but volcanology is nothing if not an inventive field—few off-the-shelf solutions are available for any volcanological application, and it is common for volcanologists and volcano observatories to adapt instruments and infrastructure for their specific applications.

Finally, there is the issue of data interpretation. This is not a problem of technology, nor of cost. In fact, it is not a problem at all, but rather a misconception carried over from times when geodetic data were scarce, and the interpretation of gravity was ambiguous (e.g., Eggers et al., 1976). A common refrain from those who are not familiar with recent developments in microgravity studies is that the data reflect too many processes that cannot be separated—for instance, changes in groundwater level or

environmental factors (like rain or pressure). While challenging, these issues are far from roadblocks. For example, to compensate for a lack of water wells that provide information on groundwater levels at Campi Flegrei and Etna, Battaglia et al. (2006) employed hydrologic models to compute groundwater recharge from rainfall records, while Carbone et al. (2003c) assumed that the changes in water level were seasonal and consistent and adjusted the gravity signal using a band-stop filter. Naturally, if groundwater data are available, the hydrological contributions to the gravity signal can be investigated in detail, through suitable models (Hemmings et al., 2016) and detailed analyses (Kazama and Okubo, 2009; Kazama et al., 2015). Careful installations of continuous instruments and surveying techniques during campaign measurements can drastically reduce sources of noise due to instrument setup. Changes in ambient temperature also affect the gravity signal from continuously recording instruments, but long-term records of gravity and temperature can be used to define a transfer function for removing such signals (Andò and Carbone, 2004; 2006). There is even potential for use of continuous gravity as a near-real-time monitoring tool, since comparisons between gravity and other datasets, like tilt or lava level, can provide rapid recognition of transient magma accumulation that may not be reflected in other datasets (Poland and Carbone, 2016). The idea that a “volcanic” gravity signal can never be separated from environmental or instrumental noise, or that it will only be a research tool, is therefore simply not true, and it is a poor excuse for dismissing application of microgravity to active volcanoes.

The challenges described above are not trivial; however, they have all been overcome by creative efforts in a variety of volcanic and environmental settings. The ever-growing list of volcano gravity success stories detailed in the sections above, the value of the results for understanding hazard potential and the fundamentals of how volcanoes work, and the large number of volcanoes worldwide that have been studied using microgravity methods (Fig. 1) repudiate claims that gravity is of little value, or that data collection is not worth the effort.

Hope for the future of volcano gravimetry comes not only from the development of new technology, creative solutions to deployment challenges, and better models of the sources of gravity change, but also potentially from space-based observations. Knowledge of the global gravity field of the Earth has improved dramatically in recent years thanks to dedicated satellite missions (like the Gravity Recovery and Climate Experiment (GRACE), and Gravity field and steady-state Ocean Circulation Explorer (GOCE)). Certainly improved knowledge of the regional gravity field around volcanic edifices based on satellite measurements, especially in areas that are poorly covered by ground-based data, is a major aid in assessing the tectonic/geodynamic contexts that may control volcanism. Time-variable satellite gravity has proven value in detecting changes related to large earthquakes (e.g., Mikhailov et al., 2004, 2014), helping to constrain models of fault rupture and elucidating post-seismic processes. Recent and

planned satellite gravity missions, however, provide data at spatial resolutions  $>100$  km, which is not sufficiently sensitive to record changes at an individual volcanic edifice. We expect, however, that spatial resolution will gradually improve over time, and that, one day, detecting volcano-related gravity changes from space may be possible.

We are hopeful that the case studies detailed in this paper, as well as the descriptions of instrumentation, methods, and analysis tools, will excite more volcano scientists around the world about the potential of volcano microgravity observations, spurring further applications, development, and innovations. Volcano gravity appears to be on the cusp of a small-scale revolution, given the surge in noteworthy results starting especially in the early 2000s. We see no reason that campaign and continuous microgravity work should not soon become standard tools for volcano research and monitoring, yielding insights into volcanic processes that would not otherwise be known.

## Figure captions

Figure 1 - Volcanoes where time-lapse gravity studies have been completed. Map was compiled based on both published reports and personal communications. Volcanoes with asterisks denote sites where continuous gravity data have been collected for periods of at least a few weeks.

Figure 2 - (a) L&R D-model gravimeter installed at Mt. Etna for continuous measurements. The sensor is protected from ambient temperature changes through a polystyrene box. (b) The semi-underground concrete box hosting the instrumentation is within 1km from one of the active craters of Etna. (c) Schematic showing the principle of L&R spring gravimeters. (d) L&R gPhone (formerly, Portable Earth Tide Gravity Meter, on the left) side-by-side with an L&R D-model gravimeter (on the right).

Figure 3 - A pair of Scintrex CG-5 gravimeters used to perform campaign measurements at Krafla volcano. The GPS receiver mounted on the tripod is used for precise positioning of each measurement point.

Figure 4 - Since September 2014, iGrav SGs have been installed on Etna, where a mini-array of three iGrav SGs is now in operation. One of the three sensors is installed inside the hut at La Montagnola (top), ~3 km southeast of the summit craters (2600 m asl), where electricity is available. Bottom-left: iGrav #020, installed inside La Montagnola hut. Bottom-right: schematic of the GWR SG.

Figure 5 - Left and top-right: FG5#238 absolute gravimeter in operation in the summit zone of Etna (2990m a.s.l.; within 1km from the active summit craters). Bottom-right: schematic showing the main parts of the FG5 gravimeter.

Figure 6 - The A-10 absolute gravimeter. Left: a view of the sensor and a schematic showing its main parts. Right: an A-10 on operation at La Soufrière de Guadeloupe volcano. The plastic bin, visible to the right of the sensor, is used to protect it from wind during the measurement session.

Figure 7 - Forward models used to calculate the gravity effect and deformation induced by simple geometries. (a) The Mogi model (Mogi, 1958). (b) The dike-like intrusion (Okubo, 1992; Okada, 1985; 1992). (c) The “fissure eruption” model (Okubo and Watanabe; 1989).

Figure 8 - (a) Numerical model used by Carbone et al. (2013) and Bagnardi et al. (2014) to simulate the gravity effect induced by changes in the level of the lava lake within the summit eruptive vent at Kīlauea Volcano. The model geometry consists of 252 vertical square-based parallelepipeds with changeable height to simulate varying lava levels. (b) Schematic cross section (redrawn from Orr et al., 2013) through Halema‘uma‘u Crater showing the shape of the summit eruptive vent. (c) Photo showing the summit eruptive vent of Kīlauea; the ledge in the upper part of the vent can be distinguished in the image.

Figure 9 - Free-air (FAG) and Bouguer-corrected free-air (BCFAG) gradients. Points falling along the FAG line indicate gravity changes due solely to changes in elevation, while points falling along the BCFAG indicate gravity changes due to both elevation changes and mass-related effects (intrusion or withdrawal of magma to/from the reservoir).

Figure 10 - Gravity change and deformation at Kilauea Volcano, Hawaii. (left) Residual gravity change (error bars) and vertical deformation (derived from InSAR data; filled circles, TSX=TerraSAR-X; open circles, CSK=Cosmo-SkyMed) near the SE rim of Halema‘uma‘u Crater (adjacent to the summit eruptive vent). These sites show the maximum residual gravity changes during 2009-2012 due to both an increase in the lava level within the summit eruptive vent and due to a mass increase about 1.5 km beneath the caldera. Plot colors correspond to station colors on the map to the right. Error bars indicate 1 standard deviation of uncertainty for the residual gravity measurements. (right) Two-dimensional scatterplot of the latitude and longitude positions for the sources of inflation (red) and deflation (blue) in the summit area during 2009-2012 based on InSAR data. Black ellipse labeled "HMM" marks the area of the summit eruptive vent. Star is modeled location of gravity increase. Sources of gravity change, inflation, and deflation are similar, located at about 1.5 km depth beneath the SE margin of Halema‘uma‘u Crater. Figure adapted from Bagnardi et al. (2014).

Figure 11 - Results obtained by Bonvalot et al. (2008), who analyzed time-lapse gravity data spanning the March 1998 eruption at Piton de la Fournaise volcano. Top-left graphs: Simulated gravity effect of the best-fitting composite model: (a) contribution from the shallow dike-like intrusion (S1 source); (b) contribution from the deeper reservoir (S2 source); (c) cumulative contribution from sources S1 and S2. Bottom-left graphs: (d) gravity changes observed between November 1997 and March 1998; (e) computed gravity changes for the best model deduced from inversion of the data; (f) difference between observed and

calculated gravity data (RMS = 10  $\mu\text{Gal}$ ). Note that a different color scale is used to better present the data in the residual gravity map. Right: position of the best-fitting composite source involving a shallow dike-like intrusion (S1) and a deeper point source model (S2).

Figure 12 - Vertical deformation (solid lines and boxes) and residual gravity change (dashed lines and diamonds) at Kīlauea Volcano, Hawai‘i. A: Sites located in south caldera. B: Sites located near east margin of Halema‘uma‘u Crater. Plot colors correspond to station colors on maps. Error bars indicate one standard deviation of uncertainty and are smaller than symbols for vertical deformation results. Vertical deformation and residual gravity change scales are same in both plots to highlight differences in behavior of two areas. Vertical deformation is from all leveling surveys completed between 1975 and 2008, not just those completed during gravity surveys. Residual gravity change in the south caldera tracked deformation, suggesting coincident mass and volume changes. Near Halema‘uma‘u Crater, however, residual gravity increased throughout 1975-2008, suggesting an increase in mass in the absence of collocated bulk pressure change. Figure taken from Johnson et al. (2010).

Figure 13 - Top: gravity and elevation changes (contour intervals: 1 cm and 50  $\mu\text{Gal}$ , respectively) observed over the summit and upper eastern flank of Mt. Etna between 1990-1991. Middle: Cross-section along a profile through the summit and along the SSE fracture zone of Etna. Bottom: a 2.5D computed model involving (i) a 50 m diameter feeder pipe rising towards the summit, and (ii) a 4 m wide dyke extending along the fracture zone, which together can account for the gravity changes observed between June 1990 and June 1991 if the density of the intrusion is assumed to be  $2800 \text{ kg}\cdot\text{m}^{-3}$ . Figure taken from Rymer et al., 1993.

Figure 14 - Top: analysis of the gravity changes observed at Mt. Komagatake (Hokkaido, Japan) between November 1997 and May 1998 revealed that they were induced by two different source processes, namely, (i) a mass increase at depth of 4–5 km below the surface, and (ii) a shallower mass decrease within the upper 500-1000m below the surface. Bottom: Schematic model of volcanic activity at Komagatake. The deeper mass increase was interpreted as the effect of magma intrusion, while boiling and evaporation of water caused the shallower mass decrease (after Jousset et al., 2000a).

Figure 15 - (a) Gravity changes from stations in the southern crater of Poás volcano, corrected for earth tides, deformation and variations in lake level and water table. The coherent 1985-1990

gravity increases (400-600  $\mu\text{Gal}$ ) correspond to a fall in lake level (b) and related temperature increase (c). The sulphate concentration (d), which was constant between 1982 and 1987, rose rapidly in 1988–1989. Hence, the observed gravity changes heralded the catastrophic drop in the level of the acidic crater lake, which was associated with intense outgassing and sulphur eruptions.

Figure 16 - (a) Map of Montserrat island (West Indies) showing the position of the benchmarks for time-lapse gravity measurements (black dots). The solid line indicates the location of the Belham Valley fault, while the dashed line correspond to the Centre Hills fault (not fully known), as proposed by Hautmann et al. (2010). Gravity changes observed during June/July 2006 to Jan/Feb 2007 (7 months; b) and during Jan/Feb 2007 to Aug/Sept 2008 (19 months; c) could have been caused by changes in the fracturing rate along the fault zone beneath central Montserrat. Figure taken from Hautmann et al. (2010).

Figure 17 - Panels a–h: sketch maps showing gravity changes and earthquake epicenters at Mt. Etna for different time intervals. Hypocentral depth ranges are indicated by color. Gravity changes are contoured at 10  $\mu\text{Gal}$  intervals. Bottom left panel: map showing the position of the FM4 gravity station, the surface projection of the NNW–SSE fracture/weakness zone (yellow box) and the main eruptive fissures (orange lines; black lines indicate fissures that opened during the 2001 eruption). Bottom right graph: temporal changes in gravity observed at the FM4 station during the 1994–2006 period (gray squares). The red curve is the same sequence corrected for the water-table effect (see Carbone et al., 2009a) and low-pass filtered with a cut-off period of about 2.5 years. The solid blue curve is the seismic strain release after removal of a linear trend and multiplication by a negative coefficient ( $-5 \times 10^{-4}$ ). Figure taken from Carbone et al. (2014).

Figure 18 - Effect of ambient temperature on the signal from a continuously running spring gravimeter. (a) Raw gravity series recorded at Mt Etna (PDN station; 2820m a.s.l.) during October 1998 to March 2001. (b) Ambient temperature recorded at the same site, inside (black curve) and outside (red curve) the thermally insulating polystyrene box hosting the gravimeter (a LaCoste & Romberg D-meter). (c, d) Joint analyses in the frequency domain between gravity and ambient temperature. The coherence plot indicates that a significant correlation appears over the lowest frequency band (T greater than about 10 days), while, moving towards the higher frequencies, after a sharp drop, the coherence values remain within 0.2, indicating the absence of correlation. The admittance plot

indicates that, over the lowest frequency band, the maximum admittance value is close to  $200 \mu\text{Gal}/^\circ\text{C}$ , implying that apparent changes on the order of hundreds of  $\mu\text{Gal}$  can result from changes in ambient temperature. (e) If a suitable setup is adopted for the field stations, the signal from a continuously running spring gravimeter is free from effect driven by ambient temperature over short periods (seconds to days).

Figure 19 - Left : variation of % weight of exsolved  $\text{H}_2\text{O}$  in basalt, as a function of pressure (after Wilson and Head, 1981). The second x-axis scale is the corresponding depth, assuming lithostatic pressure. Right: density changes of a magma body induced, through diffusion of water, by pressure changes. Starting pressures of 20 and 50 MPa are assumed for the upper and lower curves, respectively, while an initial water content of 2% wt is assumed in both cases. The calculations are performed using the equations reported in Wilson and Head (1981).

Figure 20 - Gravity effect of a rising gas slug. The calculation is performed assuming (i) an amount of gas (mainly  $\text{CO}_2$ ) of  $2 \cdot 10^7$  kg (as estimated by Allard (2010) for the 5 April 2003 paroxysmal explosion of Stromboli), (ii) a gas volume at the different depths controlled by ideal gas expansion, and (iii) a distance between crater and observation point of 300m (following Carbone et al., 2012).

Figure 21 - Top: gravity sequence observed at Mt. Etna (PDN station; 2820m a.s.l.) after removal of (i) the best linear fit, (ii) the theoretical Earth Tide and (iii) longer wavelength components (cut off frequency of the high-pass filter equal to  $2.8 \cdot 10^{-6}$  Hz, corresponding to a period of 100 h). In the bottom part of the figure, signals during the intervals marked by I, II and III are shown. In particular, the upper panels show gravity, the middle graphs show velocity seismograms (vertical component from a station on the E flank of the volcano, at an elevation of about 1700m), and the lower panels show overall spectral amplitudes of the vertical velocity component. The overall spectral amplitude of each tremor sequence was calculated within the 0.02–10 Hz frequency range (0.5–50 s). A 4096-sample sliding window (about 10% overlap) was used for the FFT calculation (after Carbone et al., 2006).

Figure 22 - Using the data from a continuous gravity station very close to the summit craters of Etna, Carbone et al. (2015) observed, during the summer of 2011, marked gravity decreases, each occurring during the transition from Strombolian (B) to lava fountaining (C) activity. Two of the above gravity decreases are shown in the top graphs (marked by the yellow arrows), together with the height of the lava fountains (meters above the vent). Grey

curves indicate unfiltered data, while black (gravity) and red (fountain height) curves indicate low-pass filtered data. The cartoons in the lower part of the figure illustrate the conceptual model proposed by Carbone et al. (2015). (A) The first stages of accumulation of a foam layer in the shallow reservoir take place during phases of quiescent degassing from the summit craters. (B) At later stages of foam accumulation, gas leakage occurs from the foam, and bubbles flow towards the conduit. The flow regime gradually changes from bubbly to slug flow, leading to the onset of Strombolian activity. A feedback loop establishes involving an increase in the gas volume fraction in the conduit and a decrease in the magmastatic pressure in the trapping zone, which results in further growth of a foam, a local density decrease, and the observed gravity decrease. (C) Eventually, the foam collapses, and transition from slug to annular flow takes place in the conduit, marking the passage from Strombolian to lava fountaining activity. Increasingly higher seismic energy is radiated, and the signal from the gravimeter is severely degraded by inertial effects (lacking filtered data in the gravity graphs). Modified after Carbone et al. (2015).

Figure 23 - Left: Sketch map of Stromboli showing the position of gravity (continuous measurements) and seismic stations. Right: wavelet transforms of gravity (top; after removal of the instrumental drift and the theoretical Earth tide) and RMS tremor amplitude (middle; seismic station co-located with the gravity station), both for periods up to 128 min. Bottom right: time changes in the explosion rate, computed using the seismic signal from STRA, STR8, STR9 and VANC stations. Figure adapted from Carbone et al. (2012).

Figure 24 - Top: Reduced gravity, after removal of the best linear fit and the theoretical Earth Tide effect, observed at the Mt. Etna PDN station (2820m a.s.l.) during a 48-hour period encompassing the start of the 2002 NE-Rift eruption. The solid curve shows low-pass filtered data (cutoff frequency of 24 cycles/day). Bottom: (1) gravity decrease (about 400  $\mu$ Gal in less than one hour), which was interpreted as due to the opening, by external forces, of a shallow fracture system 1 km W of the gravity station. The subsequent gravity increase (2), which matched the magnitude of the preceding decrease within a few hours, was due to the filling of this fracture system by magma transported from the central conduit. The magma exploited the fractures as a path to reach lower portions of the NE Rift, where an eruption occurred. Figure adapted from Branca et al. (2003).

Figure 25 - Gravity change due to a sudden drop in lava level within the summit eruptive vent at Kilauea Volcano. Top images are from a thermal camera overlooking the eruptive vent

and showing the drop in lava level that occurred over 5-6 March, 2011. Middle plot shows lava level over time, with blue shaded area indicating uncertainty. Bottom plot gives residual gravity change (black line) over time after correction for the free-air effect due to subsidence and mass removal from the shallow magma reservoir. Red line is calculated residual gravity change given the lava level change and a numerical model of the vent based on measured vent dimensions. To fit the observed gravity, the density of that portion of the lava lake that drained (the upper ~120 m of the lake) must be  $950 \pm 300$  kg/m<sup>3</sup>. Figure adapted from Carbone et al. (2013).

Figure 26 - Time series of geophysical data from the summit area of Kilauea Volcano during 2011-2015. (a) Level of lava within the summit eruptive vent in meters above sea level as measured by a thermal camera on the rim of Halema'uma'u Crater. (b) Radial tilt measured at a site 2 km NW of the summit eruptive vent. Positive change indicates inflation and negative, deflation. (c) Gravity change (after correction for Earth tides, a second-order polynomial adjustment for instrument drift, and high-pass filtering to remove long-period variations due to change in ambient temperature), with yellow bar marking period when the instrument was off level and the data unreliable. (d) Wavelet coherence plot between lava level and gravity signals. Black bars at top of plot indicate periods of no gravity data. Significant, in-phase coherence (warm colors and arrows pointing right) occurs across time spans of days to a few weeks at most, indicating good correlation between lava level and gravity at those time scales. (e) Density of lava within the summit eruptive vent based on a sliding window analysis (15 day window, 5 day step) of the gravity and lava level data and assuming the vent model of Carbone et al. (2013). Red dashed line is 2-month smoothed density value. Correlation coefficient is given by the blue curve. Calculated densities are shown for correlation coefficients  $>0.75$  (closed squares) and  $>0.65$  (open and closed squares). An overall density increase, from about 1000 to 1500 kg/m<sup>3</sup>, is indicated, with some spikes (red arrows) that may be related to specific volcanic events. Insets in (a), (b) and (c) are from the gray shaded period and demonstrate the good correspondence between tilt, lava level, and gravity change at Kilauea's summit. Figure adapted from Poland and Carbone (2016).

Figure 27 - (a) Sketch map of Etna showing the benchmarks for time-lapse relative measurements (circles) and the sites where Greco et al. (2012) performed absolute gravity measurements (triangles). (b) Schematic of the hybrid gravity measurements. Crosses represent benchmarks where only relative measurements are performed, while circled crosses are

sites where both absolute and relative gravity measurements are carried out. Figure adapted from Greco et al. (2012).

Figure 28 - (a) Sketch map of Etna showing the benchmarks for time-lapse measurements along the summit profile (triangles) and PDN continuous gravity station (circle). Gravity changes observed through time-lapse measurements during (b) the June-July 1999 and (c) June-September 1999 periods. Analysis of the time-lapse data revealed that the gravity decrease since June 1999 was due to a mass decrease of up to about  $2 \times 10^{10}$  kg, which occurred at shallow depth along the southern side of the NE rift (see Carbone et al., 2003b for details). In (c), we report the calculated gravity effect (red dots) of the model source, whose projection onto the surface is shown in (a). (d) Time series of gravity data from PDN station (black curve) after removal of effects driven by instrumental drift, Earth tide, ground tilt, ambient temperature, and pressure (see Carbone et al., 2003b, for details). The blue squares are gravity changes assessed by time-lapse measurements at CO (red triangle in (a)), a site within 1km from PDN continuous station. Continuous and time lapse data agree within uncertainty (errors affecting gravity changes along the Summit Profile of Etna are typically 10-15  $\mu\text{Gal}$ ). Figure redrawn from Carbone et al. (2003b).

## References

- Aiuppa, A., Cannata, A., Cannavò, F., Di Grazia, G., Ferrari, F., Giudice, G., Gurrieri, S., Liuzzo, M., Mattia, M., Montalto, P., Patanè, D. and Puglisi, G., 2010. Patterns in the recent 2007–2008 activity of Mount Etna volcano investigated by integrated geophysical and geochemical observations. *Geochem. Geophys. Geosys.* 11 (Q09008), doi:10.1029/2010GC003168
- Allard, P., 2010. A CO<sub>2</sub>-rich gas trigger of explosive paroxysms at Stromboli basaltic volcano, Italy. *J. Volcanol. Geotherm. Res.* 189 (3–4), 363–374, doi:10.1016/j.jvolgeores.2009.11.018.
- Aloisi, M., Cocina, O., Neri, G., Orecchio, B., Privitera, E., 2002. Seismic tomography of the crust underneath the Etna volcano, Sicily. *Phys. Earth Planet. Inter.* 134, 139–155.  
[http://dx.doi.org/10.1016/S0031-9201\(02\)00153-X](http://dx.doi.org/10.1016/S0031-9201(02)00153-X).
- Andò, B., Carbone, D., 2001. A methodology for reducing a continuously recording gravity meter for the effect of meteorological parameters. *IEEE Trans. Instrum. Meas.* 50 (5), 1248–1254, doi:10.1109/19.963193.
- Andò, B. and Carbone, D., 2004. A test on a Neuro-Fuzzy algorithm used to reduce continuous gravity records for the effect of meteorological parameters. *Phys. Earth Planet. Inter.* 142 (1–2), 37–47, doi:10.1016/j.pepi.2003.12.006.
- Andò, B. and Carbone, D., 2006. A new computational approach to reduce the signal from continuously recording gravimeters for the effect of atmospheric temperature. *Phys. Earth Planet. Inter.*, 159 (3–4), 247–256, doi:10.1016/j.pepi.2006.07.009.
- Bagnardi, M., Poland, M.P., Carbone, D., Baker, S., Battaglia, M. and Amelung, F., 2014. Gravity changes and deformation at Kīlauea Volcano, Hawaii, associated with summit eruptive activity, 2009–2012. *J. Geophys. Res.* 119 (9), 7288–7305, doi:10.1002/2014JB011506.
- Battaglia, M., Roberts, C. and Segall, P., 1999. Magma intrusion beneath Long Valley Caldera confirmed by temporal changes in gravity. *Science* 285 (5436), 2119–2122, doi:10.1126/science.285.5436.2119.
- Battaglia, M., Segall, P. and Roberts, C., 2003. The mechanics of unrest at Long Valley caldera, California. 2. Constraining the nature of the source using geodetic and micro-gravity data. *J. Volcanol. Geotherm. Res.* 127 (3–4), 219–245, doi:10.1016/S0377-0273(03)00171-9.
- Battaglia, M., Troise, C., Obrizzo, F., Pingue, F. and De Natale, G., 2006. Evidence for fluid migration as the source of deformation at Campi Flegrei caldera (Italy). *Geophys. Res. Lett.* 33 (1), doi:10.1029/2005GL024904.

- Battaglia, M., Gottsmann, J., Carbone, D. and Fernández, J., 2008. 4D volcano gravimetry. *Geophysics*, 73(6): WA3-WA18, doi: 10.1190/1.2977792.
- Berrino, G., 2000. Combined gravimetry in the observation of volcanic processes in Southern Italy. *J. Geodynamics* 30 (3), 371–388, doi:10.1016/S0264-3707(99)00072-1.
- Berrino, G., Corrado, G., Luongo, G., Toro, B., Barberi, F., Hill, D.P., Innocenti, F., Luongo, G. and Treuil, M., 1984. Ground deformation and gravity changes accompanying the 1982 Pozzuoli uplift. *Bull. Volcanol.* 47 (2), 187–200, doi:10.1007/BF01961548.
- Berrino, G., Corrado, G. and Ricciardi, U., 2006. On the capability of recording gravity stations to detect signals coming from volcanic activity: the case of Vesuvius. *J. Volcanol. Geotherm. Res.* 150 (1–3), 270–282, doi:10.1016/j.jvolgeores.2005.07.015.
- Berrino, G., d’Errico, V. and Ricciardi, G., 2013. Thirty years of precise gravity measurements at Mt. Vesuvius: an approach to detect underground mass movements. *Ann. Geophys.* 56 (4), S0436; doi:10.4401/ag-6442.
- Bonvalot, S., Diament, M. and Germinal, G., 1998. Continuous gravity recording with Scintrex CG-3M meters: A promising tool for monitoring active zones, *Geophys. J. Int.* 135 (2), 470–494, doi:10.1046/j.1365-246X.1998.00653.x.
- Bonvalot, S., Remy, D., Deplus, C., Diament, M. and Gabalda, G., 2008. Insights on the March 1998 eruption at Piton de la Fournaise volcano (La Réunion) from microgravity monitoring. *J. Geophys. Res.* 113 (B5), doi:10.1029/2007JB005084.
- Branca, S., Carbone, D. and Greco, F., 2003. Intrusive mechanism of the 2002 NE-Rift eruption at Mt. Etna (Italy) inferred through continuous microgravity data and volcanological evidences. *Geophys. Res. Lett.* 30 (20), doi:10.1029/2003GL018250.
- Budetta, G., and Carbone, D., 1997. Potential application of the Scintrex CG-3M gravimeter for monitoring volcanic activity: results of field trials on Mt. Etna, Sicily. *J. Volcano. Geotherm. Res.* 76 (3), 199–214, doi:10.1016/S0377-0273(96)00080-7.
- Budetta, G., Carbone, D., and Greco, F., 1999. Subsurface mass redistribution at Mount Etna (Italy) during the 1995–96 explosive activity detected by microgravity studies. *Geophys. J. Int.* 138 (1), 77–88, doi:10.1046/j.1365-246x.1999.00836.x.
- Camacho, A.G., González, P.J., Fernández, J. and Berrino, G., 2011. Simultaneous inversion of surface deformation and gravity changes by means of extended bodies with a free geometry: Application to deforming calderas. *J. Geophys. Res.* 116 (B10401), doi:10.1029/2010JB008165.

- Carbone, D. and Greco, F., 2007. Insights into the internal dynamics of Etna volcano through discrete and continuous microgravity observations. *Pure App. Geophys.* 164 (4), 769–790.
- Carbone, D. and Poland, M.P., 2012. Gravity fluctuations induced by magma convection at Kīlauea Volcano, Hawai‘i. *Geology*, 40(9): 803–806, doi:10.1130/G33060.1.
- Carbone, D., Budetta, G., Greco, F., 2003a. Bulk processes prior to the 2001 Mount Etna eruption, highlighted through microgravity studies. *J. Geophys. Res.* 108 (2556), doi:10.1029/2003JB002542.
- Carbone, D., Budetta, G., Greco, F. and Rymer, H., 2003b. Combined discrete and continuous gravity observations at Mount Etna. *J. Volcanol. Geotherm. Res.* 123 (1–2), 123–135, doi:10.1016/S0377-0273(03)00032-5.
- Carbone, D., Budetta, G. and Greco, F., 2003c. Possible mechanisms of magma redistribution under Mt. Etna during the 1994 – 1999 period detected through microgravity measurements. *Geophys. J. Int.* 153 (1), 187–200, doi:10.1046/j.1365-246X.2003.01901.x
- Carbone, D., Zuccarello, L., Saccorotti, G. and Greco, F., 2006. Analysis of simultaneous gravity and tremor anomalies observed during the 2002–2003 Etna eruption. *Earth Planet. Sci. Lett.* 245 (3–4), 616–629, doi:10.1016/j.epsl.2006.03.055.
- Carbone, D., Currenti, G. and Del Negro, C., 2008a. Multiobjective genetic algorithm inversion of ground deformation and gravity changes spanning the 1981 eruption of Etna volcano. *J. Geophys. Res.* 113 (7), doi:10.1029/2006JB004917.
- Carbone, D., Zuccarello, L. and Saccorotti, G., 2008b. Geophysical indications of magma uprising at Mt Etna during the December 2005 to January 2006 non-eruptive period. *Geophys. Res. Lett.* 35 (6), doi:10.1029/2008GL033212.
- Carbone, D., D'Amico, S., Musumeci, C. and Greco, F., 2009a. Comparison between the 1994–2006 seismic and gravity data from Mt. Etna: New insight into the long-term behavior of a complex volcano. *Earth Planet. Sci. Lett.* 279 (3–4), 282–292, doi:10.1016/j.epsl.2009.01.007.
- Carbone, D., Jousset, P. and Musumeci, C., 2009b. Gravity “steps” at Mt. Etna volcano (Italy): Instrumental effects or evidences of earthquake-triggered magma density changes? *Geophys. Res. Lett.* 36 (L02301), doi:10.1029/2008GL0361.
- Carbone, D., Zuccarello, L., Montalto, P. and Rymer, H., 2012. New geophysical insight into the dynamics of Stromboli volcano (Italy). *Gondwana Res.* 22 (1), 290–299, doi:10.1016/j.gr.2011.09.007.

- Carbone, D., Poland, M.P., Patrick, M.R. and Orr, T.R., 2013. Continuous gravity measurements reveal a low-density lava lake at Kīlauea Volcano, Hawai‘i. *Earth Planet. Sci. Lett.* 376, 178–185, doi:10.1016/j.epsl.2013.06.024.
- Carbone, D., Aloisi, M., Vinciguerra, S. and Puglisi, G., 2014. Stress, strain and mass changes at Mt. Etna during the period between the 1991–93 and 2001 flank eruptions. *Earth Sci. Rev.* 138, 454–468, doi:10.1016/j.earscirev.2014.07.004.
- Carbone, D., Zuccarello, L., Messina, A., Scollo, S. and Rymer, H., 2015. Balancing bulk gas accumulation and gas output before and during lava fountaining episodes at Mt. Etna. *Sci. Rep.* 5, 18049, doi:10.1038/srep18049.
- Cerutti, G., Cannizzo, L., Sakuma, A. and Hostache, J., 1974. A transportable apparatus for absolute gravity measurements. *VDI-Berichte*, 212, 49–51.
- Charco, M., Luzón, F., Fernández, J., Tiampo, K.F. and Sánchez-Sesma, F.J., 2007. Three-dimensional indirect boundary element method for deformation and gravity changes in volcanic areas: Application to Teide volcano (Tenerife, Canary Islands). *J. Geophys. Res.* 112 (B8), doi:10.1029/2006JB004740.
- Clark, D.A., Saul, S.J. and Emerson, D.W., 1986. Magnetic and gravity anomalies of a triaxial ellipsoid. *Exploration Geophys.* 17 (4), 189–200, doi:10.1071/EG986189.
- Currenti, G., 2014. Numerical evidences enabling to reconcile gravity and height changes in volcanic areas. *Geophys. J. Int.* 197 (1), 164–173, doi:10.1093/gji/ggt507.
- D’Agostino, G., Desogus, S., Germak, A., Origlia, C., Quagliotti, D., Berrino, G., Corrado, G., d’Errico, V. and Ricciardi, G., 2008. The new IMG-C-02 transportable absolute gravimeter: measurement apparatus and applications in geophysics and volcanology. *Ann. Geophys.* 51 (1), 39–49, doi:10.4401/ag-3038.
- de Zeeuw-van Dalftsen, E., Rymer, H., Sigmundsson, F. and Sturkell, E., 2004. Net gravity decrease at Askja volcano, Iceland: Constraints on processes responsible for continuous caldera deflation, 1988–2003. *J. Volcanol. Geotherm. Res.* 139 (3–4), 227–239, doi:10.1016/j.jvolgeores.2004.08.008.
- de Zeeuw-van Dalftsen, E., Rymer, H., Williams-Jones, G., Sturkell, E. and Sigmundsson, F., 2006. Integration of micro-gravity and geodetic data to constrain shallow system mass changes at Krafla volcano, N Iceland. *Bull. Volcanol.* 68 (5), 420–431, doi:10.1007/s0445-005-0018-5.
- de Zeeuw-van Dalftsen, E., Pedersen, R., Hooper, A. and Sigmundsson, F., 2012. Subsidence of Askja caldera 2000–2009: Modelling of deformation processes at an extensional plate boundary,

- constrained by time series InSAR analysis. *J. Volcanol. Geotherm. Res.* 213-214, 72–82, doi:10.1016/j.jvolgeores.2011.11.004.
- Deroussi, S., Diament, M., Feret, J.B., Nebut, T. and Staudacher, T., 2009. Localization of cavities in a thick lava flow by microgravimetry. *J. Volcanol. Geotherm. Res.* 184 (1), 193–198, doi:10.1016/j.jvolgeores.2008.10.002.
- Dickerson, S.M., Hogan, J.M., Sugarbaker, A., Johnson, D.M. and Kasevich, M.A., 2013. Multiaxis inertial sensing with long-time point source atom interferometry. *Phys. Rev. Lett.* 111 (8), 083001, doi:10.1103/PhysRevLett.111.083001.
- Dzurisin, D., Anderson, L.A., Eaton, G.P., Koyanagi, R.Y., Lipman, P.W., Lockwood, J.P., Okamura, R.T., Puniwai, G.S., Sako, M.K. and Yamashita, K.M., 1980. Geophysical observations of Kilauea Volcano, Hawaii; 2, Constraints on the magma supply during November 1975-September 1977. *J. Volcanol. Geotherm. Res.* 7 (3–4), 241–269, doi:10.1016/0377-0273(80)90032-3.
- Eggers, A.A., 1983. Temporal gravity and elevation changes at Pacaya volcano, Guatemala. *J. Volcanol. Geotherm. Res.* 19 (3–4), 223–237, doi:10.1016/0377-0273(83)90111-7.
- Eggers, A.A., and Chavez, D., 1979. Temporal gravity variations at Pacaya Volcano, Guatemala. *J. Volcanol. Geotherm. Res.* 6 (3–4), 391–402, doi:10.1016/0377-0273(79)90012-X.
- Eggers, A.A., Krausse, J., Rush, H., and Ward, J., 1976. Gravity changes accompanying volcanic activity at Pacaya Volcano, Guatemala. *J. Volcanol. Geotherm. Res.* 1 (3), 229–236, doi:10.1016/0377-0273(76)90009-3.
- El Wahabi, A., Ducarme, B., Van Ruymbeke, M., d'Oreye', N., Somerhausen, A., 1997. Continuous gravity observations at Mount Etna (Sicily) and Correlations between temperature and gravimetric records. *Cah. Cent. Eur. Geodyn. Seismol.* 14, 105–119.
- El Wahabi, A., Ducarme, B. & Van Ruymbeke, M., 2001. Humidity and temperature effects on LaCoste & Romberg gravimeters. *Proceedings of the 14th International Symposium on Earth Tides*, Mizusawa, Japan, *J. Geodetic Soc. Japan.* 47 (1), 10-15.
- Fernández, J. and Rundle, J.B., 1994. Gravity changes and deformation due to a magmatic intrusion in a two-layered crustal model. *J. Geophys. Res.* 99 (B2), 2737–2746, doi:10.1029/93JB02449.
- Fialko, Y., Khazan, Y. and Simons, M., 2001. Deformation due to a pressurized horizontal circular crack in an elastic half-space, with application to volcano geodesy. *Geophys. J. Int.* 146 (1), 181–190.

- Furuya, M., Okubo, S., Kimata, F., Miyajima, R., Meilano, I., Sun, W., Tanaka, Y. and Miyazaki, T., 2003. Mass budget of the magma flow in the 2000 volcano-seismic activity at Izu-islands, Japan. *Earth, Planets, and Space* 55 (7), 375–385, doi:10.1186/BF03351771.
- Gailler L.S., Lénat J.F., Lambert M., Levieux G., Villeneuve N. and Froger J.L., 2009. Gravity structure of Piton de la Fournaise volcano and inferred mass transfer during the 2007 crisis. *J. Volcanol. Geotherm. Res.* 184, 31–48. doi:10.1016/j.jvolgeores.2009.01.024.
- Gerlach, T.M., 1986. Exsolution of H<sub>2</sub>O, CO<sub>2</sub>, and S during eruptive episodes at Kilauea Volcano, Hawaii. *J. Geophys. Res.* 91 (B12), 12,177–12,185, doi:10.1029/JB091iB12p12177.
- Gillot, P., Francis, O., Landragin, A., Dos Santos, F.P. and Merlet, S., 2014. Stability comparison of two absolute gravimeters: optical versus atomic interferometers. *Metrologia* 51 (5), L15, doi:10.1088/0026-1394/51/5/L15.
- Goodkind, J.M., 1999. The superconducting gravimeter. *Rev. Sci. Instrum.* 70 (11), 4131–4152, doi:10.1063/1.1150092.
- Gottsmann, J., Berrino, G., Rymer, H. and Williams-Jones, G., 2003. Hazard assessment during caldera unrest at the Campi Flegri Italy: a contribution from gravity-height gradients. *Earth Planet. Sci. Lett.* 211 (3–4), 295–305, doi:10.1016/S0012-821X(03)00225-5.
- Gottsmann, J., Wooller, L., Martí, J., Fernández, J., Camacho, A.G., Gonzalez, P.J., Garcia, A. and Rymer, H., 2006. New evidence for the reawakening of Teide volcano. *Geophys. Res. Lett.* 33 (L20311), doi:10.1029/2006GL027523.
- Gottsmann, J., Carniel, R., Coppo, N., Wooller, L., Hautmann, S. and Rymer, H., 2007. Oscillations in hydrothermal systems as a source of periodic unrest at caldera volcanoes: Multiparameter insights from Nisyros, Greece. *Geophys. Res. Lett.* 34 (L07307), doi:10.1029/2007GL029594.
- Gottsmann, J., De Angelis, S., Fournier, N., Van Camp, M., Sacks, S., Linde, A. and Ripepe, M., 2011. On the geophysical fingerprint of Vulcanian explosions. *Earth Planet. Sci. Lett.* 306 (1–2), 98–104, doi:10.1016/j.epsl.2011.03.035.
- Greco, F., Currenti, G., Del Negro, C., Napoli, R., Budetta, G., Fedi, M. and Boschi, E., 2010. Spatiotemporal gravity variations to look deep into the southern flank of Etna volcano. *J. Geophys. Res.* 115 (B11411), doi:10.1029/2009JB006835.
- Greco, F., Currenti, G., D’Agostino, G., Germak, A., Napoli, R., Pistorio, A. and Del Negro, C., 2012. Combining relative and absolute gravity measurements to enhance volcano monitoring. *Bull. Volcanol.* 74 (7), 1745–1756, doi:10.1007/s00445-012-0630-0.
- Greco, F., Currenti, G., Palano, M., Pepe, A. and Pepe, S., 2016. Evidence of a shallow persistent magmatic reservoir from joint inversion of gravity and ground deformation data: the 25-26

- October 2013 Etna lava fountaining event. *Geophys. Res. Lett.*, 43 (7), 3246–3253, doi:10.1002/2016GL068426.
- Hagiwara Y., 1977. The Mogi model as a possible cause of the crustal uplift in the eastern part of Izu Peninsula and the related gravity change. *Bull. Earthquake Res. Inst.* 52, 301–309.
- Hautmann, S., Gottsmann, J., Camacho, A.G., Fournier, N., Sacks, I.S. and Sparks, R.S.J., 2010. Mass variations in response to magmatic stress changes at Soufrière Hills Volcano, Montserrat (W.I.): Insights from 4-D gravity data. *Earth Planet. Sci. Lett.* 290 (1–2), 83–89, doi:10.1016/j.epsl.2009.12.004.
- Hautmann, S., Gottsmann, J., Camacho, A.G., Van Camp, M. and Fournier, N., 2014. Continuous and campaign-style gravimetric investigations on Montserrat 2006 to 2009. In: Wadge, G., Robertson, D.E.A., and Voight, B., *The Eruption of Soufrière Hills Volcano, Montserrat from 2000 to 2010*, Geological Society of London, Memoirs 39, 241–251.
- Hemmings, B., Gottsmann, J., Whitaker, F. and Coco, A., 2016. Investigating hydrological contributions to volcano monitoring signals. A time-lapse gravity example. *Geophys. J. Int.* 207(1), 259–273, doi: 10.1093/gji/ggw266.
- Hill, D.P., Pollitz, F. and Newhall, C., 2002. Earthquake-volcano interactions. *Phys. Today* 55 (11), 41–47.
- Hinderer, J., Crossley, D., and Warburton, R., 2007. Superconducting gravity meters. In *Treatise on Geophysics*, chap. 4, vol. 3, ed. T. Herring and G. Schubert. Boston, Massachusetts: Elsevier, p. 65–122, doi:10.1016/B978-044452748-6.00172-3.
- Iida, K., Hayakawa, M. and Katayose, K., 1952. Gravity Survey of Mihara Volcano Ooshima Island and changes in gravity caused by the eruption. *Geol. Surv. Jpn.* 152.
- Jachens, R.C., and Eaton, G.P., 1980. Geophysical observations of Kilauea volcano, Hawaii, 1. temporal gravity variations related to the 29 November, 1975,  $M = 7.2$  earthquake and associated summit collapse. *J. Volcanol. Geotherm. Res.* 7 (3–4), 225–240, doi:10.1016/0377-0273(80)90031-1.
- Johnsen, G.V., Bjornsson, A., and Sigurdsson, S., 1980. Gravity and elevation changes caused by magma movement beneath the Krafla caldera, northeast Iceland. *J. Geophys.* 47 (1–3), 132–140.
- Johnson, D.J., 1987. Elastic and inelastic magma storage at Kilauea Volcano. In: R.W. Decker, T.L. Wright and P.H. Stauffer (Editors), *Volcanism in Hawaii*. U.S. Geological Survey Professional Paper 1350, 1297–1306.

- Johnson, D.J., Eggers, A.A., Bagnardi, M., Battaglia, M., Poland, M.P. and Miklius, A., 2010. Shallow magma accumulation at Kīlauea Volcano, Hawai‘i, revealed by microgravity surveys. *Geology* 38 (12), 1139–1142, doi:10.1130/G31323.1.
- Jousset, P., Mori, H. and Okada, H., 2000a. Possible magma intrusion revealed by temporal gravity, ground deformation and ground temperature observations at Mount Komagatake (Hokkaido) during the 1996–1998 crisis. *Geophys. J. Int.* 143 (3), 557–574, doi:10.1046/j.1365-246X.2000.00218.x.
- Jousset, P., Dwipa, S., Beauducel, F., Duquesnoy, T. and Diament, M., 2000b. Temporal gravity at Merapi during the 1993-1995 crisis: an insight into the dynamical behaviour of volcanoes. *J. Volcanol. Geotherm. Res.* 100 (1–4), 289–320, doi:10.1016/S0377-0273(00)00141-4.
- Jousset, P., Mori, H., and Okada, H., 2003. Elastic models for the magma intrusion associated with the 2000 eruption of Usu Volcano, Hokkaido, Japan. *J. Volcanol. Geotherm. Res.* 125 (1), 81–106, doi:10.1016/S0377-0273(03)00090-8.
- Kauahikaua, J. and Miklius, A., 2003. Long-term trends in microgravity at Kilauea's summit during the Pu‘u ‘O‘o-Kupaianaha eruption. In: C. Heliker, D.A. Swanson and T.J. Takahashi (Editors), *The Pu'u O'o-Kupaianaha Eruption of Kilauea Volcano, Hawaii: The First 20 Years*, United States Geological Survey Professional Paper 1676, 165–171.
- Kazama, T. and Okubo, S., 2009. Hydrological modeling of groundwater disturbances to observed gravity: Theory and application to Asama Volcano, Central Japan. *J. Geophys. Res.* 114 (B08402), doi:10.1029/2009JB006391.
- Kazama, T., Okubo, S., Sugano, T., Matsumoto, S., Sun, W., Tanaka, Y. and Koyama, E., 2015. Absolute gravity change associated with magma mass movement in the conduit of Asama Volcano (Central Japan), revealed by physical modeling of hydrological gravity disturbances. *J. Geophys. Res.* 120 (2), 1263–1287, doi:10.1002/2014JB011563.
- LaCoste, L., 1988. The zero-length spring gravity meter. *The Leading Edge*, 7 (7), 20–21, doi:10.1190/1.1439525.
- LaCoste & Romberg, 2004. Instruction manual. Model G and D gravity meters. <http://www.gravitymeter-repair.com/LinkClick.aspx?fileticket=53JUtKBPTmg%3d&tabid=66> (last accessed August, 15, 2016)..
- Le Gouët, J., Mehlstäubler, T.E., Kim, J., Merlet, S., Clairon, A., Landragin, A. and Dos Santos, F.P., 2008. Limits to the sensitivity of a low noise compact atomic gravimeter. *App. Phys. B.* 92 (2), 133–144, doi:10.1007/s00340-008-3088-1.

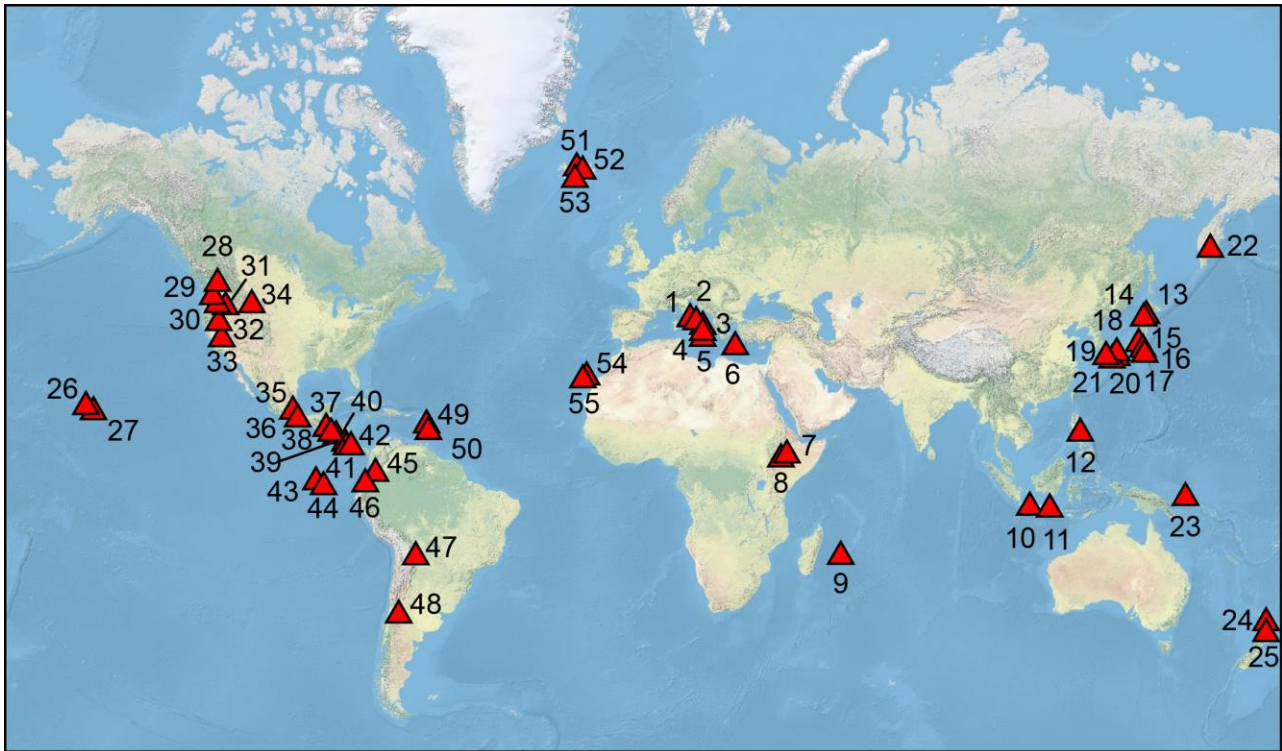
- Longo, A., Vassalli, M., Papale, P. and Barsanti, M., 2006. Numerical simulation of convection and mixing in magma chambers replenished with CO<sub>2</sub>-rich magma. *Geophys. Res. Lett.* 33 (21), doi:10.1029/2006GL027760.
- Malone, S.D., 1979. Gravity changes accompanying increased heat emission at Mount Baker, Washington. *J. Volcanol. Geotherm. Res.* 6 (3–4): 241–256, doi:10.1016/0377-0273(79)90004-0.
- Middlemiss, R.P., Samarelli, A., Paul, D.J., Hough, J., Rowan, S. and Hammond, G.D., 2016. Measurement of the Earth tides with a MEMS gravimeter. *Nature* 531 (7596), 614–617, doi:10.1038/nature17397.
- Mikhailov, V., Tikhotsky, S., Diament, M., Panet, I. and Ballu, V., 2004. Can tectonic processes be recovered from new gravity satellite data?. *Earth Planet. Sci. Lett.*, 228(3), 281–297, doi:10.1016/j.epsl.2004.09.035.
- Mikhailov, V., Panet, I., Hayn, M., Timoshkina, E.B., Bonvalot, S., Lyakhovsky, V., Diament, M., and de Viron, O., 2014, Comparative study of temporal variations in the Earth's gravity field using GRACE gravity models in the Regions of Three Recent Giant Earthquakes, *Phys. Solid Earth*, 50(2), 177–191, doi:10.1134/S1069351314020062.
- Mogi, K., 1958. Relations between the eruptions of various volcanoes and the deformations of the ground surfaces around them. *Bull. Earthquake Res. Inst.* 36 (2), 99–134.
- Nabighian, M.N., Ander, M.E., Grauch, V.J.S., Hansen, R.O., LaFehr, T.R., Li, Y., Pearson, W.C., Peirce, J.W., Phillips, J.D., and Ruder, M.E., 2005. Historical development of the gravity method in exploration. *Geophys.* 70 (6), 63ND–89ND, doi: 10.1190/1.2133785.
- Niebauer, T.M., Sasagawa, G.S., Faller, J.E., Hilt, R. and Klopping, F., 1995. A new generation of absolute gravimeters. *Metrologia*, 32 (3), 159, doi:10.1088/0026-1394/32/3/004.
- Okada, Y., 1985. Surface deformation due to shear and tensile faults in a half-space. *Bul. Seismol. Soc. Am.*, 75 (4), 1135–1154,.
- Okada, Y., 1992. Internal deformation due to shear and tensile faults in a half-space. *Bull. Seismol. Soc. Am.* 82 (2), 1018–1040.
- Okubo, S., 1992. Gravity and potential changes due to shear and tensile faults in a half-space. *J. Geophys. Res.* 97 (B5), 7137–7144, doi:10.1029/92JB00178.
- Okubo, S. and Watanabe, H., 1989. Gravity change caused by a fissure eruption. *Geophys. Res. Lett.* 16 (5) 445–448, doi:10.1029/GL016i005p00445.

- Orr, T.R., Thelen, W.A., Patrick, M.R., Swanson, D.A. and Wilson, D.C., 2013. Explosive eruptions triggered by rockfalls at Kīlauea volcano, Hawai‘i. *Geology* 41 (2), 207–210, doi:10.1130/G33564.1.
- Orr, T.R., Poland, M.P., Patrick, M.R., Thelen, W.A., Sutton, A.J., Elias, T., Thornber, C.T., Parcheta, C. and Wooten, K.M., 2015. Kīlauea's 5–9 March 2011 Kamoamoā fissure eruption and its relation to 30+ years of activity from Pu‘u ‘Ō ‘ō. In: *Hawaiian Volcanoes From Source to Surface*, American Geophysical Union Monograph 208, edited by R. Carey, V. Cayol, M. Poland, and D. Weis, pp. 393–420, doi:10.1002/9781118872079.ch18.
- Peltier, A., Bachèlery, P. and Staudacher, T., 2009. Magma transport and storage at Piton de La Fournaise (La Réunion) between 1972 and 2007: A review of geophysical and geochemical data. *J. Volcanol. Geotherm. Res.* 184 (1–2), 93–108, doi:10.1016/j.jvolgeores.2008.12.008.
- Peters, A., Chung, K.Y., Chu, S., 2001. High-precision gravity measurements using atom interferometry. *Metrologia*, 38, 25.
- Poland, M.P. and Carbone, D., 2016. Insights into shallow magmatic processes at Kīlauea Volcano, Hawai‘i, from a multiyear continuous gravity time series. *J. Geophys. Res.* 121 (7), 5477–5492, doi:10.1002/2016JB013057.
- Poland, M.P., Sutton, A.J. and Gerlach, T.M., 2009. Magma degassing triggered by static decompression at Kīlauea Volcano, Hawai‘i. *Geophys. Res. Lett.* 36 (L16306), doi:10.1029/2009GL039214.
- Prothero, W.A. and Goodkind, J.M., 1968. A superconducting gravimeter. *Rev.Sci. Instrum.* 39 (9), 1257–1262, doi:10.1063/1.1683645.
- Reid, M. E., 2004. Massive collapse of volcano edifices triggered by hydrothermal pressurization, *Geology*, 32, 373–376, doi: 10.1130/G20300.1.
- Ripepe, M. and Harris, A.J.L., 2008. Dynamics of the 5 April 2003 explosive paroxysm observed at Stromboli by a near-vent thermal, seismic and infrasonic array. *Geophys. Res. Lett.* 35 (L07306), doi:10.1029/2007GL032533.
- Rose, W.I. and Stoiber, R.E., 1969. The 1966 eruption of Izalco volcano, El Salvador. *J. Geophys. Res.* 74 (12), 3119–3130, doi:10.1029/JB074i012p03119.
- Rosi, G., Sorrentino, F., Cacciapuoti, L., Prevedelli, M. and Tino, G.M., 2014. Precision measurement of the Newtonian gravitational constant using cold atoms. *Nature*. 510 (7506), 518–521, doi:10.1038/nature13433.
- Rymer, H., 1989. A contribution to precision microgravity data analysis using Lacoste and Romberg gravity meters. *Geophys. J. Int.* 97 (2), 311–322, doi:10.1111/j.1365-246X.1989.tb00503.x.

- Rymer, H. and Brown, G.C., 1984. Periodic gravity changes at Poas volcano, Costa Rica. *Nature*, 311 (5983) 243–245, doi:10.1038/311243a0.
- Rymer, H. and Brown, G.C., 1987. Causes of microgravity change at Poas volcano, Costa Rica: an active but non-erupting system. *Bull. Volcanol.* 49 (1), 389–398, doi:10.1007/BF01046632.
- Rymer, H. and Brown, G.C., 1989. Gravity changes as a precursor to volcanic eruption at Poas volcano, Costa Rica. *Nature* 342 (6252), 902–905, doi:10.1038/342902a0.
- Rymer, H. and Williams-Jones, G., 2000. Volcanic eruption prediction: Magma chamber physics from gravity and deformation measurements. *Geophys. Res. Lett.* 27 (16) 2389–2392, doi:10.1029/1999GL011293.
- Rymer, H., Murray, J.B., Brown, G.C., Ferrucci, F. and McGuire, W.J., 1993. Mechanisms of magma eruption and emplacement at Mt. Etna between 1989 and 1992. *Nature* 361 (6411), 439–441, doi:10.1038/361439a0.
- Rymer, H., van Wyk de Vries, B., Stix, J., Williams-Jones, G., 1998. Pit crater structure and processes governing persistent activity at Masaya Volcano, Nicaragua. *Bull. Volcanol.* 59 (5), 345–355, doi:10.1007/s004450050196.
- Rymer, H., Locke, C.A., Borgia, A., Martinez, M., Brenes, J., Van der Laat, R. and Williams-Jones, G., 2009. Long-term fluctuations in volcanic activity: implications for future environmental impact. *Terra Nova* 21 (4), 304–309, doi:10.1111/j.1365-3121.2009.00885.x.
- Rymer, H., Locke, C., Ofeigsson, B.G., Einarsson, P. and Sturkell, E., 2010. New mass increase beneath Askja volcano, Iceland—a precursor to renewed activity? *Terra Nova* 22 (4), 309–313, doi:10.1111/j.1365-3121.2010.00948.x.
- Sainz-Maza Aparicio, S., Arnosó Sampedro, J., González Montesinos, F. and Martí Molist, J., 2014. Volcanic signatures in time gravity variations during the volcanic unrest on El Hierro (Canary Islands). *J. Geophys. Res.* 119 (6), 5033–5051, doi:10.1002/2013JB010795.
- Schiavone, D., and Loddo, M., 2007. 3-D density model of Mt. Etna volcano (Southern Italy). *J. Volcanol. Geotherm. Res.* 164 (3), 161–175. doi:10.1016/j.jvolgeores.2007.04.016.
- Segall, P., 2010. *Earthquake and Volcano Deformation*. Princeton University Press: Princeton. 465 pp.
- Sofyan, Y., Nishijima, J., Fujimitsu, Y., Yoshikawa, S., Kagiya, T. and Ohkura, T., 2014. Monitoring Geothermal Activity at Aso Volcano, Japan, After Small Eruption in May 2011. *Proceedings, 38<sup>th</sup> Workshop on Geothermal Reservoir Engineering, SGP-TR-202*.
- Tarantola, A., 1987. *Inverse Problem Theory*. 613 pp., Elsevier, Amsterdam.

- Tiampo, K.F., Rundle, J.B., Fernandez, J. and Langbein J., 2000. Spherical and ellipsoidal volcanic sources at Long Valley Caldera, California using a genetic algorithm inversion technique, *J. Volcanol. Geotherm. Res.* 102 (3–4), 189–206, doi:10.1016/S0377-0273(00)00185-2.
- Tikku, A.A., McAdoo, D.C., Schenewerk, M.S. and Willoughby, E.C., 2006. Temporal fluctuations of microseismic noise in Yellowstone's Upper Geyser Basin from a continuous gravity observation. *Geophys. Res. Lett.* 33 (11), doi:10.1029/2006GL026113.
- Tizzani, P., Castaldo, R., Pepe, A., Zeni, G., Lanari, R. and Battaglia, M., 2015. Magma and fluid migration at Yellowstone Caldera in the last three decades inferred from InSAR, leveling and gravity measurements. *J. Geophys. Res.* 120 (4), 2627–2647, doi:10.1002/2014JB011502.
- Todesco, M. and Berrino, G., 2005. Modeling hydrothermal fluid circulation and gravity signals at the Phlegraean Fields caldera. *Earth Planet. Sci. Lett.* 240 (2), 328–338, doi:10.1016/j.epsl.2005.09.016.
- Torge, W., 1981. Gravity and height variations connected with the current rifting episode in northern Iceland. *Tectonophysics* 71 (1–4), 227–240, doi:10.1016/0040-1951(81)90068-8.
- Torge, W., 1989. *Gravimetry*. Walter de Gruyter: Berlin. 465 pp.
- Trasatti, E., and Bonafede, M., 2008. Gravity changes due to overpressure sources in 3D heterogeneous media: Application to Campi Flegrei caldera, Italy. *Ann. Geophys.* 51 (1), 119–133, doi:10.4401/ag-4442.
- Vajda, P., Prutkin, I., Tenzer, R. and Jentzsch, G., 2012. Inversion of temporal gravity changes by the method of local corrections: A case study from Mayon volcano, Philippines. *J. Volcanol. Geotherm. Res.*, 241–242, 13–20, doi:10.1016/j.jvolgeores.2012.06.020.
- Vandemeulebrouck, J., Sohn, R.A., Rudolph, M.L., Hurwitz, S., Manga, M., Johnston, M.J.S., Soule, S.A., McPhee, D., Glen, J.M.G., Karlstrom, L. and Murphy, F., 2014. Eruptions at Lone Star geyser, Yellowstone National Park, USA: 2. Constraints on subsurface dynamics. *J. Geophys. Res.* 119 (12), 8688–8707, doi:10.1002/2014JB011526.
- Vassalli, M., Longo, A., Montagna, C.P., O'Brien, G.S., Bean, C.J., Bisconti, L., Papale, P. and Saccorotti, G., 2009. An integrated method to model volcanic processes and associated geophysical signals, in Bean, C.J., et al., eds., *The VOLUME project, VOLcanoes: Understanding subsurface mass movement: Dublin, Ireland, The Volume Consortium*, p. 162–174.
- Vigouroux, N., Williams-Jones, G., Chadwick, W., Geist, D., Ruiz, A. and Johnson, D., 2008. 4D gravity changes associated with the 2005 eruption of Sierra Negra volcano, Galápagos. *Geophys.*, 73 (6), WA29–WA35, doi:10.1190/1.2987399.

- Voight, B., 2000. Structural stability of andesite volcanoes and lava domes, *Phil. Trans. R. Soc. Lond.*, A, 358, 1663-1703, doi: 10.1098/rsta.2000.0609.
- Walsh, J.B. and Rice, J.R., 1979. Local changes in gravity resulting from deformation. *J. Geophys. Res.* 84 (B1), 165–170, doi:10.1029/JB084iB01p00165.
- Watermann H., 1957. Über systematische Fehler bei Gravimetermessungen. *DGK, München*, 21(C).
- Williams-Jones, G. and Rymer, H., 2002. Detecting volcanic eruption precursors: a new method using gravity and deformation measurements. *J. Volcanol. Geotherm. Res.* 113 (3–4), 379–389, doi:10.1016/S0377-0273(01)00272-4.
- Williams-Jones, G., Rymer, H., Mauri, G., Gottsmann, J., Poland, M. and Carbone, D., 2008. Toward continuous 4D microgravity monitoring of volcanoes. *Geophys.* 73 (6), WA19–WA28, doi:10.1190/1.2981185.
- Wilson, L. and Head, J.W., 1981. Ascent and eruption of basaltic magma on the Earth and Moon. *J. Geophys. Res.* 86 (B4), 2971–3001, doi:10.1029/JB086iB04p02971.
- Wilson, C., Wu, H., Scanlon, B., and Sharp, J., 2007. Taking the superconducting gravimeter to the field for hydrologic and other investigations. *EOS Trans. Am. Geophys. Union* 88 (53), Fall Meeting Supplement, Abstract H11A-050.
- Yang, X.-M., Davis, P.M. and Dieterich, J.H., 1988. Deformation from inflation of a dipping finite prolate spheroid in an elastic half space as a model for volcanic stressing. *J. Geophys. Res.* 93 (B5), 4249–4257, doi:10.1029/JB093iB05p04249.
- Zhou M.K., Duan X.C., Chen L.L., Luo Q., Xu Y.Y., and Hu Z.K., 2015. Micro-Gal level gravity measurements with cold atom interferometry. *Chin. Phys. B* 24 (5), doi:10.1088/1674-1056/24/5/050401.



- |                          |                      |                          |
|--------------------------|----------------------|--------------------------|
| 1. Campi Flegrei         | 21. Sakurajima       | 41. Irazu                |
| 2. Vesuvio*              | 22. Karymsky*        | 42. Turrialba            |
| 3. Stromboli*            | 23. Rabaul           | 43. Fernandina           |
| 4. Vulcano               | 24. White Island*    | 44. Sierra Negra         |
| 5. Etna*                 | 25. Tongariro        | 45. Galeras              |
| 6. Nisyros*              | 26. Mauna Loa        | 46. Cotopaxi             |
| 7. Alutu                 | 27. Kilauea*         | 47. Uturuncu             |
| 8. Corbetti              | 28. Baker            | 48. Laguna del Maule*    |
| 9. Piton de la Fournaise | 29. Mount St. Helens | 49. Soufrière Hills*     |
| 10. Merapi*              | 30. South Sister     | 50. Soufrière Guadeloupe |
| 11. Ijen                 | 31. Newberry         | 51. Krafla               |
| 12. Mayon                | 32. Lassen           | 52. Askja                |
| 13. Usu                  | 33. Long Valley      | 53. Hekla                |
| 14. Hokkaido-Komagatake  | 34. Yellowstone      | 54. Teide                |
| 15. Asama                | 35. Popocatepetl     | 55. El Hierro*           |
| 16. Izu-Oshima           | 36. Pacaya           |                          |
| 17. Miyakejima           | 37. Izalco           |                          |
| 18. Aso                  | 38. Telica           |                          |
| 19. Unzen                | 39. Masaya*          |                          |
| 20. Kuju                 | 40. Poas             |                          |

\* Denotes volcano with continuous gravity observations

**Figure 1**

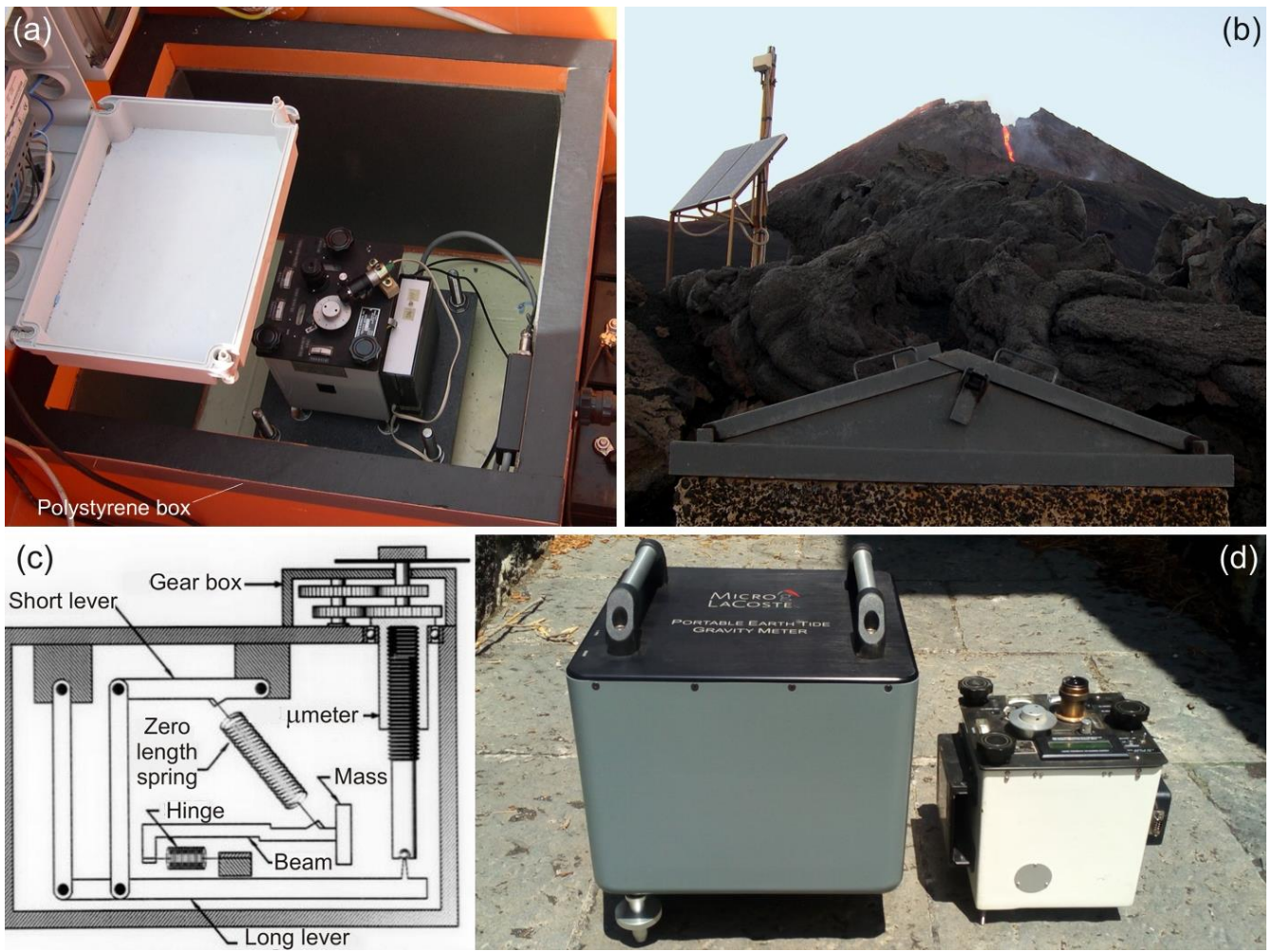


**Figure 2**

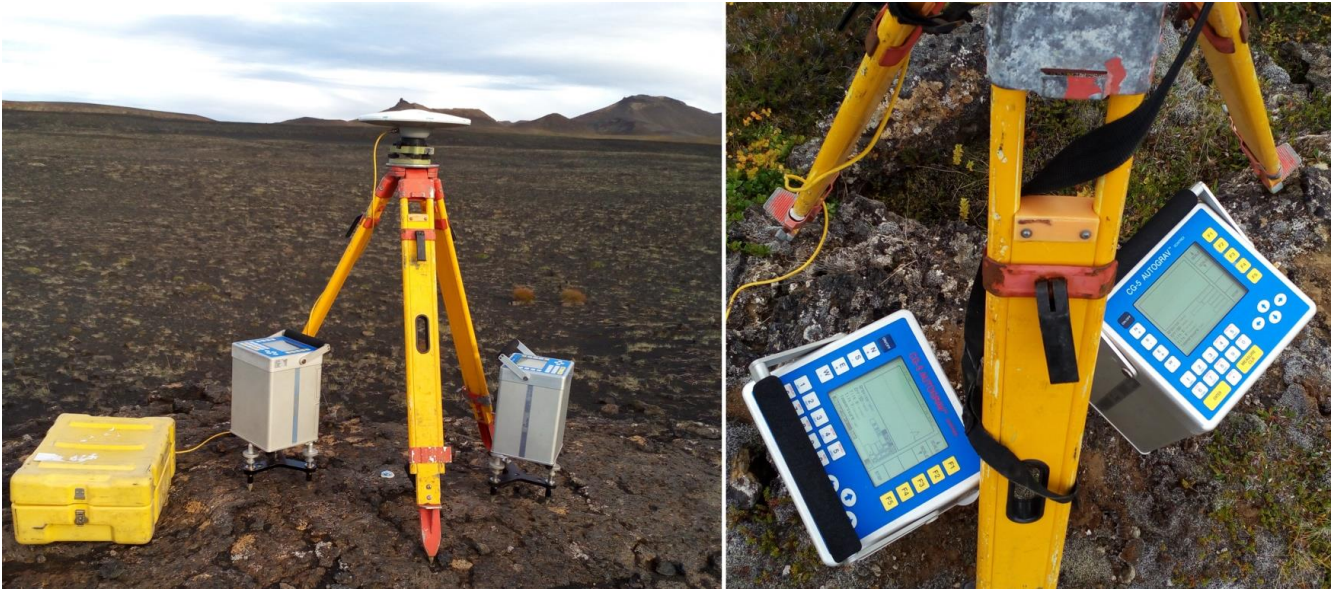


**Figure 3**

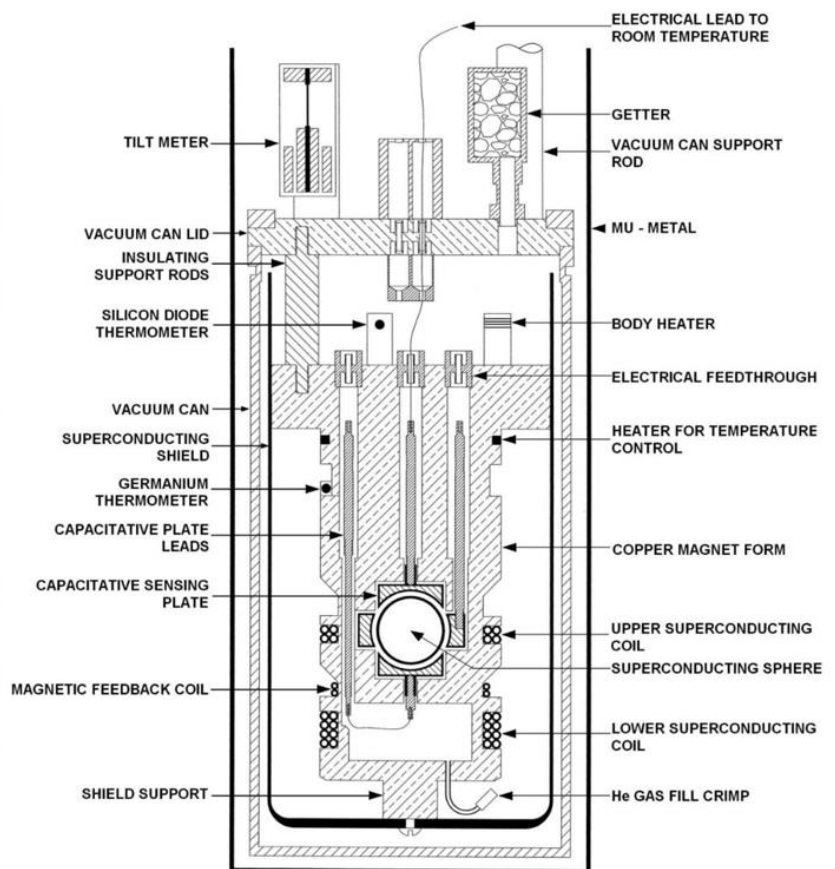
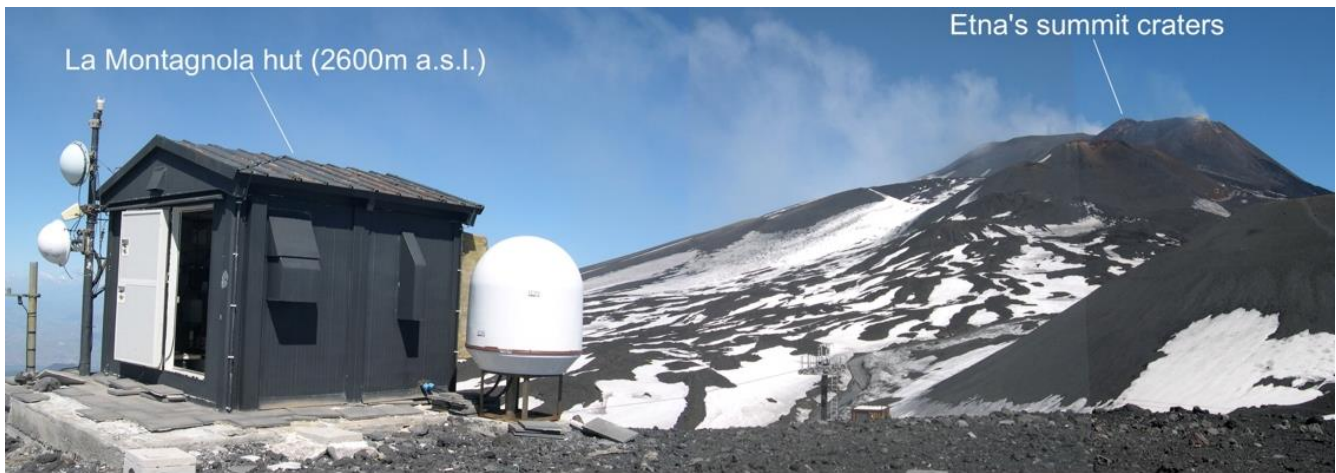


**Figure 4**

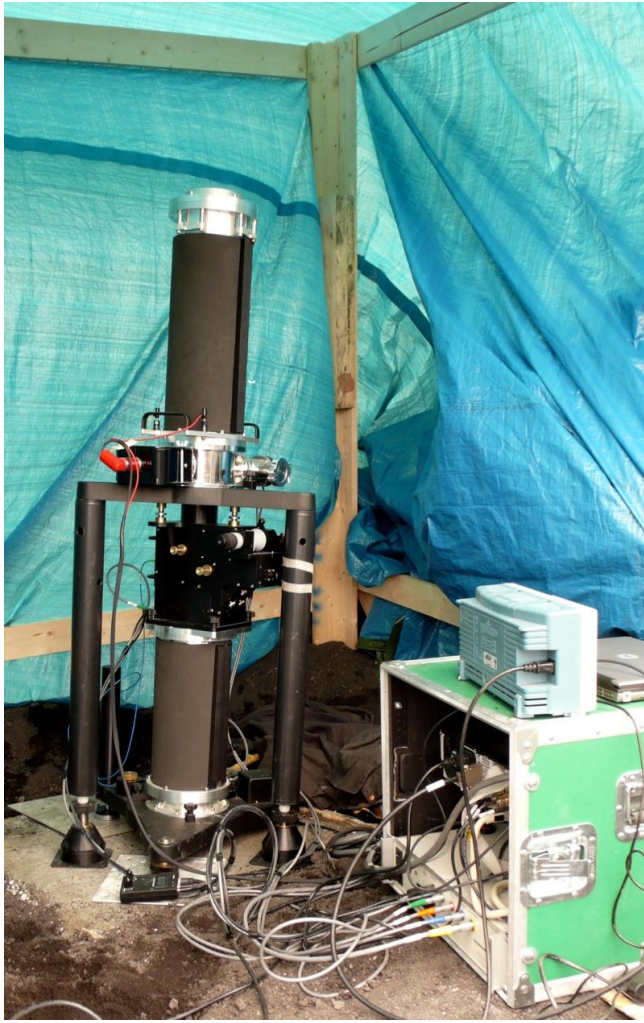


**Figure 5**



**Figure 6**

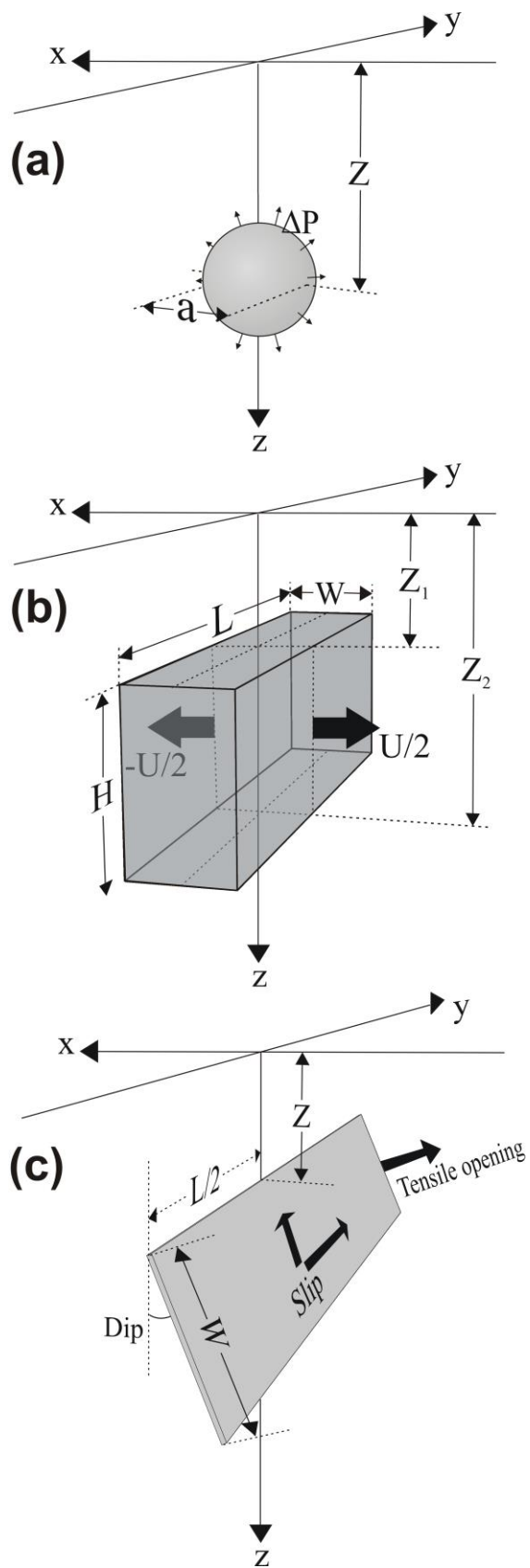


**Figure 7**

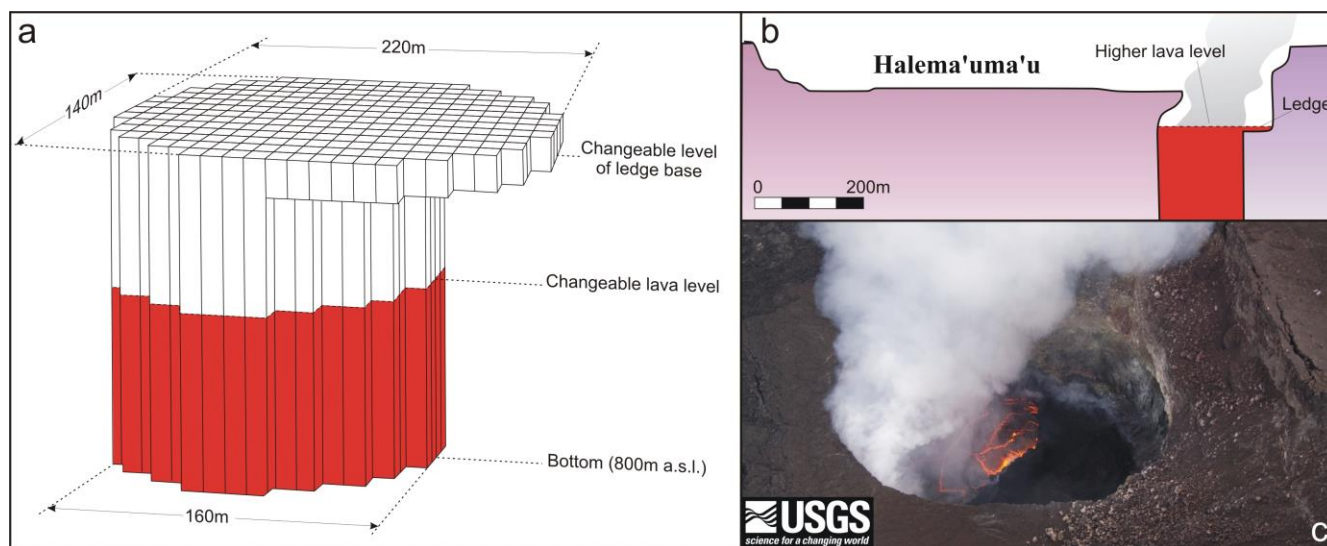


**Figure 8**

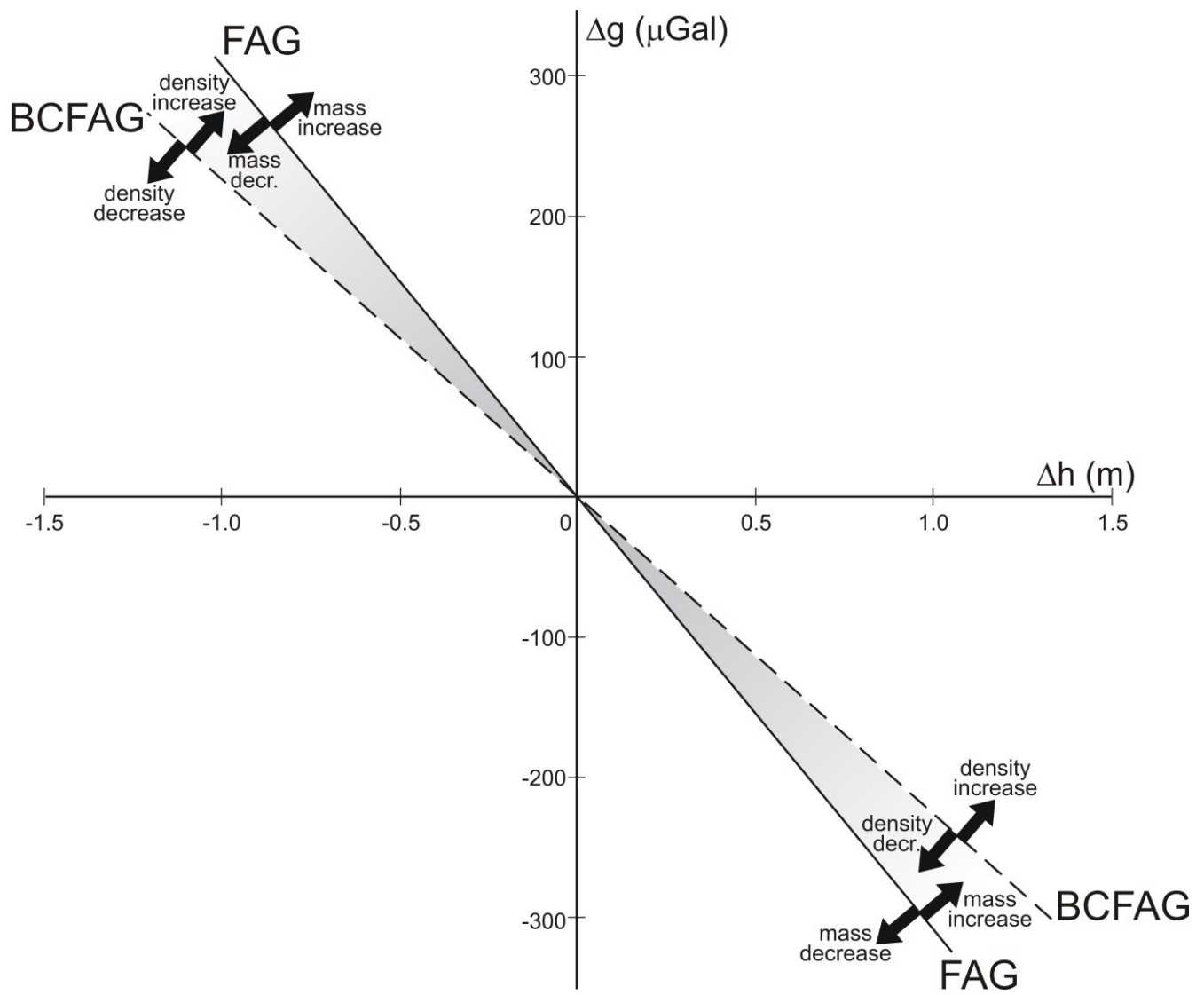


**Figure 9**

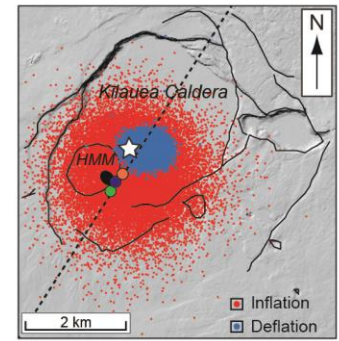
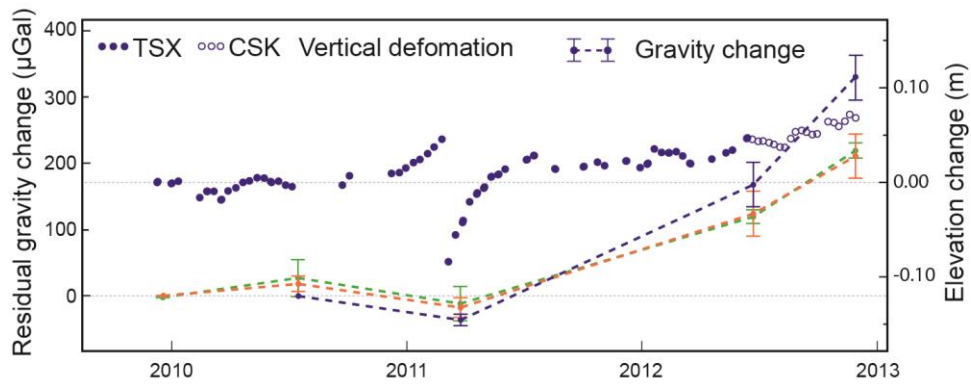


**Figure 10**

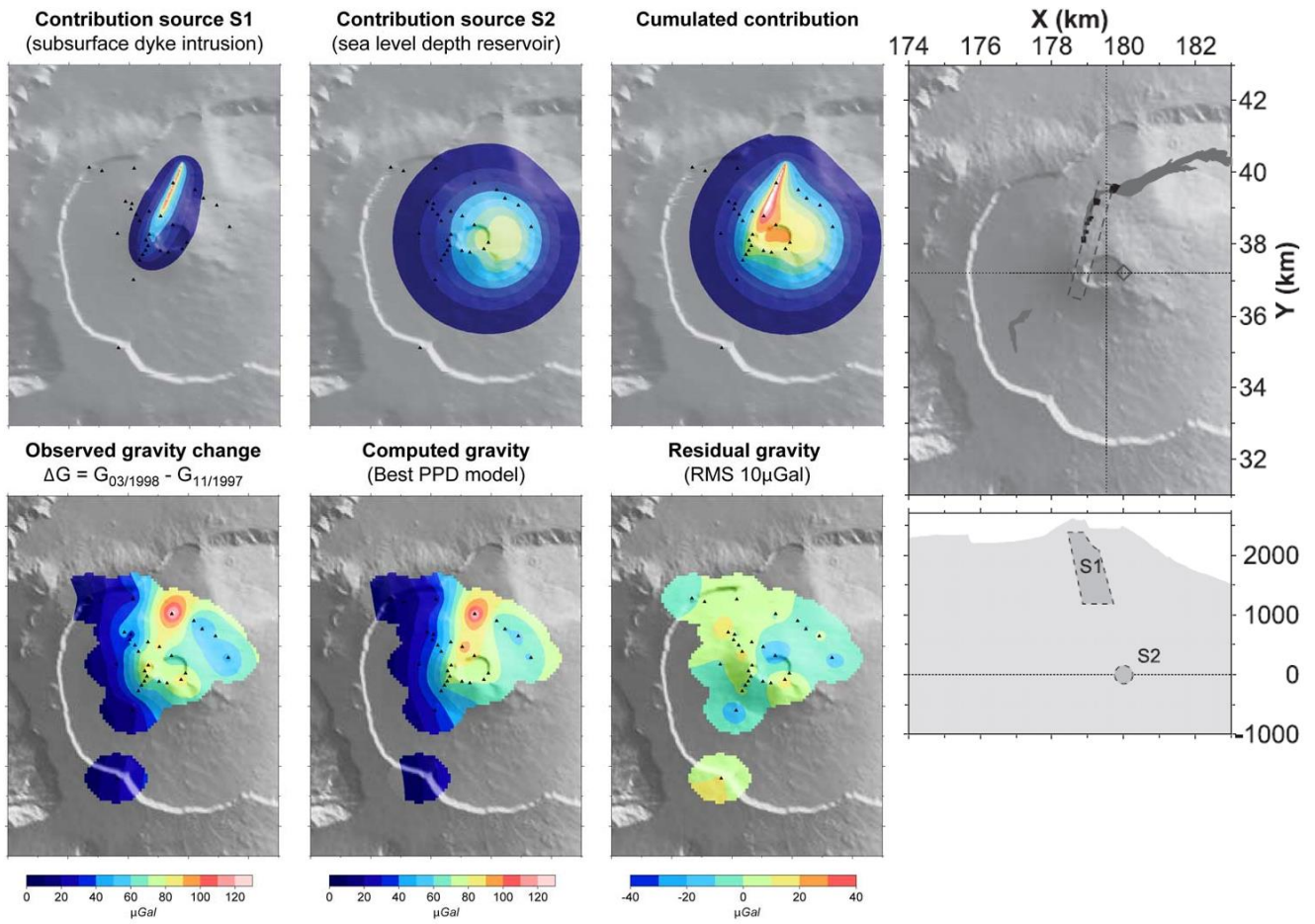


**Figure 11**

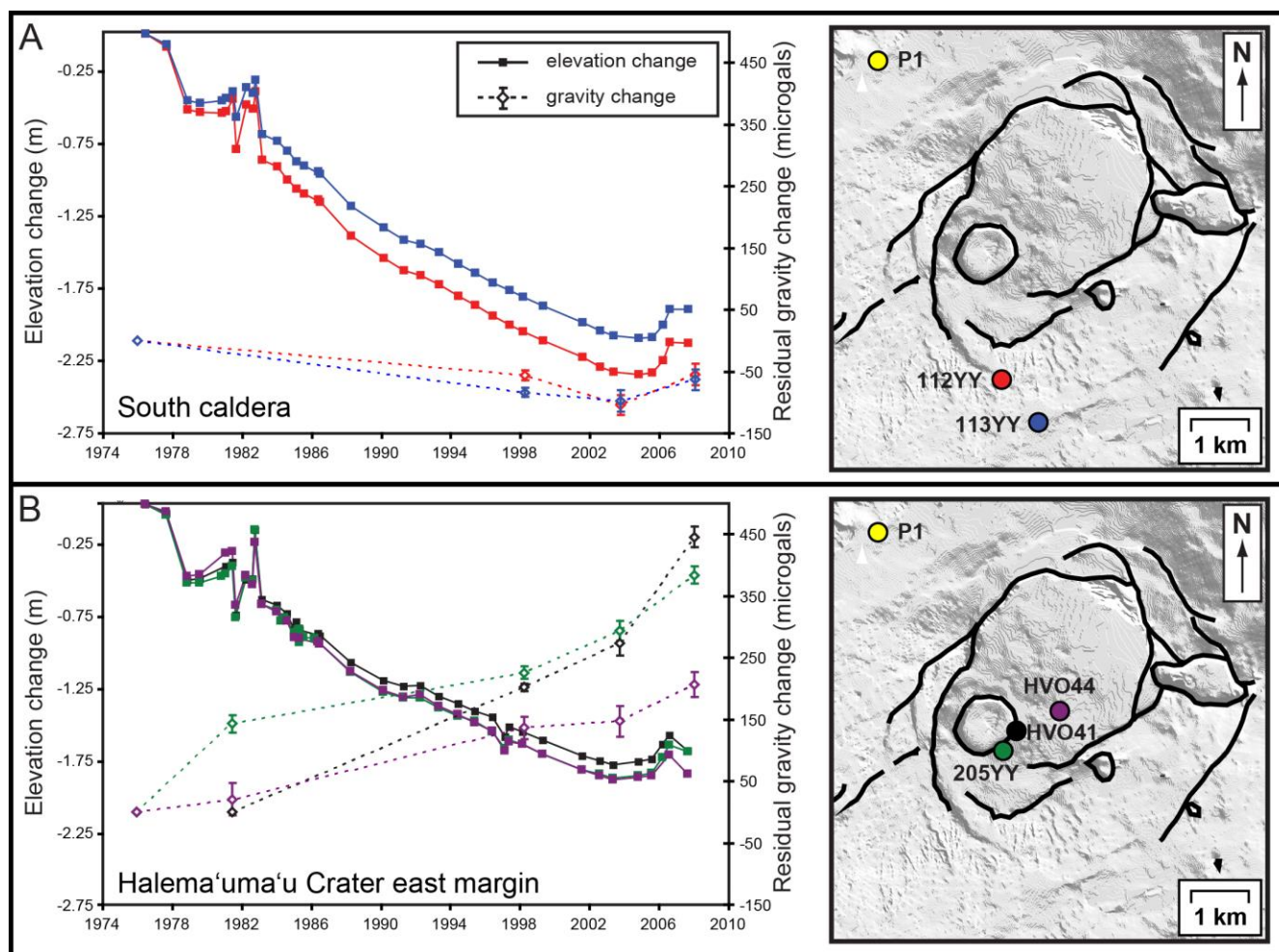


**Figure 12**

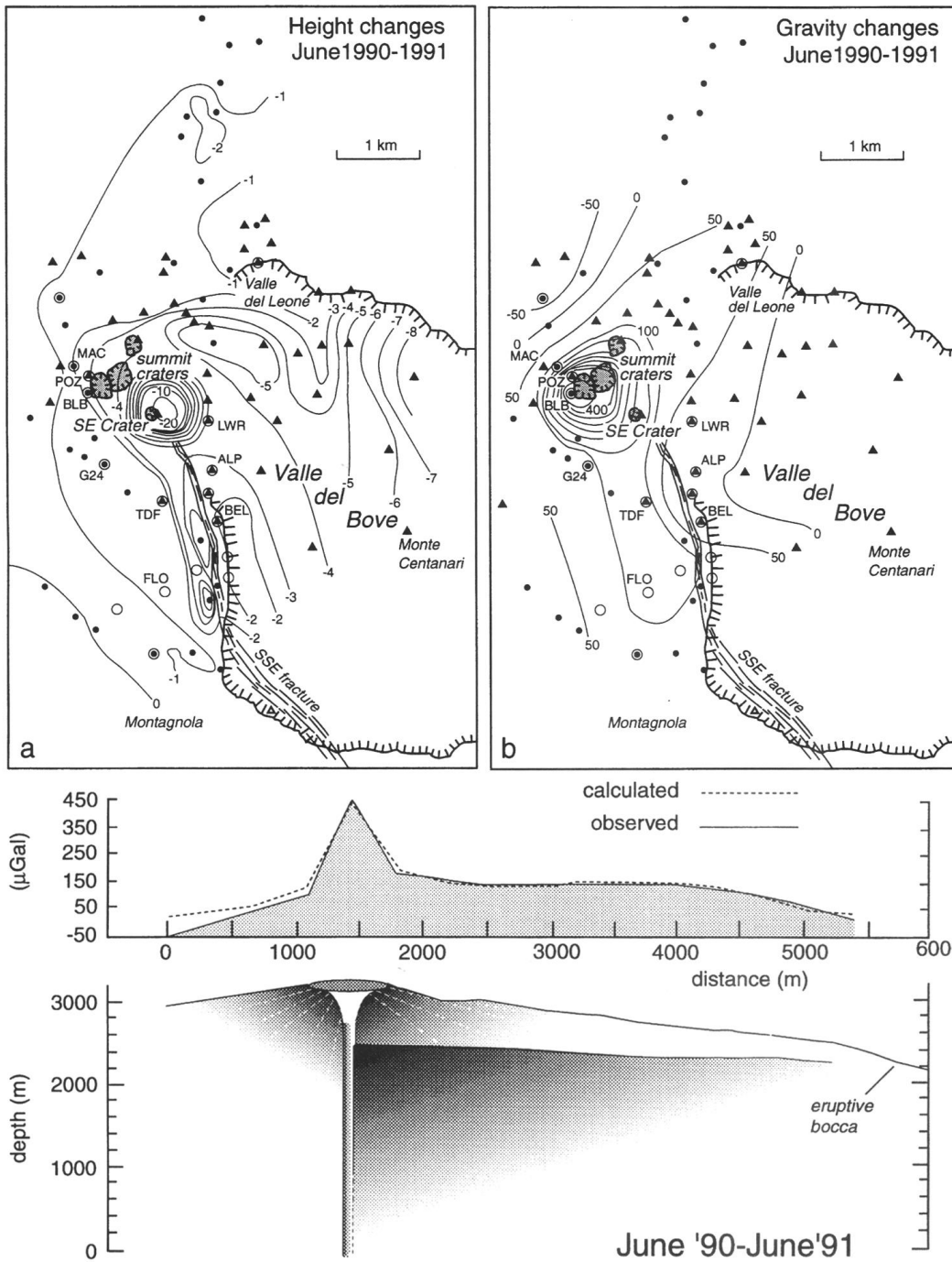


**Figure 13**

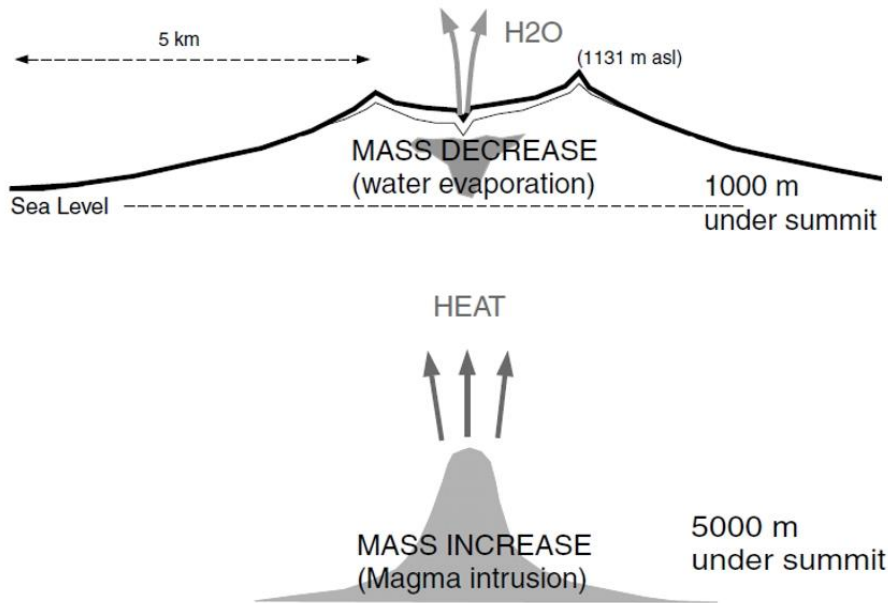
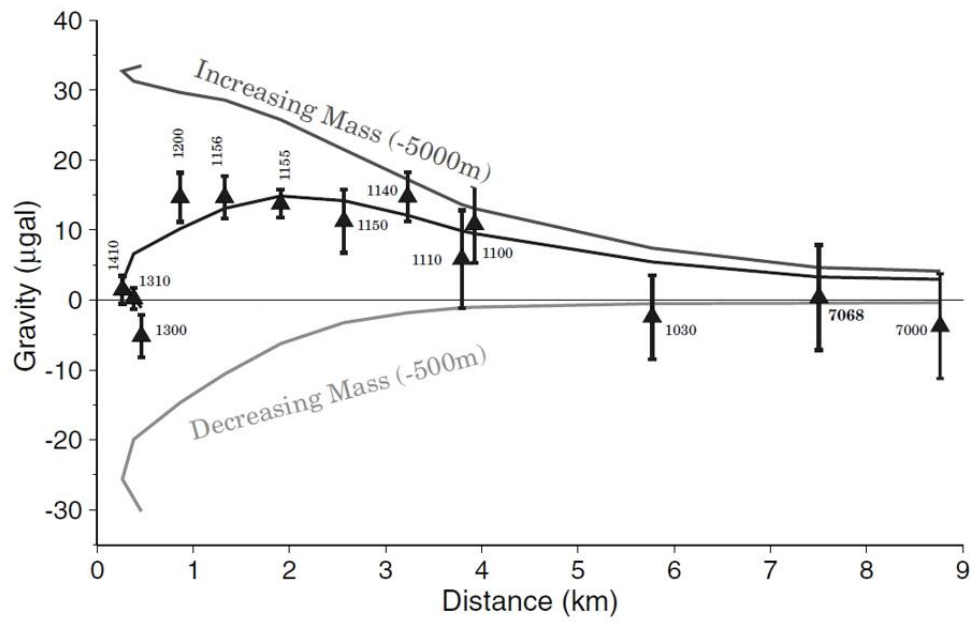


**Figure 14**

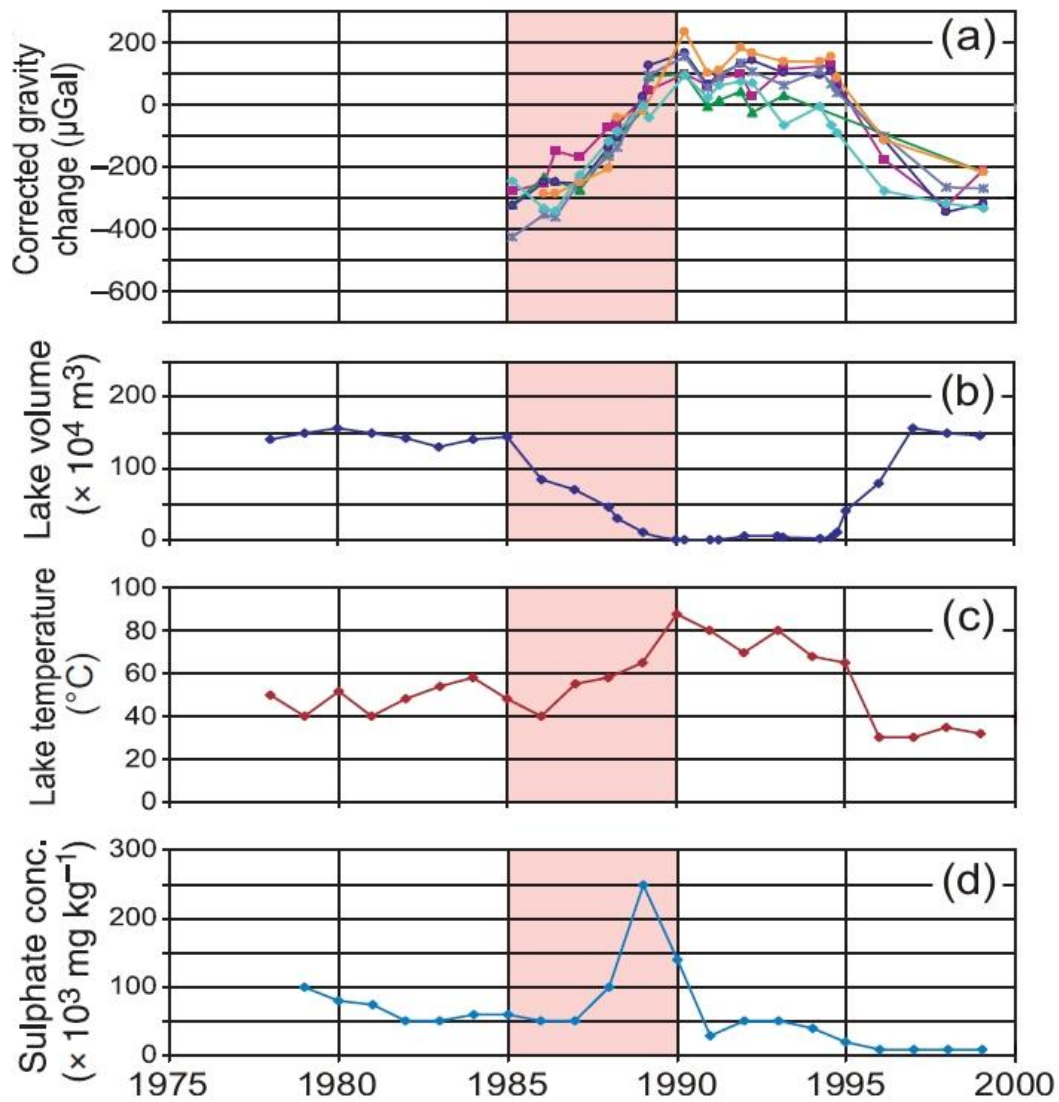


**Figure 15**

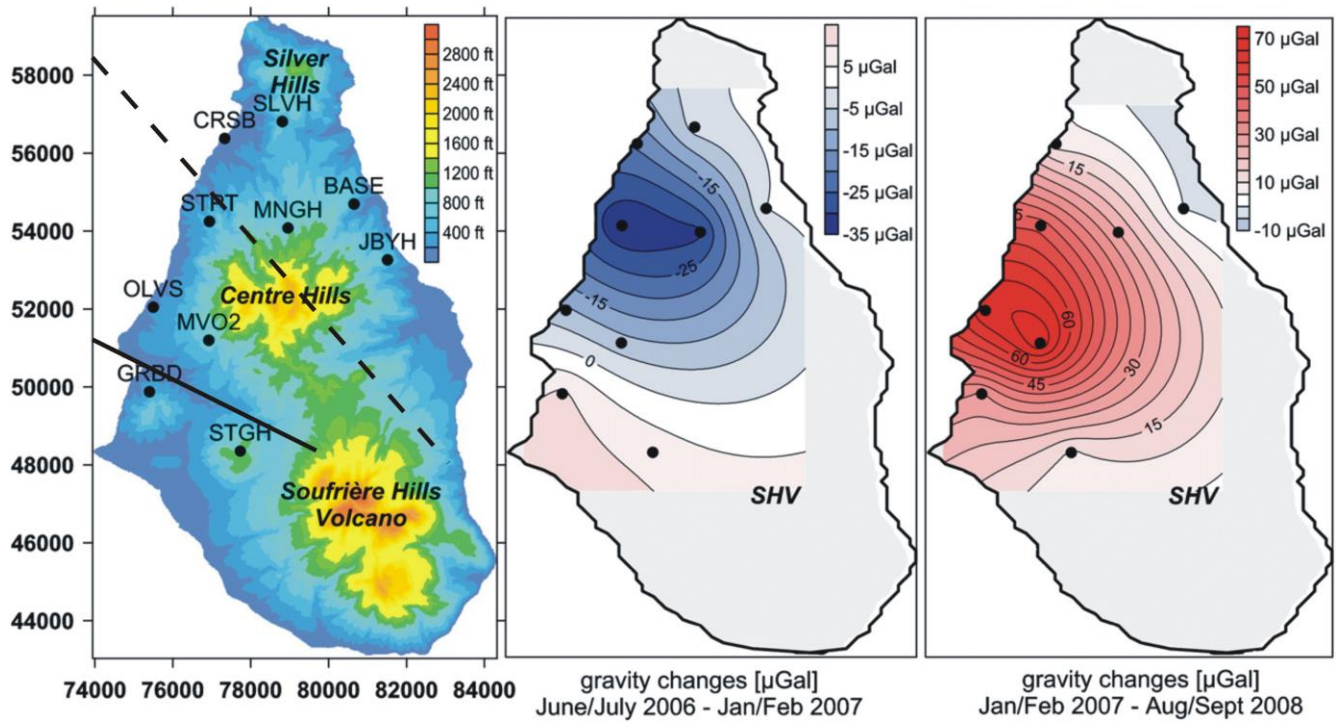


**Figure 16**

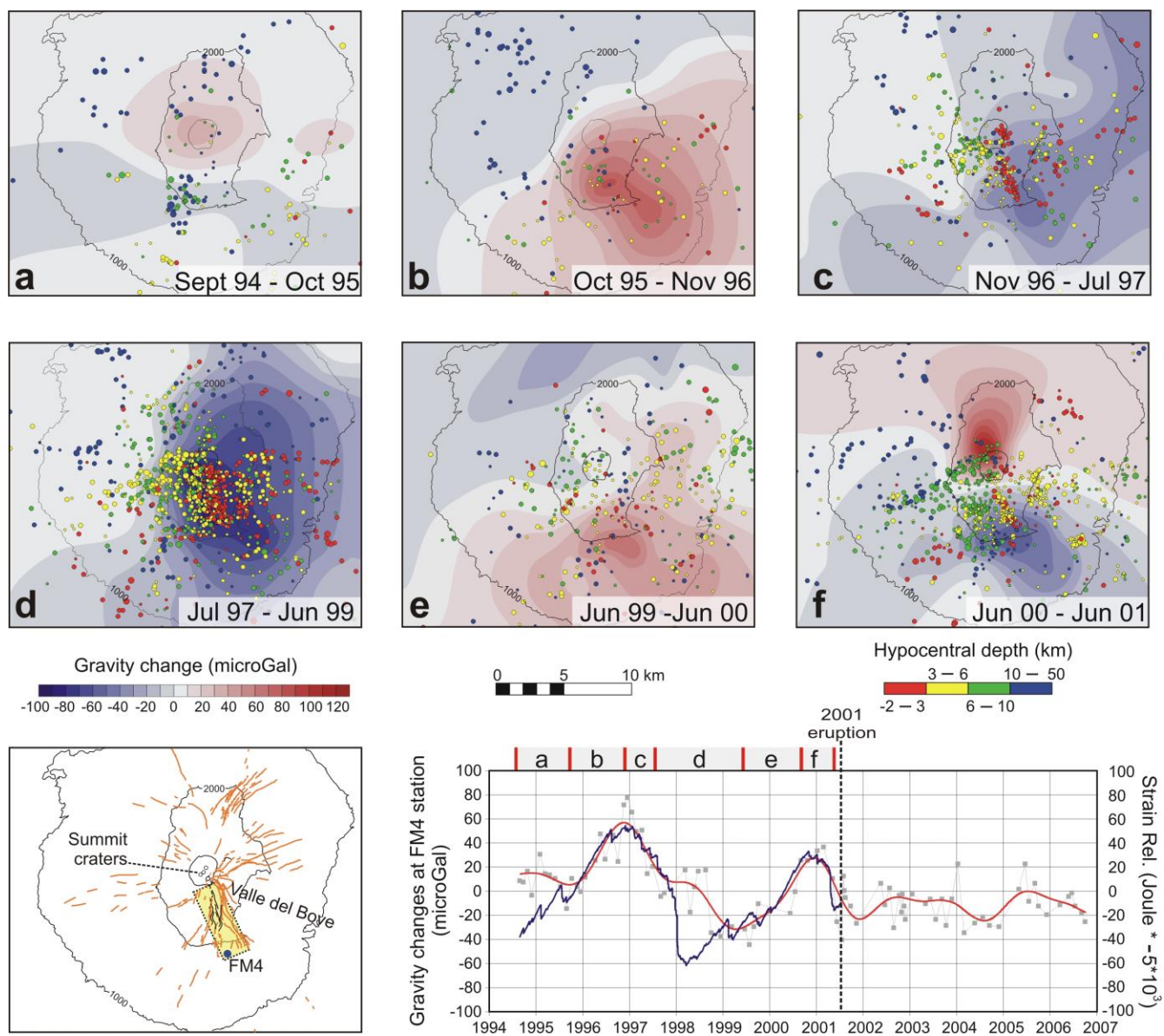


**Figure 17**

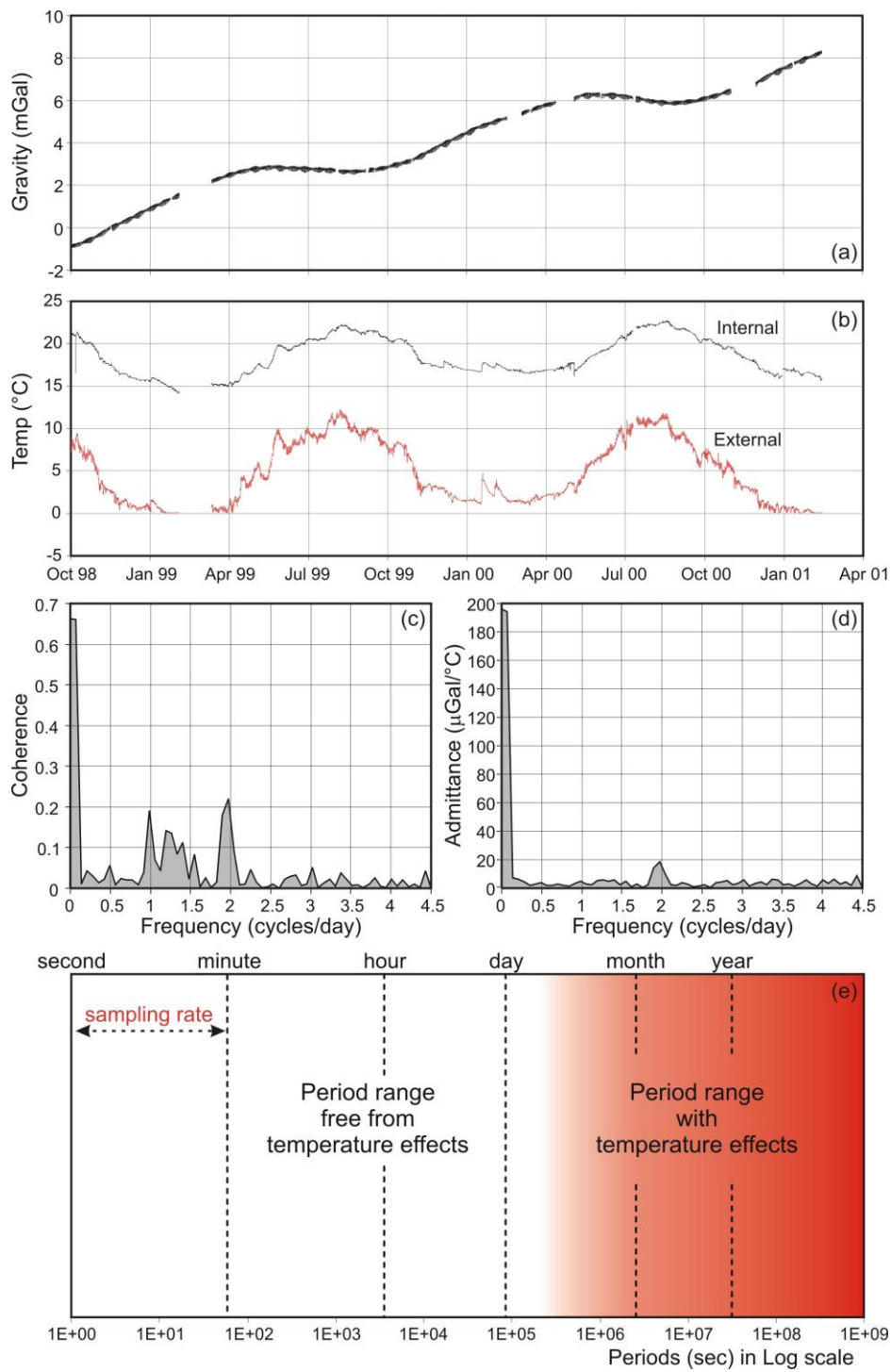


**Figure 18**

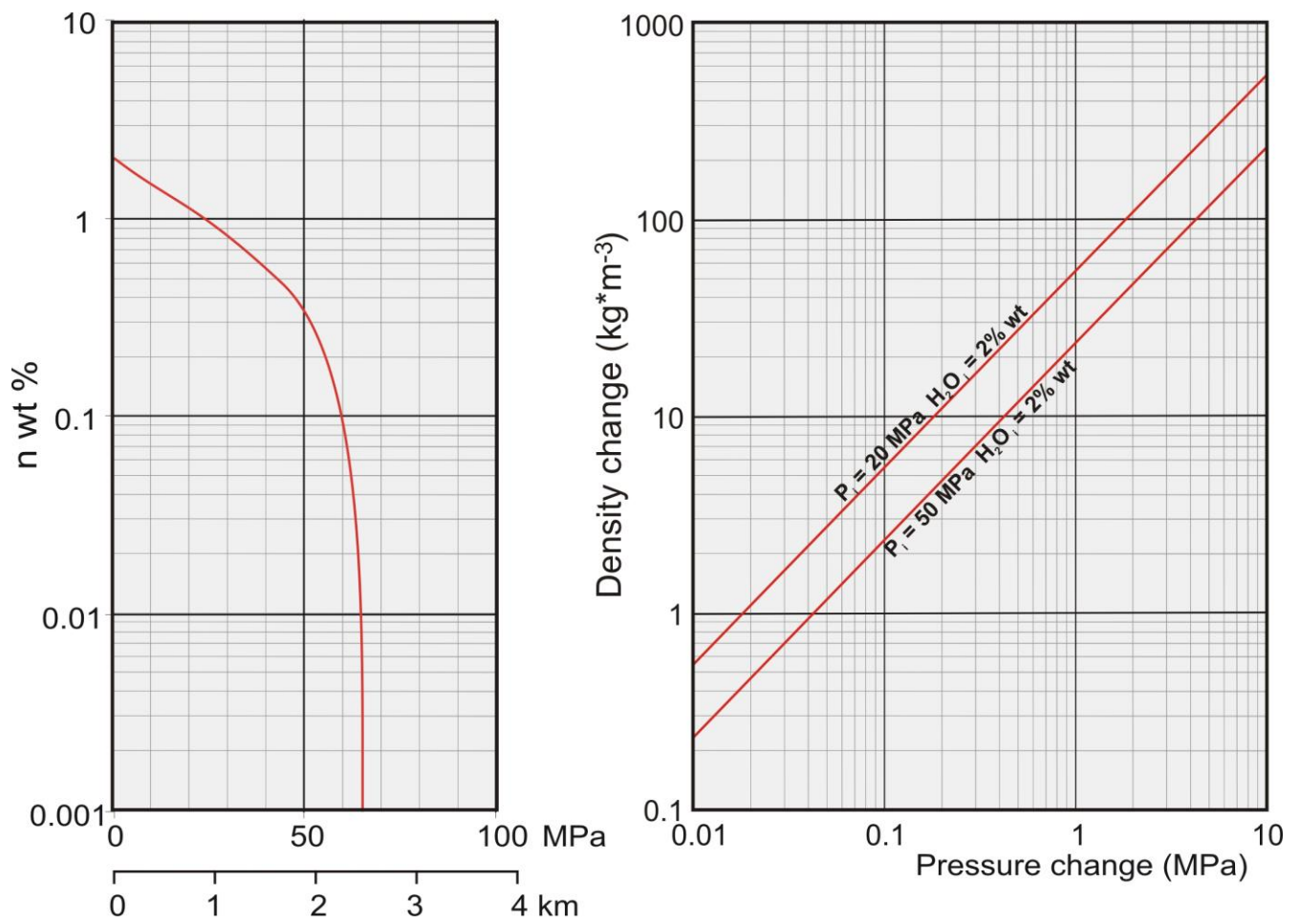


**Figure 19**

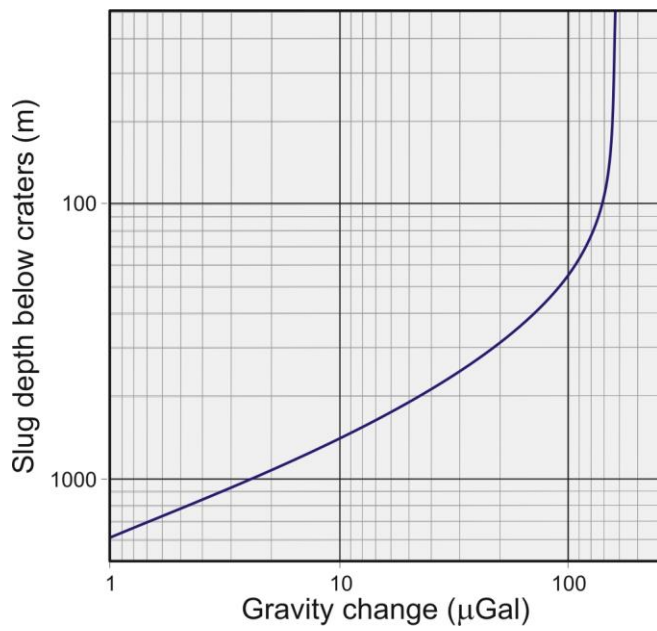


**Figure 20**

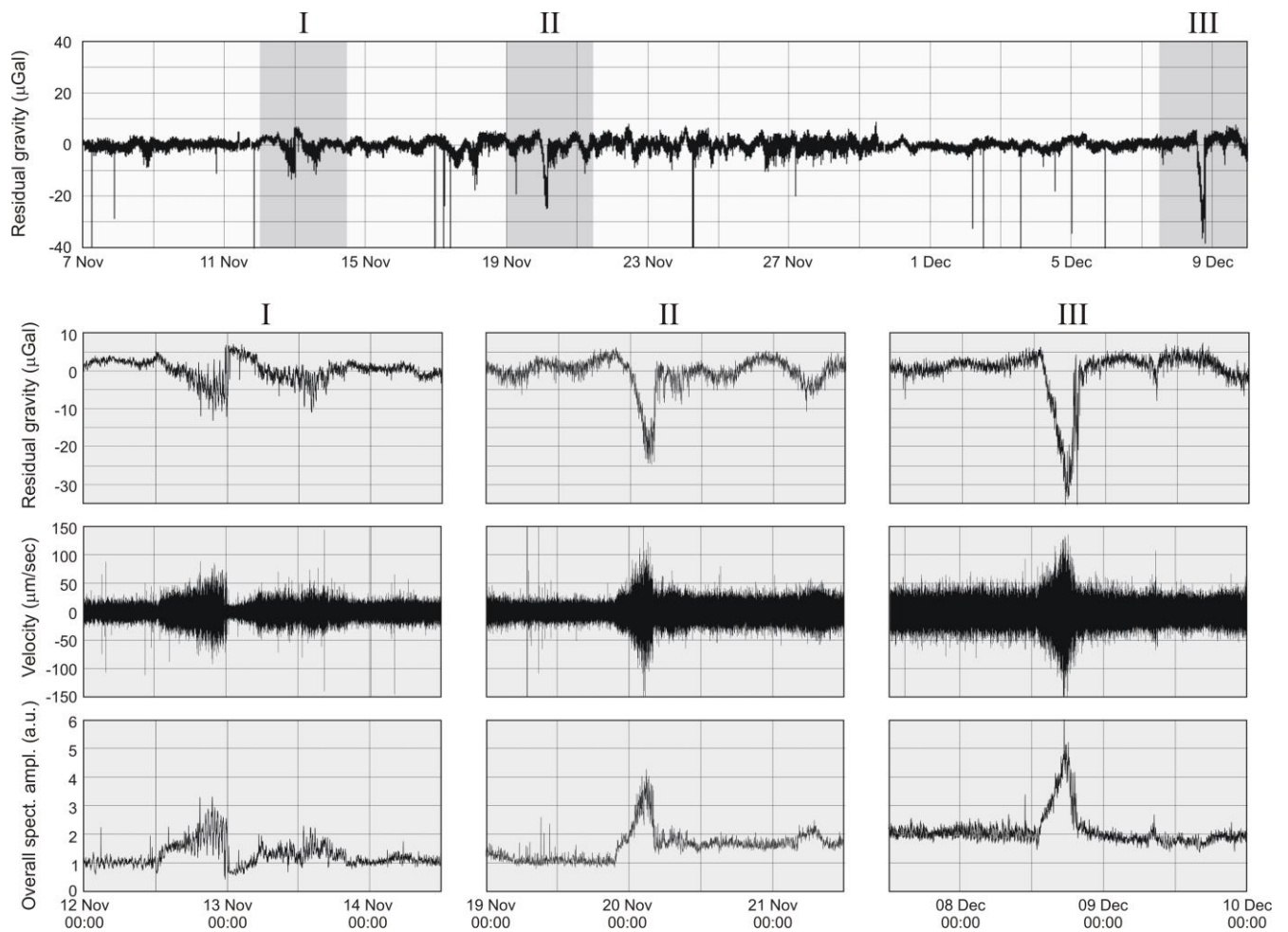


**Figure 21**

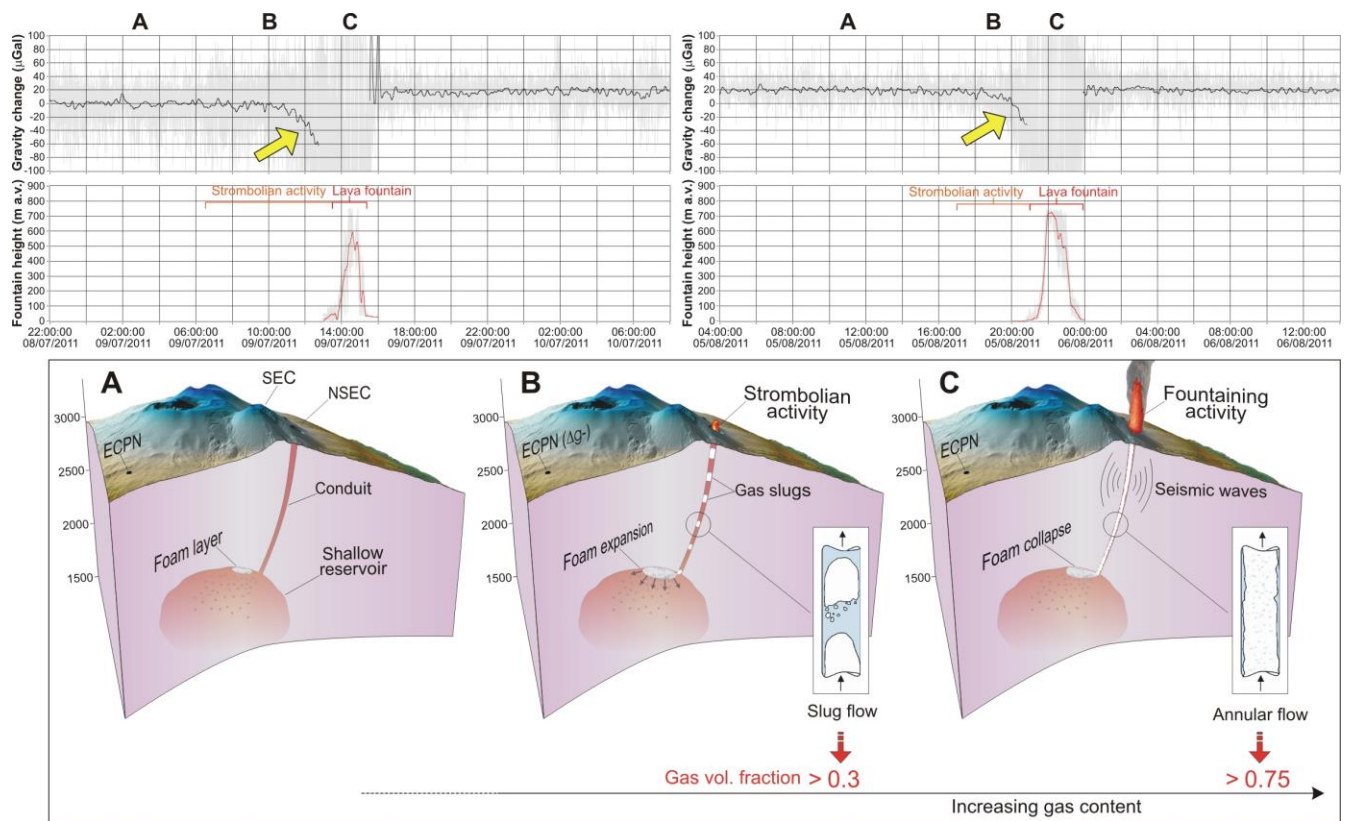


**Figure 22**

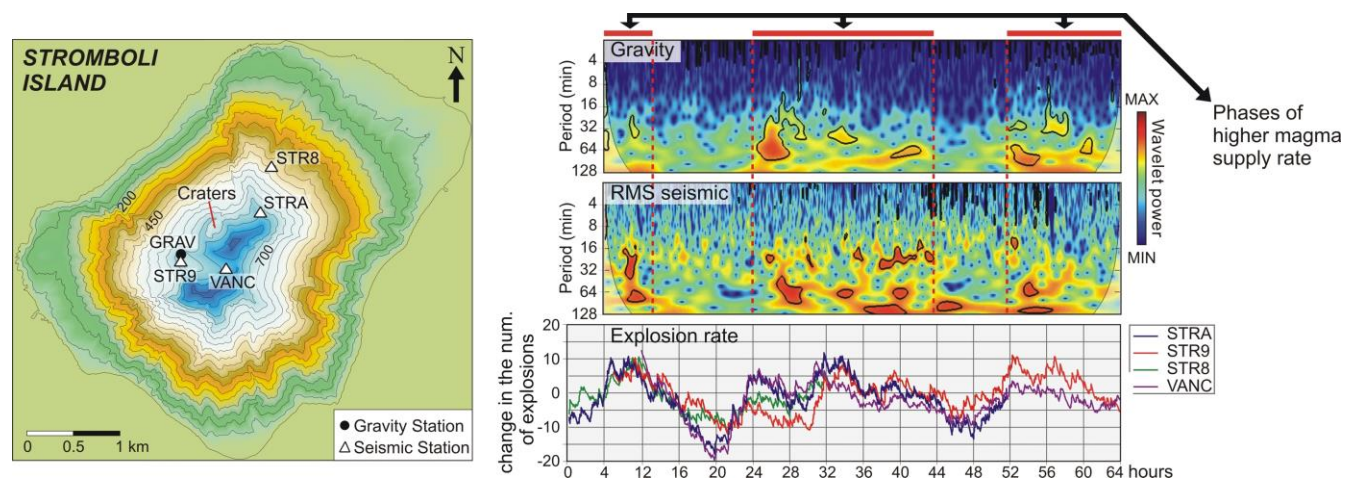


**Figure 23**

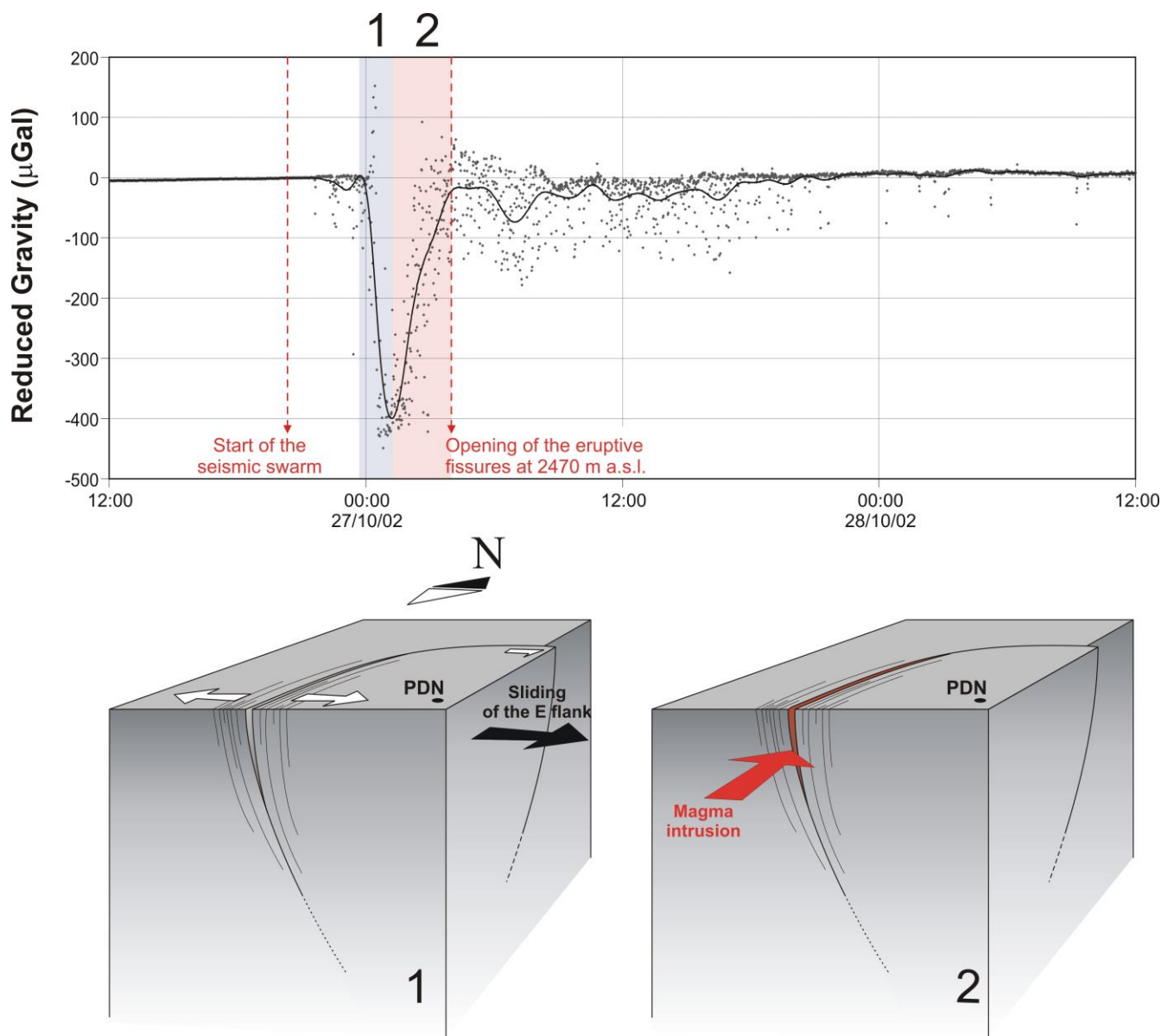


**Figure 24**

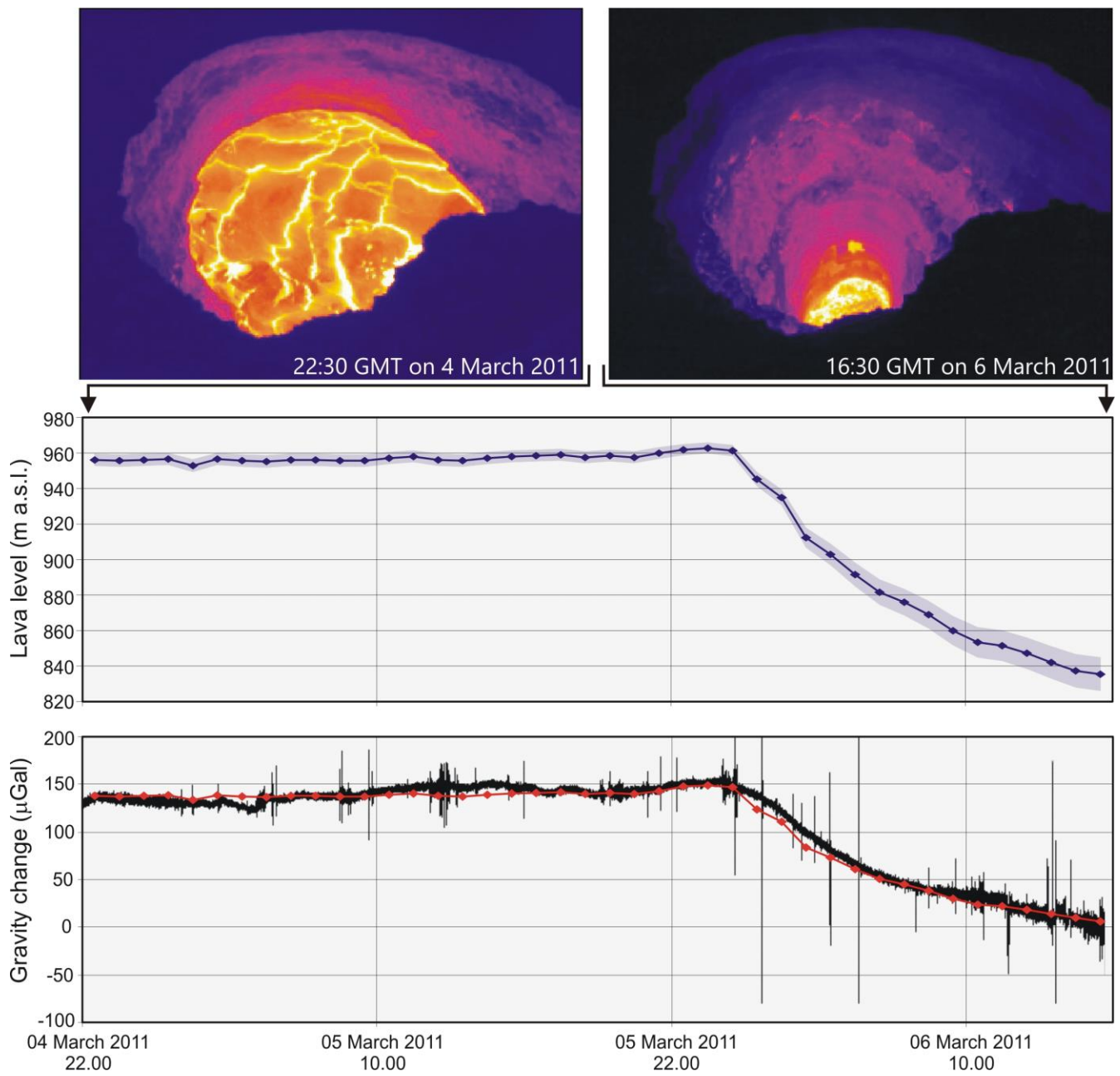


**Figure 25**

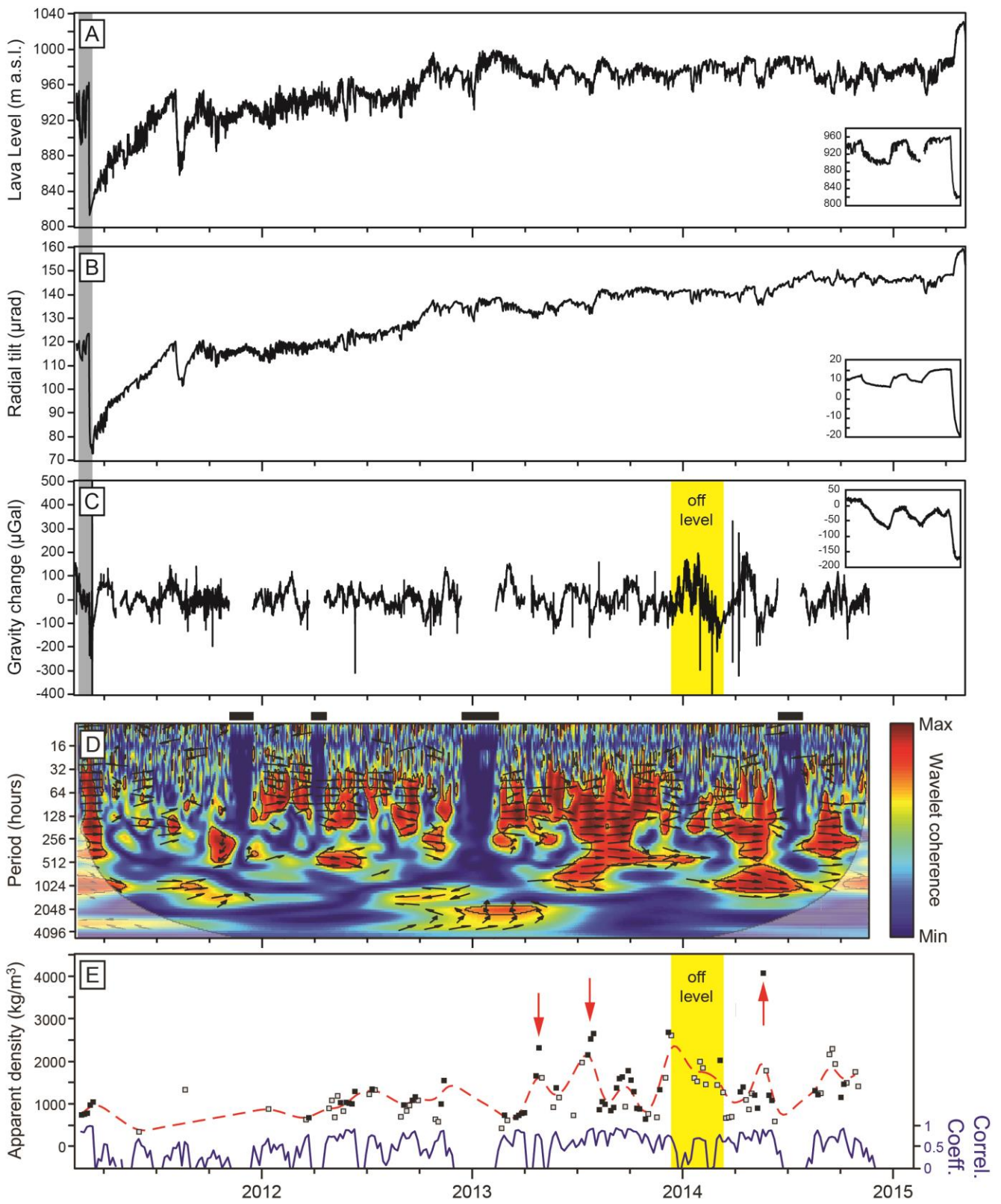


**Figure 26**

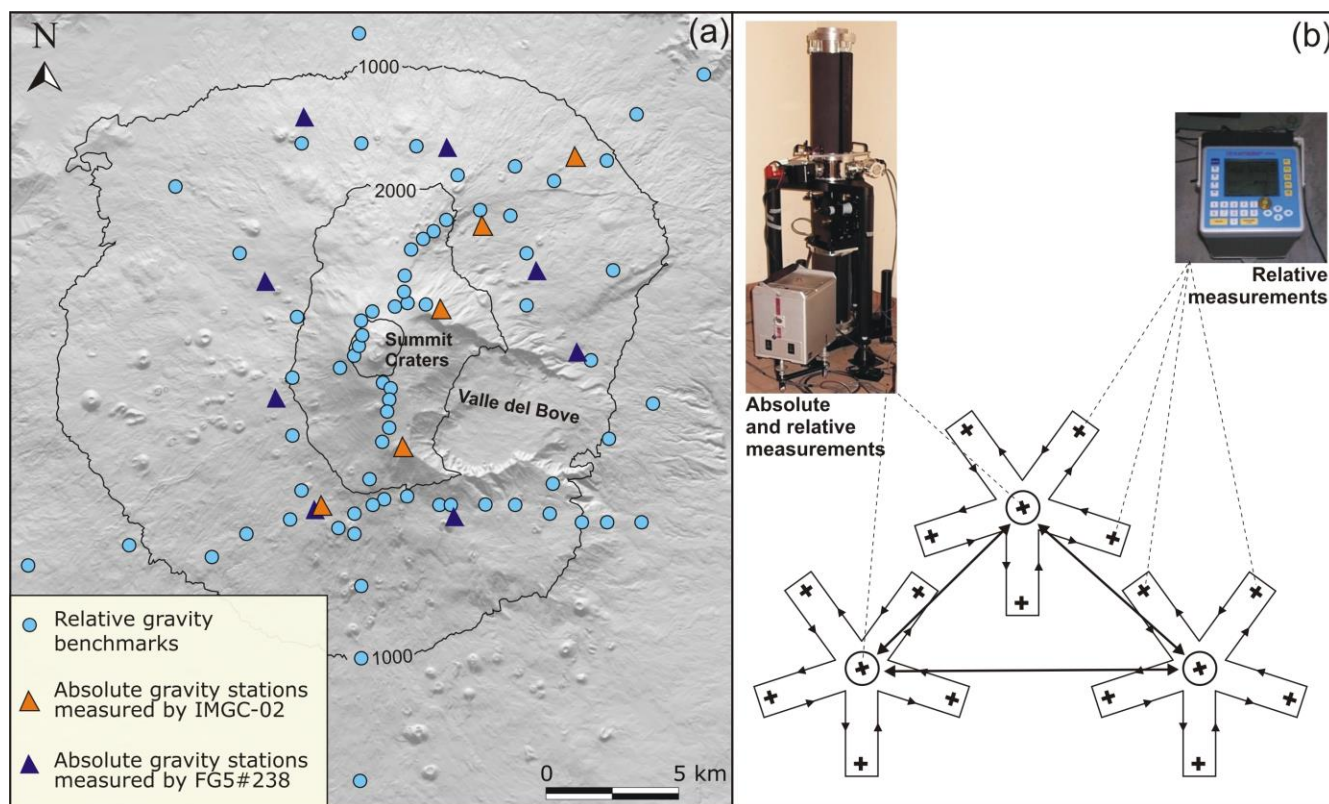


**Figure 27**

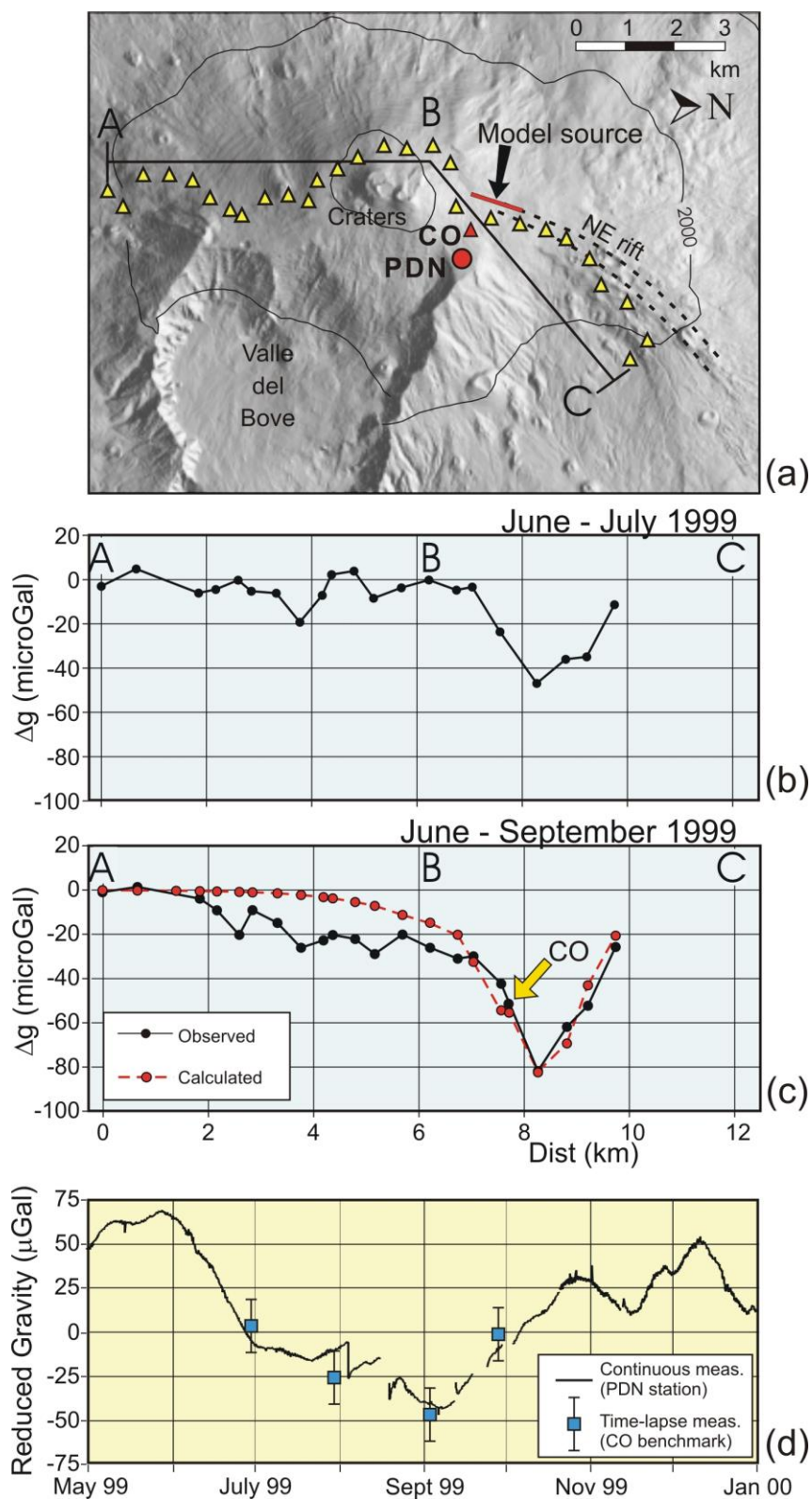


**Figure 28**